Thermodynamics for a hadronic gas of fireballs with internal color structures and chiral fields

Ismail Zakout[1,2,3] and Carsten Greiner[1]

[1]*Institut für Theoretische Physik, J. W. Goethe Universität, Max von Laue Straβe 1, D-60054 Frankfurt am Main, Germany*

[2]*Frankfurt Institute for Advanced Studies, J. W. Goethe Universität, Ruth Moufang Straβe 1, D-60438 Frankfurt am Main, Germany*

[3]*Laboratory for Particle Physics and Cosmology, Harvard University, Cambridge, Massachusetts 02138, USA*

(Received 26 December 2007; revised manuscript received 27 July 2008; published 29 September 2008)

The thermodynamic partition function for a gas of color-singlet bags consisting of fundamental and adjoint particles in both U(N_c) and SU(N_c) group representations is reviewed in detail. The constituent particle species are assumed to satisfy various thermodynamic statistics. The gas of bags is probed to study the phase transition for nuclear matter in extreme conditions. These bags are interpreted as the Hagedorn states, and they are the highly excited hadronic states produced below the phase transition point to the quark-gluon plasma (QGP). The hadronic density of states has the Gross-Witten critical point and exhibits a third-order phase transition from a hadronic phase dominated by the discrete low-lying hadronic mass spectrum particles to another hadronic phase dominated by the continuous Hagedorn states. The Hagedorn threshold production is found just above the highest known experimental discrete low-lying hadronic mass spectrum. The subsequent Hagedorn phase undergoes a first-order deconfinement phase transition to an explosive QGP. The role of the chiral phase transition in the phases of the discrete low-lying mass spectrum and the continuous Hagedorn mass spectrum is also considered. It is found to be crucial in the phase transition diagram. Alternative scenarios are briefly discussed for the Hagedorn gas undergoing a higher order phase transition through multiple processes of internal color-flavor structure modification.

DOI: 10.1103/PhysRevC.78.034916 PACS number(s): 25.75.Nq, 12.38.Mh, 24.85.+p

I. INTRODUCTION

The thermodynamic description of strongly interacting hadronic matter can be approximated by a free gas with a modified level density of hadronic states. This new level density is given by the statistical bootstrap equation. A solution to this equation exists only for a certain range of parameters [1,2]. It has been argued that the statistical evaluation of the mass spectrum in the bag made using the microcanonical ensemble behaves as a strong bootstrap model [3,4]. Naively, the thermodynamics implied by this hadronic mass spectrum has a limiting temperature T_0. The bootstrap model with internal symmetry [5,6] of the fireball provides subsidiary variables and allows for new types of phase transitions. The fireballs, described by the bags of confined quark and gluon components, stand for excited exotic hadrons. They are denoted as the hadronic bubbles or more definitely as the Hagedorn states. The Hagedorn states are defined by fireballs that consist of quarks and gluons in the color-singlet states. The confrontation with the experiment is made by projecting the color-singlet states for the non-Abelian color gauge symmetry. The simple model assumes that there are no interactions among the color charges, except for a color-singlet constraint from the confinement, assuming the results are stable to the introduction of small interaction terms. Gross and Witten [7] have studied the action for fundamental particles in the large-N_c limit of the two-dimensional U(N_c) lattice gauge theory. Using the functional integral method of Brezin, Itzykson, Parisi, and Zuber [8] in the large N_c limit. The action is explicitly evaluated for all fixed weak-strong coupling $\lambda_{\rm WS} = N_c g^2$ by steepest-descent methods. In this limit, a particular configuration totally dominates the functional integral. The Vandermonde determinant, which appears in the measure of the lattice gauge theory, also contributes a potential term. Their solution suggests the existence of a Gross-Witten point for a third-order phase transition from the weak-to-strong coupling $\lambda_{\rm WS}$ interaction in the large-N_c four-dimensional lattice gauge theory. They also mentioned that the occurrence of such a phase transition would not mean that the large-N_c theory does not confine, but more precisely that the occurrence of such a phase transition is not described by the same analytic functions. This means that the behavior of the mass spectral density must be modified at the Gross-Witten point.

The Gross-Witten solution [7] is also obtained for quarks and gluons by solving the singular integral equation. The third-order phase transition point is determined when the solution of the singular integration is evaluated over an open contour rather than a closed one [9–11]. The method given by Azakov, Salomonson and Skagerstam [11] leads to the singular integration over either a closed or an open contour. They considered gluons and quarks by solving the resultant singular integral equation, and they obtained a third-order phase transition point. They derived the phase transition point considering two possibilities. The first one is the integration over a closed contour, while the other possibility is the integration over an open contour. The phase transition takes place when the integration is performed over an open contour rather than the closed one. These two possibilities complicate the solution in the realistic case. The order of the phase transition is assumed to be the same even for an arbitrary constituent mass [12]. It is interesting to note here that the authors of Ref. [11] have shown the existence of a critical chemical potential μ_c such that for $T > 0$, the physical properties for the low-lying spectrum are unaffected by the chemical potential $|\mu| < \mu_c$. This means that generalizing and extending the results for zero chemical potential to the diluted

nuclear matter with a small chemical potential is satisfactory, though more thorough investigation is required in particular when the chemical potential exceeds the critical value. The low-temperature phase has free energy of $O(N_c^0)$, interpreted as a gas of mesons and glueballs, while the high-temperature phase has free energy of order $O(N_c^2)$, which is interpreted as exotic color-singlet bags of adjoint gluons and fundamental and antifundamental quarks.

The deconfining phase transition in SU(N_c) gauge theories has been studied at nonzero temperature using a matrix model of Polyakov loops [13–15]. This model has been also extended for nonzero density. The effective action for loops starts with a potential term. At large N_c, the action is dominated by the loop potential. It has been demonstrated that the Gross-Witten model represents an ultracritical point where the deconfining transition at $N_c = \infty$ is close to but not at the Gross-Witten point. Although masses vanish at the Gross-Witten point, the transition is found of first order, and it has been suggested that at finite N_c, the fluctuations can derive the theory much closer to the Gross-Witten point [13–15].

The thermodynamics of quark jets with an internal color structure has been considered in the context of a one-dimensional quark gas [16–18]. It is considered based on an exact Hamiltonian formalism in which the quarks are treated as classical particles, but their interactions through the group theory U(N_c) or SU(N_c) gauge fields are treated exactly [16–20].

The class of theories on a compact spatial manifold with fundamental flavors and adjoint gluons are also found to undergo a third-order deconfinement phase transition at a temperature T_c proportional to the inverse length scale of the compact manifold [21]. The same thermodynamic behavior of the deconfinement transition for large N_c at zero and weakly coupling is found for a wide class of toy models such as $\mathcal{N} = 4$ super Yang-Mills theory. It is argued that anti–de Sitter space (AdS) black hole thermodynamics is related to Hagedorn thermodynamics [22]. Sundborg [22] has calculated the partition sums for $\mathcal{N} = 4$ super Yang-Mills on S^3 and has discussed the connections with gravitational physics. It has been speculated that on a dual string theory interpretation, the deconfinement transitions are always associated with black hole formation and furthermore that the intermediate-temperature phase associated with second-order deconfinement transitions would be dual to a string theory in a background dominated by a strange new type of stable black hole [23–25]. Indeed, the Gross-Witten point and the Hagedorn states remain very exciting and rich physics. For example, in the language of anti–de Sitter-space/conformal-field-theory (AdS/CFT) duality, the Horowitz-Polchinski point for a small black hole should correspond to a Gross-Witten transition. This can be related to the phase transition from the small black hole to a big black hole [26].

The internal color symmetry of the bound state remains to be of a color-singlet state even for finite temperature and chemical potential due to the color confinement. The discrete low-lying hadronic mass spectrum is generated by the broken chiral symmetry. The internal color structure of the hadronic bag of quarks and gluons for hadronic states above the known discrete low-lying hadronic mass spectrum remains in a total color-singlet state. In realistic calculations, the internal color structure is imposed in the partition function for the hadronic bubbles [27]. When the temperature reaches the critical one, color is expected to be liberated and chiral symmetry is restored. QCD predicts a phase transition from the hadronic phase to a deconfined quark-gluon plasma (QGP). The hadronic phase consists of the whole hadronic mass spectrum including resonances of all known particles. Hardcore repulsive forces can be represented by the excluded volume. The effects from strong interactions are included by adding a free gas of hadronic bubbles which are bags of constituent quarks and gluons with a specific internal color-flavor structure. The hadronic bubbles remain in overall color-singlet states, despite the complexity of the internal color-flavor structure. The bubble size grows, but the bubble retains its own internal color symmetry with increasing baryonic density at low temperature. The volume fluctuations are expected to be suppressed whenever the bags start to overlap with each other at large chemical potential. When the temperature increases, the bag's surface is deformed and smeared out until the bubbles dissociate eventually at the critical temperature. It is expected that the bubble's volume fluctuation increases at high temperature in contrast to cold dense hadronic matter in which the bubbles tend to squeeze each other. The strength of the volume fluctuation is presumed to modify the details of the phase transition diagram [28].

The (grand-) canonical ensemble and its Laplace transform to the microcanonical ensemble for gluonic bags or glueballs were derived by Kapusta [3,4] without imposing any color constraint. The internal symmetry constraint was originally introduced for the statistical bootstrap model [5,6]. The bootstrap density of states can be derived from the MIT bag model. In the hadronic phase, the highly excited fireballs derived from the bootstrap equation are hadronic bubbles of confined quarks and gluons in a net color-singlet state [29–34]. Gorenstein *et al.* [35–38] have studied the gas of bags using the isobaric partition function. Auberson *et al.* [39] have studied the phase transition to the deconfined QGP by considering the asymptotic Gaussian volume fluctuations. The order and shape of the phase transition have been studied in detail [28]. It has been shown that the color-singlet constraint imposed on the bag states is not the only critical condition for the existence of the phase transition to an explosive QGP. Therefore, the appearance of the deconfined phase transition depends essentially on the volume fluctuations as well as the internal color structure constraints. Recently, it has been suggested that the phenomenology of the hadronic bubble internal structure decides the order of the phase transition for low chemical potential and high temperature [28,40].

In the present work, the partition function is written as a function of the thermal running parameter λ. This thermal running parameter is related to the Gross-Witten weak-strong coupling λ_{WS} as follows: $\lambda/N_c^2 = 1/\lambda_{\mathrm{WS}}$. Therefore, the weak interaction corresponds to the large thermal running $\lambda > \lambda_{\mathrm{crit}}$, while the strong interaction is analogous to the small thermal running $\lambda < \lambda_{\mathrm{crit}}$.

The outline of the present paper is as follows. In Sec. II, we review the partition function in the Hilbert space for various statistics for the gas of particles with a specific internal

color symmetry. The partition function is derived for an ideal gas. The sum of states for particles confined in the cavity is presented for convenience in the realistic calculations. The extension to a specific geometry and other degrees of freedom in the conformal fields such as the super-symmetry Yang-Mills theory is mentioned. The invariance measure used to project a specific internal color state is presented in Sec. III. The invariance measure is given by the Vandermonde determinant for the U(N_c) and SU(N_c) theoretic groups. It is shown that the Vandermonde determinant has two different asymptotic approximations: the first is appropriate when the color charges are distributed uniformly over the entire circle; the second one is more appropriate when the color charges become more dominant in a specific physical range. In Sec. IV, we review the method based on the spectral density of the color eigenvalues (hereafter called the spectral density method). It has been studied by Gross and Witten to discover the critical Gross-Witten point. This method is reviewed for the fundamental particles, and the phase transition point is given. In Sec. V, we present an alternative method for deriving the critical point for the phase transition. This method is based on the Gaussian-like saddle points (GSP) method, and it is more appropriate in theoretical nuclear physics and realistic calculations. It has been considered by several authors [28–30,34,41]. In Sec. VI, the gas of adjoint particles is reviewed in the context of two different methods. Since in the realistic situation we have a gas of fundamental as well as adjoint particles, the physics of the phase transition for a gas consisting of different particle species and satisfying various statistics is studied in Sec. VII. At first, we demonstrate the calculation for the Maxwell-Boltzmann statistics for fundamental and adjoint particles. The realistic confined quark and gluon bag is considered in detail. The adjoint gluons which are obeying the Bose-Einstein statistics and the fundamental quarks and antiquarks which are obeying the Fermi-Dirac statistics are considered in computing the partition function and finding the phase transition's critical point. The microcanonical ensemble as a density of states is presented in Sec. VIII. The microcanonical ensemble is derived from the inverse Laplace transform of the grandcanonical one. The critical mass for emerging fireballs which are obeying the Maxwell-Boltzmann statistics is demonstrated first, and then the realistic critical mass for emerging Hagedorn states is given. In Sec. IX, the density of states is derived using the statistical evaluation of the microcanonical ensemble. The derivation is given along the lines of Kapusta [3], but the internal color symmetry is considered explicitly in our calculations. The thermodynamics for the gas of bags with the excluded volume repulsion is presented in Sec. X. We summarize the conditions for the phase transition in the context of the isobaric partition function construction. Furthermore, various scenarios for the phase transition are given. The role of the chiral symmetry restoration phase transition in the hadronic matter and QGP phase diagram is given in Sec. XI. Finally, our conclusion is given in Sec. XII.

II. CANONICAL PARTITION FUNCTION

The canonical ensemble for the gas of fundamental particles in the Hilbert space is given by the tensor product of the Fock spaces of particles and antiparticles:

$$Z_{q\bar{q}}(\beta) = \int_{\mathrm{SU}(N_c),\mathrm{U}(N_c)} d\mu(g)[\mathrm{Tr}_q \hat{U}_q(g) e^{-\beta \hat{H}_q}] \times [\mathrm{Tr}_{\bar{q}} \hat{U}_{\bar{q}}(g) e^{-\beta \hat{H}_{\bar{q}}}]. \tag{1}$$

On the other hand, the canonical ensemble for the gas of fundamental and adjoint particles is given by the tensor product of fundamental particles, antiparticles and adjoint particles' Fock spaces. This tensor product reads

$$Z_{q\bar{q}g}(\beta) = \int_{\mathrm{SU}(N_c),\mathrm{U}(N_c)} d\mu(g)[\mathrm{Tr}_q \hat{U}_q(g) e^{-\beta \hat{H}_q}] \times [\mathrm{Tr}_{\bar{q}} \hat{U}_{\bar{q}}(g) e^{-\beta \hat{H}_{\bar{q}}}][\mathrm{Tr}_g \hat{U}_g(g) e^{-\beta \hat{H}_g}], \tag{2}$$

where the notation $\mathrm{Tr}_{q,\bar{q},g}$ is the trace in each Fock space. We adopt the notation Tr in order to distinguish the single-particle statistics from the trace tr_c over the color degrees of freedom. In each Fock space, there exists the basis that diagonalizes both operators as long as $\hat{H}_q$ and $\hat{U}_q(g)$ commute. Let $|\alpha, j\rangle$ be the one-particle states of such a basis, where α labels the eigenvalues of $\hat{H}_q$ and j labels those $\mathbf{R}(g)$ of $\hat{U}_q(g)$, then the diagonalized eigenstates read

$$\begin{aligned} \langle \alpha', j' | \hat{H}_q | \alpha, j \rangle &= \delta_{\alpha,\alpha'} \delta_{jj'} E_\alpha, \\ \langle \alpha', j' | \hat{U}_q(g) | \alpha, j \rangle &= \delta_{\alpha,\alpha'} \delta_{jj'} \mathbf{R}_{jj'}(g). \end{aligned} \tag{3}$$

Any configuration of the system is defined by the set of occupation numbers $\{n_{\alpha,j}\}$. The additivity of $\hat{H}_q$ simply means that

$$\langle \{n_{\alpha,j}\} | \hat{H}_q | \{n_{\alpha,j}\} \rangle = \sum_{\alpha,j} n_{\alpha,j} E_\alpha. \tag{4}$$

Then, using the basis $|\{n_{\alpha,j}\}\rangle$ to evaluate the trace, we readily obtain

$$\begin{aligned} \mathrm{Tr}\, \hat{U}_q(g) e^{-\beta \hat{H}_q} &= \sum_{\{n_{\alpha,j}\}} \prod_{\alpha,j} (\mathbf{R}_{jj}(g) e^{-\beta E_\alpha})^{n_{\alpha,j}}_{\mathrm{boson}} \\ &\quad + \sum_{\{n_{\alpha,j}\}} \prod_{\alpha,j} (-1)^{n_{\alpha,j}+1} (\mathbf{R}_{jj}(g) e^{-\beta E_\alpha})^{n_{\alpha,j}}_{\mathrm{fermion}} \\ &= \prod_{\alpha,j} \sum_{\{n_{\alpha,j}\}} (\mathbf{R}_{jj}(g) e^{-\beta E_\alpha})^{n_{\alpha,j}}_{\mathrm{boson}} \\ &\quad + \prod_{\alpha,j} \sum_{\{n_{\alpha,j}\}} (-1)^{n_{\alpha,j}+1} (\mathbf{R}_{jj}(g) e^{-\beta E_\alpha})^{n_{\alpha,j}}_{\mathrm{fermion}}. \end{aligned} \tag{5}$$

Hence, the partition function in the each Fock space decomposes to bosonic and fermionic single-particle functions. It is reduced to

$$\begin{aligned} \mathrm{Tr}_{\mathrm{states}} \hat{U}_q(g) e^{-\beta \hat{H}_q} &= \mathrm{Tr}_{\mathrm{FD}} \hat{U}_q(g) e^{-\beta \hat{H}_q} + \mathrm{Tr}_{\mathrm{BE}} \hat{U}_q(g) e^{-\beta \hat{H}_q} \\ &\to \mathrm{Tr}_{\mathrm{FD}} \hat{U}_q(g) e^{-\beta \hat{H}_q} \\ &\to \mathrm{Tr}_{\mathrm{BE}} \hat{U}_q(g) e^{-\beta \hat{H}_q}, \end{aligned} \tag{6}$$

where the subscripts FD and BE indicate Fermi-Dirac and Bose-Einstein statistics, respectively. The resultant ensemble decomposes either to fermionic or bosonic Fock space or even the superposition of Fock spaces with different statistics. The Hilbert space of gas, which is consisting of particles satisfying

Fermi-Dirac and Bose-Einstein statistics, has the structure of tensor product of Fock spaces obeying Fermi-Dirac statistics and another one obeying Bose-Einstein statistics. The trace over Fermi-Dirac statistics is given by

$$\begin{aligned}\mathrm{Tr}_{\mathrm{FD}}\hat{U}_q(g)e^{-\beta\hat{H}_q} &= \prod_{\alpha}[1+\mathbf{R}(g)e^{-\beta E_\alpha}] \\ &= \exp\left[+\mathrm{tr}_c\sum_{\alpha}\ln[1+\mathbf{R}(g)e^{-\beta E_\alpha}]\right], \quad (7)\end{aligned}$$

while the trace over Bose-Einstein statistics is given by

$$\begin{aligned}\mathrm{Tr}_{\mathrm{BE}}\hat{U}_q(g)e^{-\beta\hat{H}_q} &= \prod_{\alpha}\frac{1}{[1-\mathbf{R}(g)e^{-\beta E_\alpha}]} \\ &= \exp\left[-\mathrm{tr}_c\sum_{\alpha}\ln[1-\mathbf{R}(g)e^{-\beta E_\alpha}]\right], \quad (8)\end{aligned}$$

where tr_c is the trace over the color degree of freedom. In the realistic physical situation, the single-particle partition function satisfies either Fermi-Dirac or Bose-Einstein statistics. The quarks and antiquarks satisfy Fermi-Dirac statistics, while gluons satisfy Bose-Einstein statistics. The sum of states $\{jn\}$ for Fermi-Dirac statistics is calculated explicitly as

$$\begin{aligned}&\mathrm{Tr}_{\mathrm{FD}}\hat{U}_q(g)e^{-\beta\hat{H}_q} \\ &= \exp\left[+\mathrm{tr}_c\sum_{\alpha}\ln[1+\mathbf{R}(g)e^{-\beta E_\alpha}]\right] \\ &= \exp\left[+\mathrm{tr}_c\sum_{\alpha}\sum_{m=1}\frac{1}{m}(-1)^{m+1}(\mathbf{R}(g)e^{-\beta E_\alpha})^m\right] \\ &= \exp\left[+\sum_{m=1}\frac{1}{m}(-1)^{m+1}\left(\mathrm{tr}_c\mathbf{R}(g^m)\sum_{\alpha}e^{-m\beta E_\alpha}\right)\right] \\ &= \exp\left[+\sum_{m=1}\frac{1}{m}(-1)^{m+1}\mathrm{tr}_c\mathbf{R}(g^m)z_{\mathrm{F}}(e^{-m\beta})\right]. \quad (9)\end{aligned}$$

In Bose-Einstein statistics, the single-particle partition function becomes

$$\begin{aligned}\mathrm{Tr}_{\mathrm{BE}}\hat{U}_q(g)e^{-\beta\hat{H}_q} &= \exp\left[-\mathrm{tr}_c\sum_{\alpha}\ln[1-\mathbf{R}(g)e^{-\beta E_\alpha}]\right] \\ &= \exp\left[+\mathrm{tr}_c\sum_{\alpha}\sum_{m=1}\frac{1}{m}(\mathbf{R}(g)e^{-\beta E_\alpha})^m\right] \\ &= \exp\left[+\sum_{m=1}\frac{1}{m}\mathrm{tr}_c\left(\mathbf{R}(g^m)\sum_{\alpha}e^{-m\beta E_\alpha}\right)\right] \\ &= \exp\left[+\sum_{m=1}\frac{1}{m}\mathrm{tr}_c\mathbf{R}(g^m)z_B(e^{-m\beta})\right], \quad (10)\end{aligned}$$

where $z_{\mathrm{F/B}}(e^{-\beta})=\sum_\alpha e^{-\beta E_\alpha}$ is the sum of energy states with a specific structure and/or geometry either for Fermi or Bose particles. Furthermore, in the high-energy limit (i.e., temperature), the Maxwell-Boltzmann statistics becomes an appropriate approximation under certain conditions. The single-particle partition function in the Maxwell-Boltzmann statistics is given by

$$\begin{aligned}\mathrm{Tr}_{\mathrm{MB}}\hat{U}_q(g)e^{-\beta\hat{H}_q} &= \sum_{\{n_{\alpha,j}\}}\prod_{\alpha,j}\frac{1}{n_{\alpha,j}}(\mathbf{R}_{jj}(g)e^{-\beta E_\alpha})^{n_{\alpha,j}} \\ &= \prod_{\alpha,j}\exp(\mathbf{R}_{jj}(g)e^{-\beta E_\alpha}) \\ &= \exp\sum_{\alpha}\ln\det_c[\exp(\mathbf{R}(g)e^{-\beta E_\alpha})] \\ &= \exp\sum_{\alpha}\mathrm{tr}_c\ln\exp(\mathbf{R}(g)e^{-\beta E_\alpha}) \\ &= \exp\left[\mathrm{tr}_c\mathbf{R}(g)\sum_{\alpha}e^{-\beta E_\alpha}\right]. \quad (11)\end{aligned}$$

The theoretical group such as $\mathrm{U}(N_c)$ and $\mathrm{SU}(N_c)$ has a special importance in the realistic physical application such as the quark and gluon bubble.

The $\mathrm{U}(N_c)$ or $\mathrm{SU}(N_c)$ internal color group symmetry is introduced in the canonical ensemble in order to project the state with a specific internal color structure. The color structure of the quark and antiquark is introduced by the fundamental representation. The Fock space single-particle partition function with fundamental representation in the Fermi-Dirac statistics reads as

$$\begin{aligned}\mathrm{Tr}_{\mathrm{FD}}\hat{U}_q(g)e^{-\beta\hat{H}_q} &= \exp\left[+\mathrm{tr}_c\sum_{\alpha}\ln[1+\mathbf{R}_{\mathrm{fun}}(g)e^{-\beta E_\alpha}]\right] \\ &= \exp\left[+\sum_{i=1}^{N_c}\sum_{\alpha}\ln[1+e^{i\theta_i}e^{-\beta E_\alpha}]\right], \quad (12)\end{aligned}$$

where the trace over group $\mathrm{U}(N_c)$ [or $\mathrm{SU}(N_c)$] fundamental representation is given by

$$\mathrm{tr}_c\mathbf{R}_{\mathrm{fun}}(g^k)=\sum_{i=1}^{N_c}e^{ik\theta_i}. \quad (13)$$

The partition function for the fundamental particle and antiparticle Hilbert space becomes

$$\begin{aligned}&[\mathrm{Tr}_q\hat{U}_q(g)e^{-\beta\hat{H}_q}][\mathrm{Tr}_{\bar{q}}\hat{U}_{\bar{q}}(g)e^{-\beta\hat{H}_{\bar{q}}}] \\ &= \exp\left[+\sum_{i=1}^{N_c}\sum_{\alpha}\ln[1+2\cos(\theta_i)e^{-\beta E_\alpha}+e^{-2\beta E_\alpha}]\right]. \quad (14)\end{aligned}$$

On the other hand, the gluons are assumed as gauge particles in the theory, and they are introduced in the context of adjoint representation. The Fock space single-particle partition function for adjoint particles satisfying Bose-Einstein statistics reads

$$\begin{aligned}\mathrm{Tr}_{\mathrm{BE}}\hat{U}_g(g)e^{-\beta\hat{H}_g} &= \exp\left[-\mathrm{tr}_c\sum_{\alpha}\ln[1-\mathbf{R}_{\mathrm{adj}}(g)e^{-\beta E_\alpha}]\right] \\ &= \exp\left[-\Re\sum_{i\neq j}^{N_c}\sum_{\alpha}\ln[1-e^{i(\theta_i-\theta_j)}e^{-\beta E_\alpha}]\right. \\ &\quad \left.-N_c\sum_{\alpha}\ln[1-e^{-\beta E_\alpha}]\right]. \quad (15)\end{aligned}$$

The trace over the adjoint representation becomes

$$\mathrm{tr}_c \mathbf{R}_{\mathrm{adj}}(g^k) = \sum_{i\neq j} \cos k(\theta_i - \theta_j) + N_c, \quad \mathrm{U}(N_c),$$
$$= \sum_{i\neq j} \cos k(\theta_i - \theta_j) + (N_c - 1), \quad \mathrm{SU}(N_c), \quad (16)$$

for the $\mathrm{U}(N_c)$ and $\mathrm{SU}(N_c)$ groups, respectively. The density of states for single-particle levels has been studied extensively using the multiple reflection expansion method [42–44]. The sum runs over the number of states which can fill the one-particle states. The sum over states for constituent particles that are confined in a spherical cavity is calculated as [42–44]

$$E_\alpha = \sqrt{p^2 + m^2} + V(r), \quad \sum_\alpha = \mathcal{D}_D \int_V d^3r \int dE\, \rho(E)$$
$$= \mathcal{D}_D V \int dE \rho(E) = \mathcal{D}_D \int \frac{V d^3p}{(2\pi)^3}. \quad (17)$$

The volume V is the spherical cavity volume in which the constituent particles are confined, and it corresponds to the total occupational space. The one-particle degeneracy is given by $\mathcal{D}_D = N_c \mathcal{D}_d$, where N_c is the number of colors and $\mathcal{D}_d$ is the particle species degeneracy. Usually we set $\mathcal{D}_d = (2j+1)$ as the spin multiplicity, where j is the spin quantum number.

Nonetheless, it is interesting to note here that when we have a thermodynamic system of particles confined in a compacted space with specific geometry and other degrees of freedom, the sum of states becomes nontrivial. It has been noted that in the conformal field theories, the partition function for scalars and chiral fermions on $S^3 \times R$ are given by [22,23]

$$z_B(e^{-\beta}) = \frac{e^{-\beta} + e^{-2\beta}}{(1 - e^{-\beta})^3}, \quad (18)$$

and

$$z_F(e^{-\beta}) = \frac{e^{-\frac{4}{3}\beta}}{(1 - e^{-\beta})^3}. \quad (19)$$

Hence, the model analysis for the partition function that is given in nuclear physics for the search for a QGP can be generalized to study the conformal fields such as pure Yang-Mills theory and $\mathcal{N} = 4$ super-symmetry Yang-Mills theory. The understanding of the partition function with various internal structures can shed light on a new phase of matter beyond the QGP. This might also be useful in constructing new models to explore new physics such as the searching for a dark matter.

III. INVARIANCE MEASURE

The invariance measure is essential to projecting the state with a specific internal structure. The invariance Haar measure reads

$$\int d\mu(g) = \frac{1}{N_c!}\left(\frac{1}{2\pi}\right)^{N_c} \times \int_{-\pi}^{\pi} \left[\prod_{m>n} 2\sin^2\left(\frac{\theta_n - \theta_m}{2}\right)\right] \prod_{k=1}^{N_c} d\theta_k,$$
$$= \frac{1}{N_c!}\left(\frac{1}{2\pi}\right)^{N_c} \int_{-\pi}^{\pi} \left[\prod_{m>n} 2\sin^2\left(\frac{\theta_n - \theta_m}{2}\right)\right] \times \prod_{k=1}^{N_c} \left[2\pi\delta\left(\sum_{i=1}^{N_c}\theta_i\right)\right] d\theta_k, \quad (20)$$

for $\mathrm{U}(N_c)$ and $\mathrm{SU}(N_c)$ group representations, respectively. The Haar invariance measure for the system with homogeneous and uniform distribution over the Fourier color variables, $|\theta_i| \leqslant \pi$, is written for $\mathrm{SU}(N_c)$ as

$$\int d\mu(g) = \frac{1}{N_c!}\left(\frac{1}{2\pi}\right)^{N_c-1} \left(2^{(N_c^2 - N_c)/2}\right) \prod_{k=1}^{N_c-1} \int_{-\pi}^{\pi} d\theta_k \times \exp\left[\frac{1}{2}\sum_{n=1}^{N_c}\sum_{m=1}^{N_c} \ln\sin^2\left(\frac{\theta_n - \theta_m}{2}\right)\right]\Bigg|_{n\neq m}. \quad (21)$$

The Vandermonde determinant, which appears in the measure, contributes to the action as an additional potential term. The Vandermonde effective potential term is soft when the color eigenvalues in the stationary condition distribute uniformly over the entire circle $|\theta_i| \leqslant \pi$. However, this will not be the case for the extreme condition in particular when the color eigenvalues are distributed in a narrow domain $|\theta_i| \ll \pi$. Under this condition, the Vandermonde effective potential becomes virtually singular, and the action must be regulated in a proper way in order to remove the Vandermonde determinant divergence. The regulated Haar measure in the extreme conditions becomes

$$\int d\mu(g) = \frac{1}{N_c!}\left(\frac{1}{2\pi}\right)^{N_c} \int \prod_{k=1}^{N_c} \left[\prod_{m>n} (\theta_n - \theta_m)^2\right] \times 2\pi\delta\left(\sum_{i=1}^{N_c}\theta_i\right) d\theta_k. \quad (22)$$

This version for the invariance measure accommodates the canonical ensemble in the hot medium. The similar results can be verified for the theoretic group $\mathrm{U}(N_c)$ representation.

IV. FUNDAMENTAL PARTICLES: SPECTRAL DENSITY METHOD

The canonical ensemble for fundamental particles in the $\mathrm{U}(N_c)$ or $\mathrm{SU}(N_c)$ representation, confined in a spherical cavity and obeying Maxwell-Boltzmann statistics, reads

$$Z(\beta) = \int d\mu(g) \exp\left[\mathcal{D}_d \int_V d^3r \int \frac{d^3p}{(2\pi)^3} \mathcal{G}_{\mathrm{fun}}(\theta) e^{-\beta E(p,r)}\right], \quad (23)$$

where $\mathcal{D}_d$ is the single-particle degeneracy due to the degree of freedom, which is not specified explicitly in the calculation such as the spin multiplicity. The trace over the color degree of freedom for particles and their antiparticle partners in the

fundamental representation is given by

$$\mathcal{G}_{\rm fun}(\theta) = \frac{1}{N_c}{\rm tr}(\mathbf{R}_{\rm fun}(g) + \mathbf{R}^*_{\rm fun}(g)) = \frac{2}{N_c}\sum_{i=1}^{N_c}\cos\theta_i. \quad (24)$$

The sum of states for a gas of particles confined in a spherical cavity is calculated as

$$\lambda = \mathcal{D}_d\int_V d^3r\int\frac{d^3p}{(2\pi)^3}e^{-\beta E(p,r)} = \mathcal{D}_d\int\frac{Vd^3p}{(2\pi)^3}e^{-\beta E(p,r)}. \quad (25)$$

The color-singlet state for the canonical partition function for a gas of fundamental particles and antiparticles is projected as

$$Z(\lambda) = \frac{1}{N_c!}2^{(N_c^2-N_c)/2}\prod_{k=1}^{N_c}\int\frac{d\theta_k}{2\pi} \times\exp\left[\frac{1}{2}\sum_{n=1}^{N_c}\sum_{m=1}^{N_c}\ln\sin^2\left(\frac{\theta_n-\theta_m}{2}\right)\Bigg|_{n\neq m} + \lambda\frac{1}{N_c}{\rm tr}(\mathbf{R}_{\rm fun}(g)+\mathbf{R}^*_{\rm fun}(g))\right]. \quad (26)$$

The multiple integrations in the partition function are evaluated using the steepest-descent method. The partition function is reduced to

$$Z(\lambda) = \frac{1}{N_c!}2^{(N_c^2-N_c)/2}\exp\left[\frac{1}{2}\sum_{n=1}^{N_c}\sum_{m=1}^{N_c}\ln\sin^2 \times\left(\frac{\overline{\theta}_n-\overline{\theta}_m}{2}\right)\Bigg|_{n\neq m} + 2\lambda\frac{1}{N_c}\sum_{n=1}^{N_c}\cos\overline{\theta}_n\right]. \quad (27)$$

The saddle points $\overline{\theta}_n$ are determined by the stationary condition

$$2\lambda\frac{1}{N_c}\sin\overline{\theta}_i = \sum_{n\neq i}^{N_c}\cot\left|\frac{\overline{\theta}_i-\overline{\theta}_n}{2}\right|. \quad (28)$$

The above equation turns out to be an eigenvalue problem for the large N_c limit, and the saddle points are determined by the eigenvalues. Hereinafter, we introduce $\lambda = N_c^2\widetilde{\lambda}$. The stationary condition becomes

$$2\widetilde{\lambda}\sin\overline{\theta}_i = \frac{1}{N_c}\sum_{n\neq i}^{N_c}\cot\left|\frac{\overline{\theta}_i-\overline{\theta}_n}{2}\right|. \quad (29)$$

The solution for the stationary condition that is given by Eq. (29) depends basically on the value of the thermal running parameter $\widetilde{\lambda}$. It can be shown numerically that the solution of $\overline{\theta}_i$ for $\widetilde{\lambda}\leqslant\frac{1}{2}$ is distributed uniformly over the entire circle range $|\overline{\theta}_i|\leqslant\pi$ and $|\overline{\theta}_i-\overline{\theta}_j|\leqslant\frac{2\pi}{N_c}$. However, this solution ceases to exist for the full range $|\theta_i|\leqslant\pi$ when the thermal running parameter $\widetilde{\lambda}$ becomes relatively large and runs over the range $\widetilde{\lambda}>\frac{1}{2}$. The eigenvalues θ_i turn out to be distributed uniformly only over the incomplete range $|\theta_i|\leqslant\theta_c<\pi$. This means that the solution for $\widetilde{\lambda}>\frac{1}{2}$ becomes problematic, and the action must be regulated thoroughly when θ_c becomes small. When that action is regulated, another analytical solution may emerge, and the change in the analytical solution characteristic becomes responsible for the existence of the phase transition.

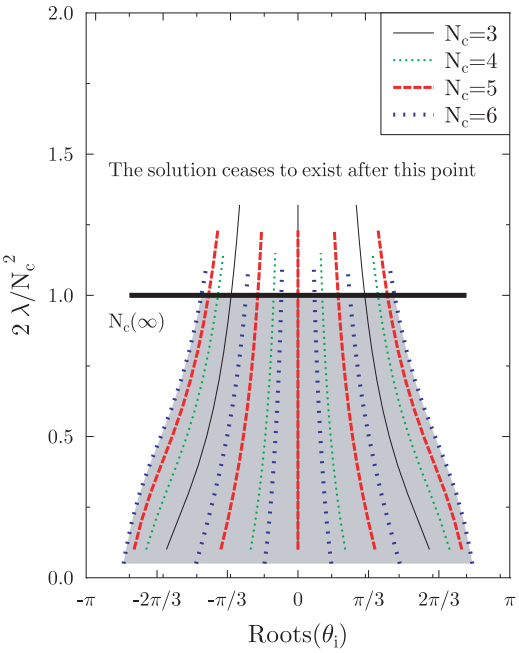

FIG. 1. (Color online) Saddle points solution for particles in the fundamental representation. The saddle points are distributed uniformly over the range $|\theta_i|\leqslant\pi$ for a parameter that runs over the range $\lambda\leqslant\lambda_0$. The numerical solution shows that saddle points cease to exist when the thermal running parameter λ exceeds the value $\frac{\lambda_0}{N_c^2}=\frac{1}{2}$ in the large N_c limit.

The numerical solution for the set of stationary conditions which are given by either Eq. (28) or Eq. (29) versus the thermal running parameter $\widetilde{\lambda}$ for various color numbers N_c with group symmetry U(N_c) is displayed in Fig. 1. The resemblance between t'Hooft coupling $\lambda_{\rm WS}=g^2_{\rm YM}N_c$ and the thermal running parameter $\widetilde{\lambda}=\lambda/N_c^2$ is given by the relation $g^2_{\rm YM}N_c=1/\widetilde{\lambda}$. The weak t'Hooft coupling corresponds to the high-lying thermal running parameter $\widetilde{\lambda}\geqslant\widetilde{\lambda}_{\rm crit}$, while the strong t'Hooft coupling is given by the low-lying $\widetilde{\lambda}\leqslant\widetilde{\lambda}_{\rm crit}$. The Vandermonde determinant contributes to the effective action. Consequently, the saddle point locations are computed using the stationary conditions where the Vandermonde determinant is included explicitly in the action as an additional potential term. It is shown numerically that the saddle points are distributed uniformly over the interval $-\pi\leqslant\theta_i\leqslant\pi$ for the low-lying thermal running parameter $\widetilde{\lambda}$ (i.e., strong t'Hooft coupling). The characteristic distribution of the saddle points is found uniform for the small $\widetilde{\lambda}$ even for a small number of colors $N_c=2$. This distribution becomes more dominant over a narrower range $|\theta_i|\leqslant\theta_0<\pi$ as $\widetilde{\lambda}$ increases and approaches the critical value. However, the numerical calculation shows that the saddle points cease to exist when the thermal running parameter $\widetilde{\lambda}$ exceeds a critical value just above $\widetilde{\lambda}\geqslant\frac{1}{2}$ (i.e., weak t'Hooft coupling). For example, in the case of $N_c=3$, the saddle points cease to exist when the thermal running parameter exceeds the value $\widetilde{\lambda}>\frac{1.32}{2}$. Furthermore, it is found that when the number of colors N_c increases, the saddle points cease to exist at smaller value of $\widetilde{\lambda}$. For example, for

$N_c = 5$, the solution for these points does not exist beyond the critical point $\widetilde{\lambda} > \frac{1.23}{2}$. In the limit of large N_c, the solution for saddle points breaks down just above the point $\widetilde{\lambda} = \frac{1}{2}$. The Vandermonde term diverges when the color saddle points become more dominant in a tiny domain around the origin. This divergence breaks the solution badly when these saddle points congregate and converge to the origin. It is found that the saddle points cease to exist when $\widetilde{\lambda} > \widetilde{\lambda}_{\rm crit}$. This implies that the stationary conditions must break down and the action must be regulated in a proper way and a new set of conditions must be formed. This proves the existence of the phase transition in the system.

In the large-N_c limit, Gross and Witten solved these equations in the case of two-dimensional U(N_c) lattice gauge theory following Brezin *et al.* [8] by introducing the spectral density of eigenvalues. Brezin *et al.* [8] have shown that the functional integrals in the large-N_c limit can be calculated by steepest-descent methods. In this limit, a particular configuration totally dominates the functional integral. The stationary equations in this limit can be replaced by their continuum version by introducing a nondecreasing function

$$\begin{aligned} \overline{\theta}_n &= \theta(x), \\ x &= \frac{n}{N_c}, \\ n &= 1, \ldots, N_c. \end{aligned} \tag{30}$$

Hence, the stationary condition becomes

$$2\widetilde{\lambda} \sin\theta(x_0) = \mathrm{P}\int_0^1 dy \cot\left(\frac{\theta(x_0) - \theta(y)}{2}\right), \tag{31}$$

where P refers to the principle part of the integral. By introducing the density of states

$$\rho(\theta) = \frac{dx}{d\theta} \geqslant 0, \tag{32}$$

and the constraint

$$\int_0^1 dx = \int_{-\theta_c}^{\theta_c} d\theta\, \rho(\theta) = 1, \tag{33}$$

where $|\theta_c| \leqslant \pi$. Hence the stationary condition becomes

$$2\widetilde{\lambda} \sin\theta = \mathrm{P}\int_{-\theta_c}^{\theta_c} d\theta' \rho(\theta') \cot\left(\frac{\theta - \theta'}{2}\right). \tag{34}$$

A. Highly thermal excited matter: $\frac{\lambda}{N_c^2} \geqslant \frac{1}{2}$

The solution of density of eigenvalues in the large N_c limit in the U(N_c) representation has attracted much attention recently. Although the solution for the spectral density of eigenvalues is difficult in the realistic situation, the approximate solution for this density has been derived for some simple specific cases for fundamental and adjoint representations in the limit of large N_c. In the following, we review the partition function using the given solution of the spectral density of color eigenvalues. Then in Sec. V we introduce another approximation to evaluate the same partition function. The other method is to approximate the resultant integral to the Gaussian-like integral, and this approximation seems to be more efficient when more complicated situations are involved. The two methods have been shown to reproduce the same results for the large thermal running parameter $\widetilde{\lambda} \geqslant \widetilde{\lambda}_0$ and $\widetilde{\lambda} = \lambda/N_c^2$.

The first method for evaluating the canonical ensemble is based essentially on the stationary equation solution for the density of color eigenvalues, and it is written for $\widetilde{\lambda} \geqslant \frac{1}{2}$ as

$$\rho(\theta) = \frac{2}{\pi}\widetilde{\lambda} \cos\frac{\theta}{2}\left[\sin^2\left(\frac{\theta_c}{2}\right) - \sin^2\left(\frac{\theta}{2}\right)\right]^{1/2}, \tag{35}$$

where

$$\sin^2\left(\frac{\theta_c}{2}\right) = \frac{1}{2\widetilde{\lambda}} \leqslant 1, \quad \frac{\lambda}{N_c^2} = \widetilde{\lambda} \geqslant \frac{1}{2}. \tag{36}$$

The color eigenvalues are not distributed uniformly over the entire color circle range $-\pi$ to π. Instead, in this solution, they are distributed over only a narrow interval $|\theta_i| \leqslant \theta_c$, where $|\theta_c| < \pi$. The canonical partition function after weighting the color density of eigenvalues becomes

$$\begin{aligned} Z(\lambda) = C \exp\Bigg[&\frac{1}{2}N_c^2 \int_{-\theta_c}^{\theta_c} d\theta \rho(\theta) \int_{-\theta_c}^{\theta_c} d\theta'\, \rho(\theta') \\ &\times \ln\sin^2\left(\frac{\theta - \theta'}{2}\right) + 2N_c^2\widetilde{\lambda}\int_{-\theta_c}^{\theta_c} d\theta\, \rho(\theta)\cos\theta\Bigg], \end{aligned} \tag{37}$$

where the preexponential constant is given by $C = \frac{2^{(N_c^2 - N_c)/2}}{N_c!}$. Under this stationary approximation, the canonical ensemble function is calculated as

$$\begin{aligned} Z(\lambda) &\cong \exp\left[2N_c^2\widetilde{\lambda} - \frac{N_c^2}{2}\ln\left(2\widetilde{\lambda}N_c^2\right) + \frac{N_c^2}{2}\ln N_c^2 - \frac{3}{4}N_c^2\right] \\ &\cong \left(\frac{1}{2\widetilde{\lambda}}\right)^{\frac{N_c^2}{2}} \exp\left(2N_c^2\widetilde{\lambda} - \frac{3}{4}N_c^2\right), \quad \text{where} \quad \widetilde{\lambda} \geqslant \frac{1}{2}. \end{aligned} \tag{38}$$

Hence, the asymptotic large running thermal coupling solution reads

$$Z(\lambda) \equiv \left(\frac{N_c^2}{2\lambda}\right)^{\frac{N_c^2}{2}} \exp\left(2\lambda - \frac{3}{4}N_c^2\right). \tag{39}$$

B. Diluted and relatively cold matter: $\frac{\lambda}{N_c^2} \leqslant \frac{1}{2}$

At low temperatures, the stationary condition for $\widetilde{\lambda} \leqslant \frac{1}{2}$ produces the following density of color eigenvalues:

$$\rho(\theta) = \frac{1}{2\pi}(1 + 2\widetilde{\lambda}\cos\theta), -\pi \leqslant \theta \leqslant \pi. \tag{40}$$

The chemical potential for the total particle number due to the rotated U$(1)_B$ symmetry is not considered here, and it is left for the forthcoming work. In the large N_c limit, the system is assumed to be highly compressed due to the large number of colors, but this is not the case for a finite number of colors such as QCD. In this case, the system is identified as a compressed one when the chemical potential for particle numbers becomes

relatively large. The density of eigenvalues given by Eq. (40) for $\frac{\lambda}{N_c^2} \leqslant \frac{1}{2}$ produces the partition function

$$Z(\lambda) = e^{N_c^2 \widetilde{\lambda}^2} = e^{\lambda^2/N_c^2}. \tag{41}$$

The occurrence of such a phase transition from the diluted and relatively cold matter (i.e., low-lying phase) to the highly thermal excited matter (i.e., high-lying phase) would not mean that the large-N_c theory does not confine. The highly excited thermal matter can be interpreted as an exotic hadronic phase dominated by the Hagedorn states. In the lattice theory, this would imply that the weak and strong λ_{WS} coupling is not described by the same analytic functions [7]. The weak and strong λ_{WS} are analogous to the large and small thermal running parameters λ/N_c^2, respectively. For the finite N_c, one could continue from the strong to the weak coupling. However, one would expect to see a sign of phase transition for large enough N_c (i.e., in the limit $N_c = \infty$) whose manifestation would be a sharp transition at $\lambda_{\mathrm{WS}} \approx \lambda_{\mathrm{WS(crit)}}$ from the weak-coupling to the strong-coupling behavior. As in the lattice theory, in the thermal and dense QCD, the strong- and weak-coupling transition is analogous to the phase transition from the discrete low-lying mass spectrum particles to the highly excited and massive Hagedorn states (i.e., continuous high-lying mass spectrum). The Hagedorn states are the color-singlet (confined) hadronic states. This phase should not be interpreted as an immediate deconfined phase. The critical Gross-Witten point is the threshold point for the Hagedorn states to emerge in the system. The deconfined phase transition can either take place immediately when unstable Hagedorn states are produced in the system or as a subsequent process when the metastable Hagedorn phase undergoes a true deconfined phase transition.

V. FUNDAMENTAL PARTICLES: GAUSSIAN-LIKE SADDLE POINTS METHOD

We introduce a novel alternative method for calculating the partition function and finding the critical point for the phase transition. This method accommodates the sophisticated physical problems such as the internal color structure for a gas consisting of particles with various statistics species in a specific space boundary and with more complicated color-flavor correlations and chiral symmetries. It may be useful in finding the equation of state for physics beyond QCD.

A. Highly thermal excited matter: $\frac{\lambda}{N_c^2} \geqslant \frac{1}{2}$

In the realistic physical situation, more calculations are involved. It becomes more difficult to calculate the density of color eigenvalues under certain conditions, in particular when the color eigenvalues populate a tiny interval $|\theta_c| \ll 1$ under extreme conditions. The canonical ensemble has a special importance for the thermal running parameter $\widetilde{\lambda}$ over the range $\widetilde{\lambda} > \frac{1}{2}$, and it corresponds to the hot hadronic matter. It is relevant to the relativistic heavy ion collisions studied at the BNL Relativistic Heavy Ion Collider (RHIC) and CERN Large Hadron Collider (LHC), and to cosmology such as the physics of the early universe.

In the following, we demonstrate a method for calculating the partition function for the coupling parameter $\frac{\lambda}{N_c^2} \geqslant \widetilde{\lambda}_0$ (in our case, $\widetilde{\lambda}_0 = \widetilde{\lambda}_{\mathrm{crit}} = \frac{1}{2}$). The integral over the color invariance measure is approximated to the Gaussian-like multi-integrals around the saddle points. The color saddle points are dominant in the narrow interval $|\theta| \leqslant \theta_c$ around the origin, where $|\theta_c| \ll 1$. Since the saddle points are populated in a small domain, we can safely approximate all the saddle points to be located near the origin. The Vandermonde potential does not appear in the action, but instead the invariance measure appears as a prefactor power function of the exponential in the Gaussian integral. The integration of the resultant multi-Gaussian integrals is straightforward. We call this method the Gaussian-like saddle points (GSP) method. In this limit, the invariance Haar measure is approximated to

$$\int_{\mathrm{U}(N_c)} d\mu(g)_{\mathrm{sp}} \approx \prod_{k=1}^{N_c} \int d\theta_k \frac{1}{N!} \left(\frac{1}{2\pi}\right)^{N_c} \left[\prod_{n>m}^{N_c} (\theta_n - \theta_m)^2\right], \tag{42}$$

and

$$\int_{\mathrm{SU}(N_c)} d\mu(g)_{\mathrm{sp}} \approx \frac{1}{N!} \left(\frac{1}{2\pi}\right)^{N_c} \prod_{k=1}^{N_c} \int d\theta_k \times \left[\prod_{n>m}^{N_c} (\theta_n - \theta_m)^2\right] 2\pi\,\delta\left(\sum_i^{N_c} \theta_i\right), \tag{43}$$

for $\mathrm{U}(N_c)$ and $\mathrm{SU}(N_c)$ symmetries, respectively. The partition ensemble is given by

$$\begin{aligned} Z(\lambda) &= \int d\mu(g) \exp\left[\frac{\lambda}{N_c} \mathrm{tr}_c(\mathbf{R}_{\mathrm{fun}}(g) + \mathbf{R}^*_{\mathrm{fun}}(g))\right] \\ &= \int d\mu(g) \exp\left(2\frac{\lambda}{N_c} \sum_{n=1}^{N_c} \cos\theta_n\right). \end{aligned} \tag{44}$$

When the thermal running parameter becomes relatively large and covers the range $\widetilde{\lambda} \geqslant \widetilde{\lambda}_{\mathrm{(II)min}}$, the partition ensemble is approximated around the saddle points, which become dominant in a small range, as follows:

$$\begin{aligned} &Z(\lambda) \approx Z_{\mathrm{(II)}}(\lambda), \text{ (for } \widetilde{\lambda} \text{ in the range } \widetilde{\lambda} \geqslant \widetilde{\lambda}_{\mathrm{(II)min}}), \\ &Z_{\mathrm{(II)}}(\lambda) = \int d\mu(g)_{\mathrm{sp}} \exp\left(2N_c\widetilde{\lambda} \sum_{n=1}^{N_c} \cos\theta_n\right) \\ &\qquad \approx e^{2N_c^2\widetilde{\lambda}} \int d\mu(g)_{\mathrm{sp}} \exp\left[-\frac{1}{2}(2N_c\widetilde{\lambda}) \sum_{n=1}^{N_c} \theta_n^2\right], \end{aligned} \tag{45}$$

where $\lambda = N_c^2\widetilde{\lambda}$.

The subscript (II) denotes the solution for the asymptotic large $\widetilde{\lambda}$ while the subscript (I) will denote the solution for the asymptotic small $\widetilde{\lambda}$. In the case of $\mathrm{U}(N_c)$ symmetry, the partition function becomes

$$\begin{aligned} Z_{\mathrm{(II)}}(\lambda) = \frac{1}{N_c!} \left(\frac{1}{2\pi}\right)^{N_c} \frac{e^{2N_c^2\widetilde{\lambda}}}{(2N_c\widetilde{\lambda})^{\frac{N_c^2}{2}}} \left(\prod_{k=1}^{N_c} \int_{-x_0}^{x_0} dx_k\right) \\ \times \left(\prod_{n>m}^{N_c} (x_n - x_m)^2\right) e^{-\frac{1}{2}\sum_{n=1}^{N_c} x_n^2}. \end{aligned} \tag{46}$$

The Gaussian-like multi-integrals are evaluated using the standard formula

$$\left(\prod_{k=1}^{N_c}\int_{-\infty}^{\infty}dx_k\right)\left(\prod_{n>m}^{N_c}(x_n-x_m)^2\right)\exp\left[-\frac{1}{2}\sum_{n=1}^{N_c}x_n^2\right] \equiv (2\pi)^{N_c/2}\prod_{n=1}^{N_c}n!. \tag{47}$$

Hence, the partition function is evaluated as

$$Z_{(\mathrm{II})}(\lambda)\cong\left(\frac{1}{2N_c\widetilde{\lambda}}\right)^{\frac{N_c^2-1}{2}}e^{2N_c^2\widetilde{\lambda}}\left[\frac{1}{(2\pi)^{\frac{N_c}{2}-1}}\frac{1}{N_c!}\frac{1}{\sqrt{2\pi N_c}}\prod_{n=1}^{N_c}n!\right], \quad (\text{for}\ \widetilde{\lambda}\geqslant\widetilde{\lambda}_{(\mathrm{II})\min}), \tag{48}$$

and

$$Z_{(\mathrm{II})}(\lambda)\cong\left(\frac{1}{2N_c\widetilde{\lambda}}\right)^{\frac{N_c^2}{2}}e^{2N_c^2\widetilde{\lambda}}\left[\frac{1}{(2\pi)^{\frac{N_c}{2}}}\frac{1}{N_c!}\prod_{n=1}^{N_c}n!\right], \quad (\text{for}\ \widetilde{\lambda}\geqslant\widetilde{\lambda}_{(\mathrm{II})\min}), \tag{49}$$

for SU(N_c) and U(N_c) symmetries, respectively. To compare the results of the present method with those derived using the spectral density method given by Eq. (39), the partition function for U(N_c) is written as

$$Z_{(\mathrm{II})}(\lambda)=C_{N_c}\left(\frac{1}{2\widetilde{\lambda}}\right)^{\frac{N_c^2}{2}}e^{2N_c^2\widetilde{\lambda}},\quad(\text{for}\ \widetilde{\lambda}\geqslant\widetilde{\lambda}_{(\mathrm{II})\min}), \tag{50}$$

where the prefactor constant is given by

$$C_{N_c}=N_c^{-\frac{N_c^2}{2}}\left[\frac{1}{(2\pi)^{\frac{N_c}{2}}}\frac{1}{N_c!}\prod_{n=1}^{N_c}n!\right]. \tag{51}$$

Using Stirling's approximation $\ln n!\approx n\ln n-n+\frac{1}{2}\ln n+\frac{1}{2}\ln 2\pi$, the prefactor given by Eq. (51) is simplified to

$$\begin{aligned}\ln C_{N_c}&=-\frac{N_c^2}{2}\ln N_c-\frac{N_c(N_c+1)}{2}-\frac{1}{2}\sum_{n=1}^{N_c}\ln n+\sum_{n=1}^{N_c}n\ln n\\&\approx-\frac{N_c^2}{2}\ln N_c-\frac{N_c(N_c+1)}{2}-\frac{1}{2}\int_1^{N_c}dn\ln n\\&\quad+\int_1^{N_c}dn\,n\ln n\\&=-\frac{3}{4}N_c^2-\frac{1}{2}N_c\ln N_c.\end{aligned} \tag{52}$$

The above expression simplifies the partition function to

$$\lim_{N_c\to\text{large}}Z_{(\mathrm{II})}(\lambda)\approx\left(\frac{1}{2\widetilde{\lambda}}\right)^{N_c^2/2}\exp\left[2N_c^2\widetilde{\lambda}-\frac{3}{4}N_c^2\right], \quad(\text{for}\ \widetilde{\lambda}\geqslant\widetilde{\lambda}_{(\mathrm{II})\min}). \tag{53}$$

The above solution is the approximate solution over the range

$$\widetilde{\lambda}\geqslant\widetilde{\lambda}_{\mathrm{crit}}\geqslant\widetilde{\lambda}_{(\mathrm{II})\min},\quad\text{where}\quad\widetilde{\lambda}_{\mathrm{crit}}=\tfrac{1}{2}. \tag{54}$$

It is in agreement with Eq. (39). This means that the GSP method is consistent with the spectral density method developed by Brezin *et. el.* [8] for the energy range $\frac{\lambda}{N_c^2}\geqslant\frac{1}{2}$.

B. Diluted and relatively cold matter: $\frac{\lambda}{N_c^2}\leqslant\frac{1}{2}$

The Fourier color angles are distributed uniformly over the entire color circle range $-\pi\leqslant\theta_i\leqslant\pi$ in the low-lying energy domain $\frac{\lambda}{N_c^2}\leqslant\frac{1}{2}$ as

$$Z(\lambda)\approx Z_{(\mathrm{I})}(\lambda),\quad(\text{for}\ \widetilde{\lambda}\ \text{in the range}\ \widetilde{\lambda}\leqslant\widetilde{\lambda}_{(\mathrm{I})\max}),$$
$$Z_{(\mathrm{I})}(\lambda)=\int_{-\pi}^{\pi}d\mu(g)\exp\left[\lambda\frac{1}{N_c}\mathrm{tr}(\mathbf{R}(g)+\mathbf{R}^*(g))\right]. \tag{55}$$

The partition function is expanded with respect to orthogonal bases over $\frac{\lambda}{N_c^2}\leqslant\widetilde{\lambda}_{(\mathrm{I})\max}$ and reads

$$\begin{aligned}Z_{(\mathrm{I})}(\lambda)&=\int_{-\pi}^{\pi}d\mu(g)\exp[N_c\widetilde{\lambda}\,\mathrm{tr}(\mathbf{R}(g)+\mathbf{R}^*(g))]\\&=\int_{-\pi}^{\pi}d\mu(g)\sum_{i=1}^{\infty}\sum_{j=1}^{\infty}\frac{1}{i!}(N_c\widetilde{\lambda}\,\mathrm{tr}\,\mathbf{R}(g))^i\\&\quad\times\frac{1}{j!}(N_c\widetilde{\lambda}\,\mathrm{tr}\,\mathbf{R}^\dagger(g))^j.\end{aligned} \tag{56}$$

Using the orthogonal relations over the U(N_c) bases, the partition function is reduced to [7]

$$\begin{aligned}Z_{(\mathrm{I})}(\lambda)&=\int_{-\pi}^{\pi}d\mu(g)\sum_{i=1}^{\infty}\left(\frac{1}{i!}\right)^2(N_c\widetilde{\lambda})^{2i}(\mathrm{tr}\,\mathbf{R}(g))^i(\mathrm{tr}\,\mathbf{R}^\dagger(g))^i\\&=\sum_{i=1}^{\infty}\frac{1}{i!}\left(N_c^2\widetilde{\lambda}^2\right)^i=e^{(N_c^2\widetilde{\lambda}^2)}\\&=e^{\left(\frac{\lambda^2}{N_c^2}\right)}\quad(\text{over the range}\ \widetilde{\lambda}\leqslant\widetilde{\lambda}_{\mathrm{crit}}\leqslant\widetilde{\lambda}_{(\mathrm{I})\max}),\end{aligned} \tag{57}$$

where $\widetilde{\lambda}_{\mathrm{crit}}=\frac{1}{2}$ and $\widetilde{\lambda}_{(\mathrm{I})\max}<1$.

The canonical ensemble with the Maxwell-Boltzmann statistics single-particle partition function reads

$$\begin{aligned}Z_{(\mathrm{I})}(\beta)&=\exp\left[\frac{1}{N_c^2}(2j+1)^2\left(\int\frac{V_{S^3}d^3p}{(2\pi)^3}e^{-\beta E}\right)^2\right]\\&=\exp\left[\frac{(2j+1)^2V_{S^3}^2}{\pi^4N_c^2\beta^6}\right]\\&\to\exp\left[\frac{(2j+1)^2V_{S^3}^2T^6}{\pi^4N_c^2}\right]\end{aligned} \tag{58}$$

for an ideal gas of fundamental particles confined in a spherical cavity in the three-dimensional space, where V_{S^3} is the cavity volume in the three-dimensional space. The free energy approaches the same value as in the free theory for low temperature, whereas we have mesonic-like and baryonic-like matter in the dilute hadronic phase. The canonical ensemble in this range does not produce an explosive phase transition. The physics for the two phases will be discussed in detail when we present the microcanonical ensemble as a density of states in Sec. VIII.

We display the function $\ln Z(\lambda)$ versus $\frac{\lambda}{N_c^2}$ for the gas of fundamental particles in the color-singlet state with various numbers of colors N_c in Figs. 2 and 3. The logarithm of the canonical ensemble in the domain $\frac{\lambda}{N_c^2}\geqslant\frac{1}{2}$ is displayed in Fig. 2. The highly thermal excited partition parameter $\frac{\lambda}{N_c^2}\geqslant\frac{\lambda_0}{N_c^2}$

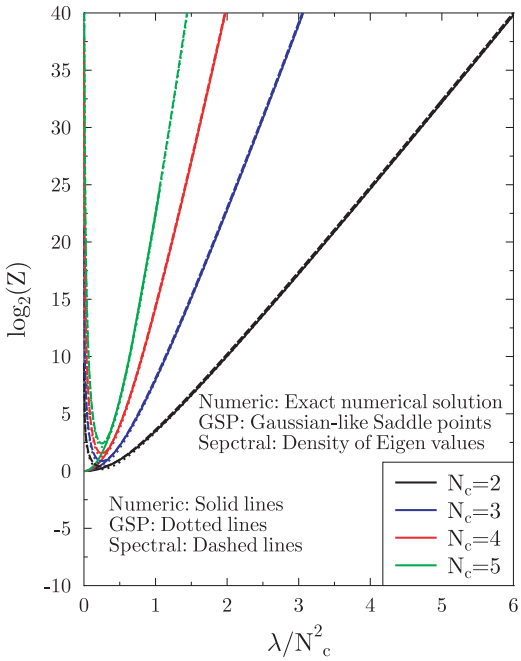

FIG. 2. (Color online) Density of states for the color-singlet fireballs (i.e., Hagedorn states) vs the thermal running parameter $\frac{\lambda}{N_c^2}$ with various color numbers N_c. The high-lying solution is calculated for a bag consisting of fundamental particles with a $\frac{\lambda}{N_c^2}$ over the range $\frac{\lambda}{N_c^2} \geqslant \frac{1}{2}$. The results for the high-lying solution calculated using the spectral density method of Brezin *et al.* [8] in the limit of large color number N_c and the results obtained using the GSP method are displayed together with the exact numerical solution. The high-lying solutions for both methods and their extrapolations to $\frac{\lambda}{N_c^2} \leqslant (\frac{\lambda}{N_c^2})_{\text{crit}}$ are compared with the exact numerical solution.

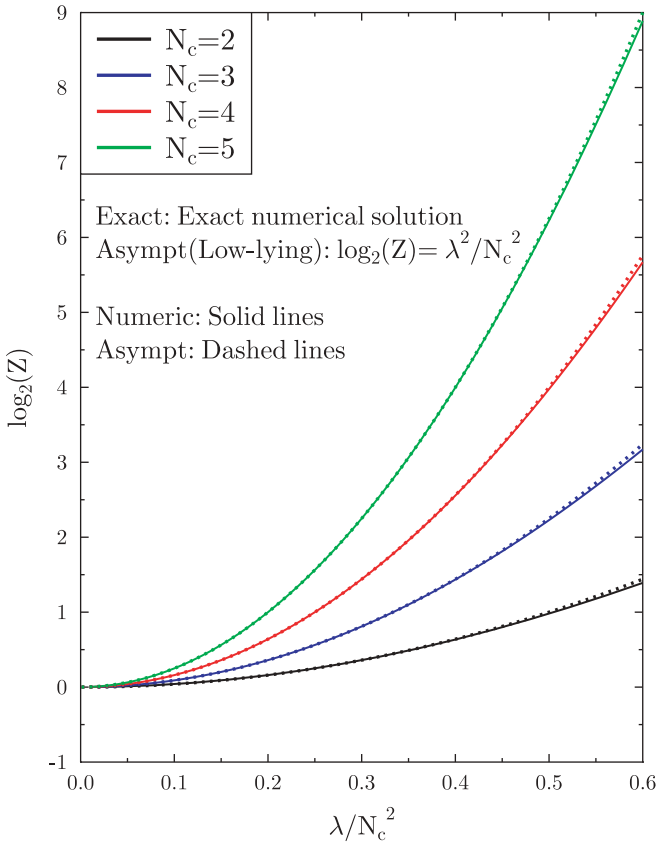

FIG. 3. (Color online) Density of states for the color-singlet fireballs (i.e., Hagedorn states) vs the thermal running parameter $\frac{\lambda}{N_c^2}$ for various color numbers N_c. The low-lying density of states is calculated for bags consisting of fundamental particles and with a thermal running parameter $\frac{\lambda}{N_c^2}$ over the range $\frac{\lambda}{N_c^2} \leqslant \frac{1}{2}$. The results derived by the orthogonal expansion given by Eqs. (56) and (57) are displayed together with the exact density of states evaluated numerically.

corresponds to the weak t'Hooft coupling, and it describes a hot gas. The partition function in the large $\widetilde{\lambda}$ regime is evaluated exactly by the exact numerical integration over the Fourier colors over the entire circle range $(-\pi \leqslant \theta_i \leqslant \pi)$. The results for the numerical integration are compared with the solution for the spectral density method introduced by Brezin *et. el.* [8] as well as the solution of the GSP method. The two methods are found to produce the same results, and they fit the exact numerical calculations when the thermal partition parameter exceeds the critical value $\frac{\lambda}{N_c^2} \geqslant \frac{1}{2}$. In the regime below the critical point $\widetilde{\lambda}_0 = \frac{\lambda_0}{N_c^2}$, the two methods deviate from the exact numerical one, and this deviation increases as $\frac{\lambda}{N_c^2}$ decreases below the critical thermal running parameter $\frac{\lambda_0}{N_c^2}$. The largest discrepancy is found for the small number of colors $N_c = 2$. Even though the spectral density method was originally derived for the large $N_c \to \infty$ limit, the solution is found satisfactory for a finite number of colors even for a relatively small one, $N_c = 2$. Furthermore, the GSP method is found to produce precisely the asymptotic solution for the large $N_c \to \infty$ limit, although it was originally derived for a finite number of colors. However, the extrapolations of both methods to $\frac{\lambda}{N_c^2} < \frac{\lambda_0}{N_c^2}$ evidently fail to reproduce the exact numerical results in the low-lying energy regime, in particular when $\frac{\lambda}{N_c^2}$ becomes sufficiently small, $\frac{\lambda}{N_c^2} \ll \frac{1}{2}$. The failure of the large energy extrapolation to reproduce the correct asymptotic low-lying energy solution indicates the existence of a possible phase transition near the point $\frac{\lambda_0}{N_c^2} = \frac{1}{2}$. This deviation from the exact numerical solution increases significantly as $\frac{\lambda}{N_c^2}$ decreases below the critical one $\frac{\lambda_0}{N_c^2}$. The low-lying energy solution for the small thermal running parameter domain $\frac{\lambda}{N_c^2} \leqslant \frac{1}{2}$ with various color numbers $N_c = 2$, 3, 4, and 5 is displayed in Fig. 3. The exact numerical solution is compared with the asymptotic analytical solution $\ln Z = \lambda^2/N_c^2$ for the low-lying energy solution which is derived for the small thermal running parameter $\frac{\lambda}{N_c^2}$. The asymptotic analytical low-lying energy solution matches the exact numerical one in the range $\frac{\lambda}{N_c^2} \leqslant \frac{1}{2}$. This agreement between the low-lying energy solution and the exact numerical one is found satisfactory even for a small color number, $N_c = 2$. The critical point $\widetilde{\lambda}_{\text{crit}} = \lambda_{\text{crit}}/N_c^2$ for the phase transition from the asymptotic low-lying energy solution for the range $\frac{\lambda}{N_c^2} \leqslant \frac{\lambda_0}{N_c^2}$ to the asymptotic high-lying energy solution for the range $\frac{\lambda}{N_c^2} \geqslant \frac{\lambda_0}{N_c^2}$ is determined when both

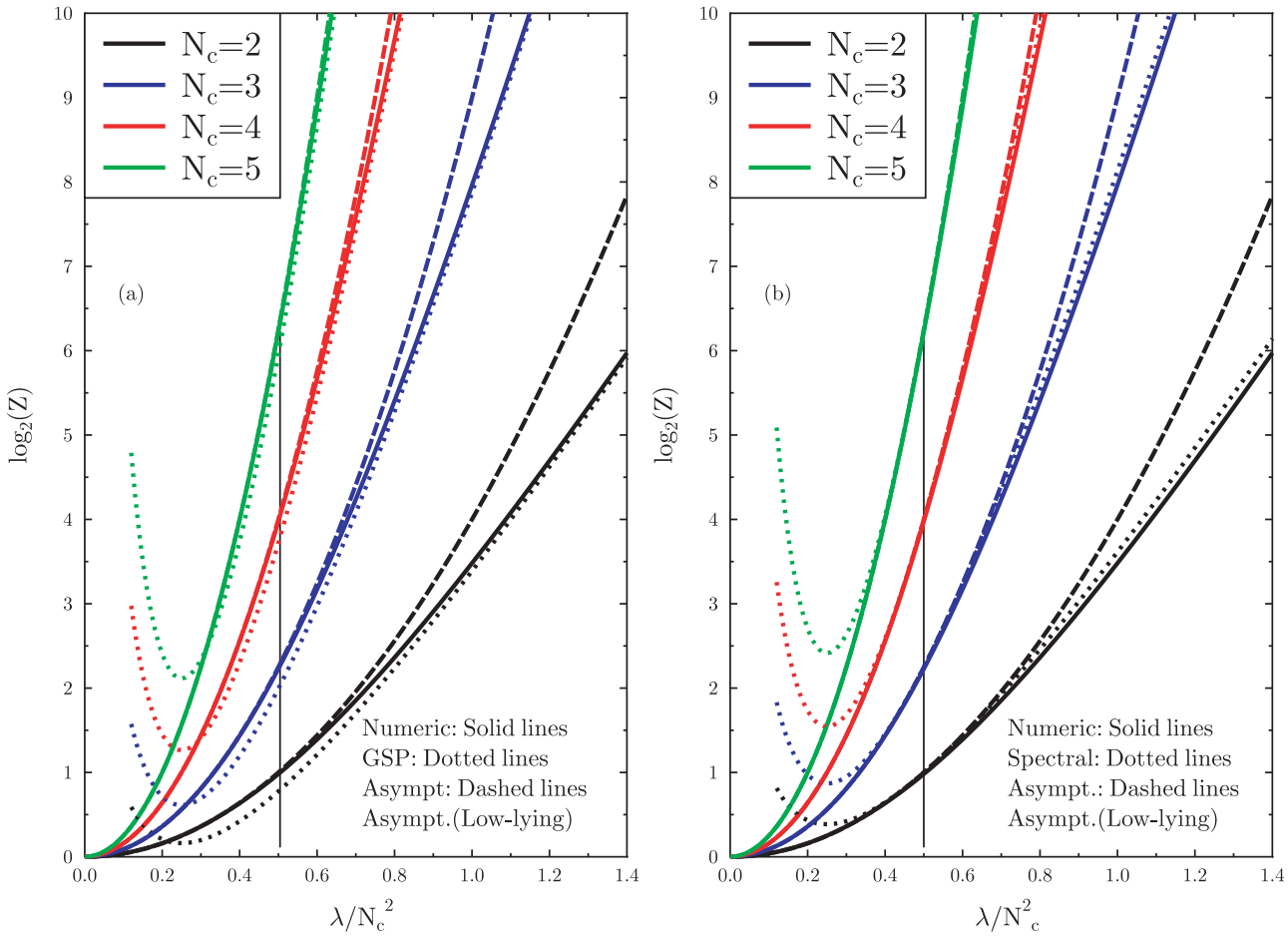

FIG. 4. (Color online) The match between the asymptotic low-lying energy for $\frac{\lambda}{N_c^2}$ over the range $\frac{\lambda}{N_c^2} \leqslant (\frac{\lambda}{N_c^2})_{\rm crit}$ and the asymptotic high-lying energy solution for $\frac{\lambda}{N_c^2}$ over the range $\frac{\lambda}{N_c^2} \geqslant (\frac{\lambda}{N_c^2})_{\rm crit}$ for a color-singlet bag consisting of only fundamental particles. The asymptotic low-lying solution is calculated using the λ-power expansion and the group orthogonality over the entire color range $|\theta| \leqslant \pi$. The asymptotic high-lying energy solution is computed using (a) the GSP method and (b) the spectral density method [8].

asymptotic solutions match each other from left and right sides, respectively. Roughly speaking, they split only with a small redundant constant due to several approximations considered in the derivation. This additive constant vanishes smoothly as the rough approximations are eliminated, and the solution approaches the exact one.

The solutions for the asymptotic low- and high-lying $\frac{\lambda}{N_c^2}$ energy domains are displayed in Fig. 4. Both solutions are displayed with various color numbers N_c and compared with the exact numerical one. The phase transition is found to be a third-order one. This means that the asymptotic low- and high-lying energy solutions and their first and second derivatives are equal. This implies that both solutions are smoothly tangent to each other and lie above each other. They look like they do not really tend to be intersected but instead are approaching each other. The critical point is the midpoint in the interpolation between the low- and high-lying $\frac{\lambda}{N_c^2}$ energy solutions. The matching of the asymptotic large $\frac{\lambda}{N_c^2}$ solution that is calculated using the GSP method with the asymptotic small $\tilde{\lambda}$ solution is displayed in Fig. 4(a). It is found that at the critical point, the low-lying and high-lying energy solutions are split to the minimum with a small redundant additive constant. This redundant constant emerges due to consequent approximations adopted in the analytical solutions with a finite N_c. Although the two solutions deviate from each other by a small redundant constant, evidently, it is always possible to find a smooth interpolation between the two solutions. Since the phase transition is a third order, then the tangent slope and its derivative are interpolated smoothly. The exact numerical solution is shown to match the low-lying energy solution; and then when $\frac{\lambda}{N_c^2}$ exceeds the critical point, the exact numerical solution deviates the asymptotic low-lying energy solution. The exact numerical solution continues to match the asymptotic high-lying energy solution instead of the low-lying energy solution. This tiny redundant constant should not worry us at all, and the location of the critical point is realized in the midway of the interpolation between the two asymptotic solutions, and this constant should be vanished in order to preserve the continuation. In this case, the interpolation between the two solutions is smooth and has a soft deflection characteristic at the critical point. On the other hand, the high-lying energy solution that is obtained by the

spectral density of eigenvalues solution for the range $\frac{\lambda}{N_c^2} \geqslant \frac{\lambda_0}{N_c^2}$ is displayed in Fig. 4(b). It is shown that the low- and high-lying energy solutions are smoothly tangent to each other and located adjacent to each other for a finite range where the Gross-Witten point $\frac{\lambda_0}{N_c^2} = \frac{1}{2}$ is located in the midway. The tangent slope and its derivative for both left and right solutions are equal. Hence, both low-lying and high-lying energy solutions are scaled to be equal at the Gross-Witten point.

C. Phase transition critical point

The critical point for the phase transition is the solution of the spectral density method, and it comes naturally when the integration over the Fourier color variable does not complete the entire circle range but rather covers an incomplete circle range $|\theta_i| \leqslant \theta_c$ where $|\theta_c| < \pi$. The spectral density method produces a solution for the small thermal running parameter $\frac{\lambda}{N_c^2} \leqslant \frac{1}{2}$ and another solution for the large parameter $\frac{\lambda}{N_c^2} \geqslant \frac{1}{2}$. The critical point is determined by matching the two solutions. It is interesting to point out that the small- and large-$\widetilde{\lambda}$ parameters correspond to the strong and weak couplings in the Gross-Witten scenario [7], respectively.

On the other hand, the GSP method produces the high-lying energy solution only for the thermal running parameter that runs over the interval $\frac{\lambda}{N_c^2} \geqslant \frac{1}{2}$. Hereinafter, this is labeled as the solution (II). In solution (II), the Fourier color variables θ_i are assumed to be dominated in a narrow domain. However, the low-lying energy solution for $\frac{\lambda}{N_c^2} \leqslant \frac{1}{2}$ is known to be distributed uniformly over the entire circle with respect to the color angle. Under this condition, the partition function is evaluated trivially by expanding the integral with respect to the group basis powers and using the orthogonality and then finally resumming the resultant terms. Hereinafter, we label the low-lying energy solution as solution (I). The extrapolation of both solutions fails to reproduce the asymptotic results far away outside their domains. The point of the phase transition is determined by examining the continuity when both solutions match each other along the axis of the thermal running parameter $\widetilde{\lambda} \equiv \frac{\lambda}{N_c^2}$. The thorough study of solution (II) sheds more light on the location of the critical point for the phase transition. Solution (II) is concave up for the small parameter $\frac{\lambda}{N_c^2}$. The extremum left-hand point for solution (II), namely,

$$\left(\lim_{N_c\to\infty} \frac{\ln Z_{(\mathrm{II})}(\widetilde{\lambda})}{N_c^2}\right) = -\frac{1}{2}\ln 2\widetilde{\lambda} + 2\widetilde{\lambda} - \frac{3}{4}, \quad \widetilde{\lambda} \geqslant \widetilde{\lambda}_{(\mathrm{II})\min}, \tag{59}$$

is determined by

$$\frac{\partial}{\partial\widetilde{\lambda}}\left(\lim_{N_c\to\infty} \frac{\ln Z_{(\mathrm{II})}(\widetilde{\lambda})}{N_c^2}\right)\Bigg|_{\widetilde{\lambda}_{(\mathrm{II})\mathrm{ext}}} = 0 \to \widetilde{\lambda}_{(\mathrm{II})\mathrm{ext}} = \frac{1}{4}. \tag{60}$$

This point is the bottom of the concave up solution (II):

$$\frac{\partial^2}{\partial\widetilde{\lambda}^2}\left(\lim_{N_c\to\infty} \frac{\ln Z_{(\mathrm{II})}(\widetilde{\lambda})}{N_c^2}\right)\Bigg|_{\widetilde{\lambda}_{(\mathrm{II})\mathrm{ext}}} \to + \text{ at } \widetilde{\lambda}_{(\mathrm{II})\min} = \frac{1}{4}. \tag{61}$$

The left-hand extremum point is found to be the minimum of the solution, and the physical solution $Z_{(\mathrm{II})}(\widetilde{\lambda})$ is found for $\widetilde{\lambda}$ runs over the range $\infty \geqslant \widetilde{\lambda} \geqslant \widetilde{\lambda}_{(\mathrm{II})\min}$. This means that solution (II) is the satisfactory solution for the range $\widetilde{\lambda} > \widetilde{\lambda}_{(\mathrm{II})\min}$. The critical point $\widetilde{\lambda}_{\mathrm{crit}}$ is located somewhere above $\widetilde{\lambda}_{(\mathrm{II})\min}$,

$$\widetilde{\lambda} \geqslant \widetilde{\lambda}_{\mathrm{crit}} \geqslant \widetilde{\lambda}_{(\mathrm{II})\min}, \quad \text{where} \quad \widetilde{\lambda}_{(\mathrm{II})\min} = \tfrac{1}{4}. \tag{62}$$

Therefore, when the low-lying energy solution $Z(\widetilde{\lambda}) \approx Z_{(\mathrm{I})}(\widetilde{\lambda})$ over the range $\widetilde{\lambda} < \widetilde{\lambda}_{\mathrm{crit}}$ is not known, the GSP method still can give much information about the critical point location and the continuous high-lying energy production threshold.

To determine the precise location of the critical point, we need solution (I) for the energy domain $\widetilde{\lambda} < \widetilde{\lambda}_{(\mathrm{I})_{\max}} = 1$. The critical point is determined whenever solution (II) from above and solution (I) from below match each other somewhere in the interval that is bounded by the interval

$$\widetilde{\lambda}_{(\mathrm{I})\max} \geqslant \widetilde{\lambda}_{\mathrm{crit}} \geqslant \widetilde{\lambda}_{(\mathrm{II})\min}. \tag{63}$$

In our case, solution (I) reads

$$\frac{\ln Z_{(\mathrm{I})}(\widetilde{\lambda})}{N_c^2} = \widetilde{\lambda}^2 \quad \text{for} \quad \widetilde{\lambda} < \widetilde{\lambda}_{(\mathrm{I})\max}. \tag{64}$$

Hence, the critical point for the phase transition between the two solutions is computed by matching the extrapolation of the left- and right-hand solutions as follows:

$$\frac{\ln Z_{(\mathrm{I})}(\widetilde{\lambda})}{N_c^2} = \frac{\ln Z_{(\mathrm{II})}(\widetilde{\lambda})}{N_c^2}, \quad \text{at } \widetilde{\lambda} = \widetilde{\lambda}_{\mathrm{crit}}. \tag{65}$$

It is found that $\widetilde{\lambda}_{\mathrm{crit}} = \frac{1}{2}$.

D. Saddle points approximation with the Vandermonde potential

To understand the validity of the Gaussian-like approximation, it is essential to show that the color saddle points are distributed in a narrow domain ($|\theta_c| \ll \pi$) as the parameter $\widetilde{\lambda}$ runs over the range $\widetilde{\lambda} \geqslant \widetilde{\lambda}_{\mathrm{crit}}$. The canonical partition function for the fundamental particles obeying $U(N_c)$ can be written as

$$Z(\widetilde{\lambda}) = \frac{1}{N_c!}\prod_k^{N_c}\int\frac{d\theta_k}{2\pi}\exp\left[\frac{1}{2}\sum_{n=1}^{N_c}\sum_{m=1}^{N_c}\ln\sin^2\left(\frac{\theta_n-\theta_m}{2}\right)\Bigg|_{n\neq m} + 2N_c\widetilde{\lambda}\sum_{n=1}^{N_c}\cos\theta_n\right]. \tag{66}$$

The above partition function is extremely difficult to be evaluated exactly. Fortunately, it can be integrated over the color variables using the saddle points approximation. The

exponent under the integral can be written as

$$\ln Z(\widetilde{\lambda}, \{\theta\}) = \left[\frac{1}{2} \sum_{n=1}^{N_c} \sum_{m=1}^{N_c} \ln \sin^2 \left(\frac{\theta_n - \theta_m}{2} \right) \Bigg|_{n \neq m} + 2N_c \widetilde{\lambda} \sum_{n=1}^{N_c} \cos \theta_n \right] + \text{const.} \quad (67)$$

To avoid the singularity in the exponent, the color saddle points are distributed uniformly over the complete circle and do not approach each other ($\overline{\theta}_i \neq \overline{\theta}_m$). However, when these points approach each other in the limit $\overline{\theta}_i \to \overline{\theta}_m$, the exponent blows up and diverges, and subsequently the saddle points integral approximation is badly broken down, and another analytic solution must emerge beyond this critical point. The color saddle points are evaluated using the stationary conditions

$$\frac{\partial}{\partial \theta_i} \ln Z(\widetilde{\lambda}, \{\theta\})|_{\theta_i = \overline{\theta}_i} = 0, \quad i = 1, 2, \ldots, N_c (\text{or } N_c - 1), \quad (68)$$

for U(N_c) or SU(N_c). Hence the saddle points are determined by the set of equations

$$2N_c \widetilde{\lambda} \sin \overline{\theta}_i = \sum_{n \neq i}^{N_c} \cot \left(\frac{\overline{\theta}_i - \overline{\theta}_n}{2} \right), \quad \overline{\theta}_i \neq \overline{\theta}_m. \quad (69)$$

These points satisfy the set of nonlinear equations as follows:

$$2\widetilde{\lambda} \left(\frac{1}{N_c} \sum_{i=1}^{N_c} \sin \overline{\theta}_i \right) = \frac{1}{N_c^2} \sum_{i}^{N_c} \sum_{n}^{N_c} \cot \left(\frac{\overline{\theta}_i - \overline{\theta}_n}{2} \right)_{i \neq n}. \quad (70)$$

This nonlinear set is the root of the spectral density that is derived using the spectral density method in the large N_c limit. The Gaussian-like integral around the saddle points is approximated as

$$Z(\widetilde{\lambda}) \sim \prod_i \int_{-\pi}^{\pi} \frac{d\theta_i}{2\pi} \exp[\ln Z(\widetilde{\lambda}, \{\theta\})] \approx Z(\widetilde{\lambda}, \{\overline{\theta}\}) \prod_i \int_{-\infty}^{\infty} \frac{d\theta_i}{2\pi} e^{-\sum_{ij} \frac{1}{2} \Delta(\overline{\theta}_i, \overline{\theta}_j) \theta_i \theta_j}, \quad (71)$$

where the exponential elements are determined at the saddle points ($\theta_i, i = 1, 2, \ldots, N_c$) as

$$\Delta(\overline{\theta}_i, \overline{\theta}_j) = -\frac{\partial^2}{\partial \theta_i \partial \theta_j} \ln Z(\widetilde{\lambda}, \{\theta\})|_{\theta_i = \overline{\theta}_i}. \quad (72)$$

Equation (71) is evaluated around the saddle points using the Gaussian integral as follows:

$$Z(\widetilde{\lambda}) \doteq \mathcal{N} \exp[\ln Z(\widetilde{\lambda}, \{\overline{\theta}\})], \quad (73)$$

where the preexponential normalization satisfies the integral $\int \frac{d\theta_i}{2\pi} = 1$ and is determined by

$$\mathcal{N} = (2\pi)^{-N_c/2} [\det \Delta(\overline{\theta}_i, \overline{\theta}_j)]^{-1/2} \leqslant 1. \quad (74)$$

However, it is not always possible to find real values for the saddle points distributed uniformly over the entire circle range for the parameter $\widetilde{\lambda}$ that runs along the real axis. These real saddle points cease to exist when the thermal running parameter $\widetilde{\lambda}$ reaches the critical value. The Vandermonde potential characteristics is modified at the critical point. This point is the threshold for another solution with a different behavior.

VI. ADJOINT PARTICLES

The color-singlet bags consisting of a gas of fundamental and antifundamental particles represent the mesonic and baryonic states with no gluonic component. On the other hand, the color-singlet bags consisting only of the adjoint particles represent glueball states with no quark component. The low-lying hadronic states are likely mesons, baryons, and glueballs. The Hagedorn states with fundamental and adjoint constituent particles are essential to understanding the highly thermal excited hadronic states near and just below the deconfinement phase transition diagram.

The canonical ensemble for the bags consisting only of the adjoint particles projected in the color-singlet state reads

$$Z(\beta) = \int d\mu(g) \exp \left[\mathcal{D}_g \int_V d^3 r \int \frac{d^3 p}{(2\pi)^3} \mathcal{G}_{\text{adj}}(\theta) e^{-\beta E(p,r)} \right], \quad (75)$$

where $\mathcal{D}_g$ is the degeneracy such as the spin multiplicity $\mathcal{D}_g = (2j + 1)$. The internal color structure for the adjoint constituents in the Fock space is given by

$$\mathcal{G}_{\text{adj}}(\theta) = \frac{1}{\dim_g} \text{tr} [\mathbf{R}_{\text{adj}}(g)], \quad (76)$$

where $\dim_g = N_c^2$ and $(N_c^2 - 1)$ for U(N_c) and SU(N_c), respectively. The partition function for the gas of free particles occupying the volume V is approximated to

$$\lambda_g = \mathcal{D}_g \int_V d^3 r \int \frac{d^3 p}{(2\pi)^3} e^{-\beta E(p,r)}, \quad (77)$$

where $E(p, r)$ is the energy for each constituent particle species. To simplify our notation, we define the following thermal running parameter

$$\tilde{\lambda}_g = \frac{\lambda_g}{\dim_g}. \quad (78)$$

Hence, the canonical ensemble is simplified as

$$Z(\lambda_g) = \int d\mu(g) \exp[\tilde{\lambda}_g \text{tr}_c [\mathbf{R}_{\text{adj}}(g)]]. \quad (79)$$

The adjoint group representation reads

$$\text{tr} [\mathbf{R}_{\text{adj}}(g^k)] = \text{tr} [\mathbf{R}_{\text{fun}}(g^k)] \, \text{tr} [\mathbf{R}^*_{\text{fun}}(g^k)] - 1 = (N_c - 1) + \sum_{n=1}^{N_c} \sum_{m=1}^{N_c} \cos k(\theta_n - \theta_m)|_{n \neq m}, \quad \theta_{N_c} = \sum_{i=1}^{N_c - 1} \theta_i, \quad (80)$$

and

$$\text{tr} [\mathbf{R}_{\text{adj}}(g^k)] = \text{tr} [\mathbf{R}_{\text{fun}}(g^k)] \, \text{tr} [\mathbf{R}^*_{\text{fun}}(g^k)], \quad (81)$$

for the groups SU(N_c) and U(N_c), respectively.

We use the GSP method developed in the previous section to calculate the asymptotic high-lying energy solution for the canonical ensemble with a large thermal running parameter $\tilde{\lambda}_g \geqslant (\tilde{\lambda}_g)_{\text{crit}}$. In this range, the Fourier color variables are assumed to be dominant only in a narrow range. The adjoint action near the saddle points is approximated to

$$\tilde{\lambda}_g \text{tr}_c[\mathbf{R}_{\text{adj}}(g)] = \tilde{\lambda}_g \left\{ (N_c - 1) + \sum_{n=1}^{N_c} \sum_{m=1}^{N_c} \cos(\theta_n - \theta_m)|_{n \neq m} \right\}$$
$$\approx \tilde{\lambda}_g \left[\left(N_c^2 - 1\right) - \frac{1}{2} \sum_{n=1}^{N_c} \sum_{m=1}^{N_c} (\theta_n - \theta_m)^2 \right]. \quad (82)$$

The above approximation reduces the canonical ensemble to

$$Z(\lambda_g)|_{\text{SU}(N_c)} \approx Z_{(\text{II})}(\lambda_g)|_{\text{SU}(N_c)},$$
$$\text{(for } \tilde{\lambda}_g \text{ over the range } \tilde{\lambda}_g \geqslant \tilde{\lambda}_{g(\text{II})\min}),$$
$$Z_{(\text{II})}(\lambda_g)|_{\text{SU}(N_c)} = e^{(N_c^2-1)\tilde{\lambda}_g} \frac{1}{N!} \int_{-\pi}^{\pi} d\theta_{N_c} \delta \left(\sum_{i=1}^{N_c} \theta_i \right)$$
$$\times \left(\prod_{k}^{N_c - 1} \int_{-\infty}^{\infty} \frac{d\theta_k}{2\pi} \right) \prod_{n>m}^{N_c} (\theta_n - \theta_m)^2$$
$$\times \exp \left[-\frac{\tilde{\lambda}_g}{2} \sum_{n=1}^{N_c} \sum_{m=1}^{N_c} (\theta_n - \theta_m)^2 \right]$$
$$\approx \left(\frac{1}{2N_c \tilde{\lambda}_g} \right)^{\frac{N_c^2-1}{2}} e^{(N_c^2-1)\tilde{\lambda}_g}$$
$$\times \left[\frac{1}{N_c! (2\pi)^{\frac{N_c}{2}-1}} \prod_{n=1}^{N_c} n! \frac{1}{\sqrt{2\pi N_c}} \right], \quad (83)$$

for the SU(N_c) group representation, where the following relation has been adopted

$$I_i = \left(\prod_{k}^{N_c} \int_{-\infty}^{\infty} \frac{d\theta_k}{2\pi} \right) 2\pi \delta \left(\sum_{i=1}^{N_c} \theta_i \right)$$
$$\times \left[\prod_{n \neq m}^{N_c} (\theta_n - \theta_m)^2 \right]^{\frac{1}{2}} e^{[-\frac{\tilde{\lambda}_g}{2} \sum_{n=1}^{N_c} \sum_{m=1}^{N_c} (\theta_n - \theta_m)^2]}$$
$$\equiv \left(\prod_{k}^{N_c} \int_{-\infty}^{\infty} \frac{d\theta_k}{2\pi} \right) 2\pi \delta \left(\sum_{i=1}^{N_c} \theta_i \right)$$
$$\times \left[\prod_{n>m}^{N_c} (\theta_n - \theta_m)^2 \right] e^{[-\frac{2N_c \tilde{\lambda}_g}{2} \sum_{n=1}^{N_c} \theta_n^2]}. \quad (84)$$

The same procedure can be followed for U(N_c) symmetry. The canonical ensemble is reduced to

$$Z_{(\text{II})}(\lambda_g)|_{\text{U}(N_c)} \approx \left(\frac{1}{2N_c \tilde{\lambda}_g} \right)^{\frac{N_c^2-1}{2}} e^{N_c^2 \tilde{\lambda}_g}$$
$$\times \left[\frac{\sqrt{N_c}}{N_c! (2\pi)^{\frac{N_c-1}{2}}} \prod_{n=1}^{N_c} n! \right] \int_{-\infty}^{\infty} \frac{d\theta_{N_c}}{2\pi}$$
$$\approx e^{N_c^2 \tilde{\lambda}_g} \left(\frac{1}{2N_c \tilde{\lambda}_g} \right)^{\frac{N_c^2-1}{2}} \left[\frac{\prod_{n=1}^{N_c} n!}{N_c! (2\pi)^{\frac{N_c}{2}}} \right]$$
$$\times \sqrt{2\pi N_c} \int_{-\pi}^{\pi} \frac{d\theta_{N_c}}{2\pi},$$
$$\text{(for } \tilde{\lambda}_g \text{ over the range } \tilde{\lambda}_g \geqslant \tilde{\lambda}_{g(\text{II})\min}). \quad (85)$$

Using Stirling's approximation as done in Eq. (52) for the large N_c limit, the partition function becomes

$$Z_{(\text{II})}(\lambda_g)|_{\text{U}(N_c)} \approx \left(\frac{1}{2\tilde{\lambda}_g} \right)^{\frac{N_c^2-1}{2}} e^{(N_c^2 \tilde{\lambda}_g - \frac{3}{4} N_c^2)}$$
$$\to \left(\frac{1}{2\tilde{\lambda}_g} \right)^{\frac{N_c^2}{2}} e^{(N_c^2 \tilde{\lambda}_g - \frac{3}{4} N_c^2 + N_c^2 C_{\text{adj}})},$$
$$\text{(for } \tilde{\lambda}_g \text{ over the range } \tilde{\lambda}_g \geqslant \tilde{\lambda}_{g(\text{II})\min}), \quad (86)$$

for the U(N_c) representation. The additional constant C_{adj} ensures that the term $\ln Z_{(\text{II})}(\lambda_g)/N_c^2$ is a non-negative quantity, and it should satisfy the boundary near the critical point; furthermore, it throws away any redundant constant. This additional constant stems from the normalization transformation in the Gaussian-like integration $\int_{-\infty}^{\infty} \frac{d\theta}{2\pi} e^0 \to \int_{-\pi}^{\pi} \frac{d\theta}{2\pi} = 1$. Hence, the solution for the large parameter $\tilde{\lambda}_g > \tilde{\lambda}_{g(\text{II})\min}$ reads

$$\left(\lim_{N_c^2 \to \text{large}} \frac{\ln Z_{(\text{II})}(\lambda_g)}{N_c^2} \right) \Bigg|_{\text{U}(N_c)} = -\frac{1}{2} \ln 2\tilde{\lambda}_g + \tilde{\lambda}_g - \frac{3}{4} + C_{\text{adj}},$$
$$\geqslant 0, \quad (87)$$

in the large N_c limit. This function is concave up. The value $\tilde{\lambda}_{g(\text{II})\min}$ is calculated as follows

$$\left(\lim_{N_c^2 \to \text{large}} \frac{\partial}{\partial \lambda_g} \frac{\ln Z_{(\text{II})}(\lambda_g)}{N_c^2} \right)_{\tilde{\lambda}_{g(\text{II})\min}} = 0 \to \tilde{\lambda}_{g(\text{II})\min} = \frac{1}{2},$$
$$\left(\lim_{N_c^2 \to \text{large}} \frac{\partial^2}{\partial \lambda_g^2} \frac{\ln Z_{(\text{II})}(\lambda_g)}{N_c^2} \right)_{\tilde{\lambda}_{g(\text{II})\min}} \to (+) \to \text{concave up}. \quad (88)$$

This means that our solution is valid only when $\tilde{\lambda}_g$ runs over the range $\tilde{\lambda}_g \geqslant \tilde{\lambda}_{g(\text{II})\min}$. The value C_{adj} is determined from

$$\left(\lim_{N_c^2 \to \text{large}} \frac{\ln Z_{(\text{II})}(\lambda_g)}{N_c^2} \right) \geqslant 0, \quad (89)$$

for the point $\tilde{\lambda}_{g(\text{II})\min}$ to ensure that our solution is non-negative in the entire $\tilde{\lambda}$ range and to preserve the analytic continuation of the solution. This leads to $C_{\text{adj}} = \frac{1}{4}$. Hence, the canonical partition in the range $\tilde{\lambda}_g \geqslant \tilde{\lambda}_{g(\text{II})\min}$ in the large N_c limit reads

$$Z_{(\text{II})}(\lambda_g) \equiv \left(\frac{1}{2\tilde{\lambda}_g} \right)^{\frac{N_c^2}{2}} \exp \left(N_c^2 \tilde{\lambda}_g - \frac{N_c^2}{2} \right). \quad (90)$$

It will be shown below [e.g., in Eq. (100)] that for $\tilde{\lambda}_g \leqslant \tilde{\lambda}_{g(\text{I})\max}$, where $\tilde{\lambda}_{g(\text{I})\max} < 1$, the canonical ensemble

becomes

$$\lim_{N_c^2\to\text{large}} \ln Z(\lambda_g) = \lim_{N_c^2\to\text{large}} \ln Z_{(\mathrm{I})}(\lambda_g), \\ = -\frac{1}{N_c^2}\ln(1-\tilde{\lambda}_g),\ \approx 0, \\ \text{(for } \tilde{\lambda}_g \text{ over the range } \tilde{\lambda}_g \leqslant \tilde{\lambda}_{g(\mathrm{I})\max}). \tag{91}$$

We are now in the position to compute the Gross-Witten critical point:

$$\tilde{\lambda}_{g(\mathrm{I})\max} \geqslant \tilde{\lambda}_{g\mathrm{crit}} \geqslant \tilde{\lambda}_{g(\mathrm{II})\min}. \tag{92}$$

The critical point for the phase transition is determined as follows:

$$\lim_{N_c^2\to\text{large}} \frac{\ln Z_{(\mathrm{I})}(\lambda)}{N_c^2} = \lim_{N_c^2\to\text{large}} \frac{\ln Z_{(\mathrm{II})}(\lambda)}{N_c^2}, \\ \text{(at the point } \tilde{\lambda}_g = \tilde{\lambda}_{g\mathrm{crit}}). \tag{93}$$

It is found that the critical point is located at $\tilde{\lambda}_{g\mathrm{crit}} = \frac{1}{2}$. This procedure is very useful in determining the point for the phase transition for a finite number of colors N_c, and it will be more appropriate when more complicated physical situations are involved. Furthermore, it seems that the GSP method is more straightforward and easier than the spectral density method.

The solution of the canonical ensemble for the adjoint particles in the range $\tilde{\lambda}_g \leqslant \tilde{\lambda}_{g(\mathrm{I})\max}$ is nontrivial because of the color structure for SU(N_c) and U(N_c) group representations. Fortunately, the adjoint color structure can be simplified to a fundamental-like structure by introducing the Lagrange multiplier. The inclusion of the Lagrange multiplier trick reduces the partition function with the U(N_c) group structure to

$$Z(\lambda_g) = \int d\mu(g) \exp\left(\lambda_g \frac{1}{\dim_g} \mathrm{tr}\mathbf{R}_{\mathrm{adj}}(g)\right) \\ = \int d\mu(g) \exp(\tilde{\lambda}_g \mathrm{tr}\,\mathbf{R}_{\mathrm{fun}}(g) \mathrm{tr}\,\mathbf{R}^*_{\mathrm{fun}}(g)) \\ = \frac{N_c^2}{2\tilde{\lambda}_g}\int_0^\infty d\xi\, \xi e^{-\frac{N_c\xi^2}{4\tilde{\lambda}_g}} \int d\mu(g) \\ \times \exp\left[\frac{N_c\xi}{2}(\mathrm{tr}\,\mathbf{R}_{\mathrm{fun}}(g) + \mathrm{tr}\,\mathbf{R}^*_{\mathrm{fun}}(g))\right]. \tag{94}$$

This equation is decomposed into two parts:

$$Z(\lambda_g) = Z_1(\lambda_g) + Z_2(\lambda_g), \tag{95}$$

where

$$Z_1(\lambda_g) = \frac{N_c^2}{2\tilde{\lambda}_g}\int_0^{\xi_0} d\xi\xi e^{-\frac{N_c^2\xi^2}{4\tilde{\lambda}_g}} e^{\frac{N_c^2\xi^2}{4}}, \tag{96}$$

and

$$Z_2(\lambda_g) = \frac{N_c^2}{2\tilde{\lambda}_g}\int_{\xi_0}^\infty d\xi\, \xi e^{-\frac{N_c^2\xi^2}{4\tilde{\lambda}_g}} (\xi)^{-N_c^2/2} e^{N_c^2\xi - 3N_c^2/4}. \tag{97}$$

The integration over the color-singlet state takes into account the splitting into the small and large domains $0 \leqslant \xi \leqslant \xi_0$ and $\xi_0 \leqslant \xi \leqslant \infty$, respectively, where $\xi_0 = 1$. The integration over the range $(0 \leqslant \xi \leqslant \xi_0)$ reduces Eq. (96) to

$$Z_1(\lambda_g) = \frac{N_c^2}{4\tilde{\lambda}_g}\int_0^{\xi_0} d\xi^2 \exp\left[-\frac{N_c^2\xi^2}{4}\left(\frac{1}{\tilde{\lambda}_g} - 1\right)\right], \tag{98}$$

where $\tilde{\lambda}_g$ is assumed to run only over the range $\tilde{\lambda}_g \leqslant \tilde{\lambda}_{g(\mathrm{I})\max} < 1$. The extrapolation of the integration upper limit $\xi_0 \to \infty$ approximates the partition function to

$$Z(\lambda_g) = Z_1(\lambda_g) + Z_2(\lambda_g) \\ \approx \frac{N_c^2}{4\tilde{\lambda}_g}\int_0^\infty d\xi^2 \exp\left[-\frac{N_c^2\xi^2(1-\tilde{\lambda}_g)}{4\tilde{\lambda}_g}\right] \\ \approx \frac{N_c^2}{4\tilde{\lambda}_g}\frac{4\tilde{\lambda}_g/N_c^2}{(1-\tilde{\lambda}_g)}. \tag{99}$$

This integration is trivial and is reduced to

$$Z(\lambda_g) \approx Z_1(\lambda_g), \\ Z_1(\lambda_g) \approx \frac{1}{1-\tilde{\lambda}_g}, \\ = \exp[-\ln(1-\tilde{\lambda}_g)] \sim \exp[\text{function}(\tilde{\lambda}_g)]. \tag{100}$$

The integration over $\xi_0 \leqslant \xi \leqslant \infty$ where $\xi_0 = 1$ for the case $\tilde{\lambda}_g \leqslant \frac{1}{2} \leqslant \tilde{\lambda}_{g(\mathrm{I})\max}$ is approximated to

$$Z_2(\lambda_g) = \frac{N_c^2}{4\tilde{\lambda}_g}\int_{\xi_0^2}^\infty d\xi^2 (\xi^2)^{-N_c^2/4} e^{-\frac{N_c^2\xi^2}{4\tilde{\lambda}_g}} e^{N_c^2\xi - \frac{3}{4}N_c^2} \\ \leqslant \frac{N_c^2}{4\tilde{\lambda}_g}\int_{\xi_0^2}^\infty d\xi^2 e^{-\frac{N_c^2\xi^2}{4\tilde{\lambda}_g}} e^{N_c^2\xi} \leqslant \frac{N_c^2}{4\tilde{\lambda}_g}\int_{x_0}^\infty dx\, e^{-\frac{N^2(1-\lambda_g)x}{4\tilde{\lambda}_g}}. \tag{101}$$

This integral complements the integral given by Eq. (99) which runs over the interval $0 \leqslant \xi \leqslant \xi_0$. In Eq. (99), when ξ_0 is extended and extrapolated to ∞ in the term $Z_1(\lambda_g)$, then the second term is suppressed.

On the other hand, the analytical solution behaves differently in the energy domain $\tilde{\lambda}_g \geqslant 1 \geqslant \tilde{\lambda}_{g(\mathrm{II})\min}$. In this energy domain, the integral over $0 \leqslant \xi \leqslant \xi_0$ is suppressed and $Z_1(\lambda_g)$ becomes negligible,

$$Z_1(\lambda_g) \propto \frac{1}{\lambda_g} \sim 0. \tag{102}$$

The integration over the range $\xi_0 \leqslant \xi \leqslant \infty$ and $\tilde{\lambda}_g \geqslant 1$ approximates Eq. (97) to

$$Z(\lambda_g) \approx Z_2(\lambda_g) \\ = \frac{N_c^2}{2\tilde{\lambda}_g}\int_{\xi_0}^\infty d\xi\xi e^{-\frac{N_c^2\xi^2}{4\tilde{\lambda}_g}} (\xi)^{-N_c^2/2} e^{N_c^2\xi - 3N_c^2/4} \\ = \int_{\xi_0}^\infty d\xi e^{f(\xi)}, \tag{103}$$

where

$$f(\xi) \approx \left[-\frac{1}{4\tilde{\lambda}_g}\xi^2 - \frac{1}{2}\ln\xi + \xi - \frac{3}{4}\right]. \tag{104}$$

When the saddle point becomes $\xi_{\mathrm{sp}} \geqslant 1$, the above equation is approximated to

$$Z(\lambda_g) \approx \int_0^\infty d\xi\, e^{f(\xi)}. \tag{105}$$

The saddle point can be found by the solution

$$(\xi^2 - 2\tilde{\lambda}_g\xi + \tilde{\lambda}_g)_{\xi=\xi_{\rm sp}} = 0. \tag{106}$$

The saddle point solution reads

$$\begin{aligned}
&\xi_{\rm sp} = 1 + \sqrt{1 - \frac{1}{\tilde{\lambda}_g}}, \text{ (with the constraint } \tilde{\lambda}_g \geqslant 1),\\
&\xi_{\rm sp} \approx \tilde{\lambda}_g\left[2 - \frac{1}{2\tilde{\lambda}_g}\right],\\
&\xi_{\rm sp} \approx 2\tilde{\lambda}_g.
\end{aligned} \tag{107}$$

The saddle point can, alternatively, be derived from Eq. (106) as follows:

$$\begin{aligned}
&\left(1 - 2\tilde{\lambda}_g\frac{1}{\xi} + \tilde{\lambda}_g\frac{1}{\xi^2}\right)_{1/\xi=1/\xi_{\rm sp}} = 0,\\
&\rightarrow 1/\xi_{\rm sp} = 1 - \sqrt{1 - \frac{1}{\tilde{\lambda}_g}} \approx \frac{1}{2\tilde{\lambda}_g}.
\end{aligned} \tag{108}$$

This result is analogous to Eq. (118). The above approximation softens and extrapolates the constraint to

$$\xi_{\rm sp} = 2\tilde{\lambda}_g, \quad \left(\text{with constraint } \tilde{\lambda}_g \geqslant \tfrac{1}{2}, \quad \text{and} \quad \xi_{\rm sp} \geqslant 1\right). \tag{109}$$

Hence, by substituting the saddle point into Eq. (104), we get

$$\begin{aligned}
f(\xi_{\rm sp}) &= -\frac{1}{4\tilde{\lambda}_g}\left[\xi_{\rm sp}^2 - 2\tilde{\lambda}_g\xi_{\rm sp} + \tilde{\lambda}_g\right] + \frac{\xi_{\rm sp}}{2} - \frac{1}{2}\ln\xi_{\rm sp} - \frac{1}{2}\\
&= \frac{\xi_{\rm sp}}{2} - \frac{1}{2}\ln\xi_{\rm sp} - \frac{1}{2}\\
&= \frac{1}{2s_0^2} + \frac{1}{2}\ln s_0^2 - \frac{1}{2} = f\left(s_0^2\right),
\end{aligned} \tag{110}$$

where we have introduced $s_0^2 = 1/\xi_{\rm sp}$ for our convenience. In terms of s_0^2, the partition function is reduced to

$$\begin{aligned}
Z_2(s_0^2) &= \mathcal{N}_\xi \exp\left[N_c^2\left(\frac{1}{2s_0^2} + \frac{1}{2}\ln s_0^2 - \frac{1}{2}\right)\right]\\
&\approx \exp\left[N_c^2\left(\frac{1}{2s_0^2} + \frac{1}{2}\ln s_0^2 - \frac{1}{2} + \mathcal{O}\left(\frac{\ln N_c^2}{N_c^2}\right)\right)\right],
\end{aligned} \tag{111}$$

where

$$\begin{aligned}
\mathcal{N}_\xi &= \frac{N_c^2}{2\tilde{\lambda}_g}\sqrt{\frac{2\pi}{-f''(\xi_0)}}\\
&= \exp\left[N_c^2\mathcal{O}\left(\frac{1}{N_c^2}\ln(N_c^2)\right)\right].
\end{aligned} \tag{112}$$

With the approximation $s_0^2 = \frac{1}{2\tilde{\lambda}_g}$ and $\tilde{\lambda}_g \geqslant \frac{1}{2}$, the partition function reads

$$Z(\tilde{\lambda}_g) = \exp\left[N_c^2\left(\tilde{\lambda}_g - \frac{1}{2}\ln 2\tilde{\lambda}_g - \frac{1}{2}\right)\right]. \tag{113}$$

This result is identical to the result in Eq. (120) to be derived using the spectral density method. However, the saddle point derived from Eq. (106) can be approximated to

$$\xi_{\rm sp} = 2\tilde{\lambda}_g - \tfrac{1}{2}. \tag{114}$$

This approximation in the large N_c limit leads to

$$\begin{aligned}
Z(\tilde{\lambda}_g) &\approx \lim_{\tilde{\lambda}_g\rightarrow\text{large}} \exp\left[N^2\left(\tilde{\lambda}_g - \frac{1}{2}\ln\left(2\tilde{\lambda}_g - \frac{1}{2}\right) - \frac{3}{4}\right)\right]\\
&\approx \exp\left[N^2\left(\tilde{\lambda}_g - \frac{1}{2}\ln(2\tilde{\lambda}_g) - \text{const.}\right)\right],\\
\text{const.} &= \frac{3}{4},
\end{aligned} \tag{115}$$

with an additive constant equivalent to the one in the GSP method. The discrepancy between the GSP method and the spectral density method comes from a redundant additive constant that emerges because of the kind of approximation considered. This redundant constant appears in the gas of only adjoint particles in the U(N_c) representation. The SU(N_c) representation does not have this kind of problem. To verify the results of the GSP method, we compare them with the results of the method of the spectral density of color eigenvalues [8]. The canonical ensemble in the adjoint representation is computed in a similar way as done in the fundamental representation. Using a similar transformation, the canonical ensemble in the term of the spectral density is reduced to

$$\begin{aligned}
Z(\lambda_g) &= C\exp\left[\frac{N_c^2}{2}\mathrm{P}\int_{-\pi}^{\pi}d\theta\rho(\theta)\right.\\
&\quad\times\int_{-\pi}^{\pi}d\theta'\rho(\theta')\ln\sin^2\left(\frac{\theta-\theta'}{2}\right)\\
&\quad+\tilde{\lambda}_g\left\{N_c + N_c^2\mathrm{P}\int_{-\pi}^{\pi}d\theta\rho(\theta)\right.\\
&\quad\left.\left.\times\int_{-\pi}^{\pi}d\theta'\rho(\theta')\cos(\theta-\theta')\right\}\right]\\
&\approx C\exp\left[N_c^2\left\{\frac{1}{2}\mathrm{P}\int_{-\pi}^{\pi}d\theta\rho(\theta)\right.\right.\\
&\quad\times\int_{-\pi}^{\pi}d\theta'\rho(\theta')\ln\sin^2\left(\frac{\theta-\theta'}{2}\right)\\
&\quad\left.\left.+\tilde{\lambda}_g\int_{-\pi}^{\pi}d\theta\rho(\theta)\int_{-\pi}^{\pi}d\theta'\rho(\theta')\cos(\theta-\theta')\right\}\right],
\end{aligned} \tag{116}$$

where the integral prefactor C is analogous to that given in the fundamental representation. Using the symmetry property of the spectral density $\rho(\theta)$ in the range $-\pi \leqslant \theta \leqslant \pi$, the stationary equation reads

$$\begin{aligned}
&2\tilde{\lambda}_g\left[\int_{-\pi}^{\pi}d\theta'\rho(\theta')\cos\theta'\right]\sin\theta\\
&\quad= \mathrm{P}\int_{-\pi}^{\pi}d\theta'\rho(\theta')\cot\left(\frac{\theta-\theta'}{2}\right).
\end{aligned} \tag{117}$$

The solution for the range $2\tilde{\lambda}_g \geqslant 1$ is already known [7,8,22,23]. The density of eigenvalues reads

$$\rho(\theta) = \frac{1}{\pi}\frac{\cos\frac{\theta}{2}}{\sin^2\frac{\theta_0}{2}}\sqrt{\sin^2\frac{\theta_0}{2} - \sin^2\frac{\theta}{2}}, \quad -\theta_0 \leqslant \theta \leqslant \theta_0,$$
$$= 0, \quad \pi \geqslant |\theta| > \theta_0, \tag{118}$$

where

$$\sin^2\left(\frac{\theta_0}{2}\right) = 1 - \sqrt{1 - \frac{1}{\tilde{\lambda}_g}}. \tag{119}$$

However, in the limit $\tilde{\lambda}_g \gg 1$, we get $\sin^2(\theta_0/2) = 1/(2\tilde{\lambda}_g)$. In the context of the spectral density method, the canonical ensemble, in the large N_c limit, becomes

$$Z(\tilde{\lambda}_g) \approx \exp\left[N_c^2\tilde{\lambda}_g - \frac{N_c^2}{2}\ln(2N_c\tilde{\lambda}_g) + \frac{N_c^2}{2}\ln N_c - \frac{N_c^2}{2}\right]$$
$$\cong \left(\frac{1}{2\tilde{\lambda}_g}\right)^{\frac{N_c^2}{2}} \exp\left[N_c^2\tilde{\lambda}_g - \frac{N_c^2}{2}\right], \quad \tilde{\lambda}_g \geqslant \frac{1}{2}. \tag{120}$$

The solution for the energy domain $\tilde{\lambda}_g \leqslant \frac{1}{2} \ll \tilde{\lambda}_{g(\mathrm{I})\max} < 1$ reads

$$\ln Z(\tilde{\lambda}_g) \approx \text{const.} \times \exp[\text{function}(\lambda_g)], \quad \tilde{\lambda}_g \leqslant \tfrac{1}{2}, \tag{121}$$

for the entire color range $|\theta_i| \leqslant \pi$, where the function of λ_g is independent of N_c. Hence, in the limit $N_c \to \infty$, we have

$$\lim_{N_c\to\infty} \frac{\ln Z(\tilde{\lambda}_g)}{N_c^2} = 0. \tag{122}$$

It means that in the limit $N_c \to \infty$, the adjoint particle contribution vanishes, and only the fundamental particles contribute to the low-lying energy solution for the energy range $\tilde{\lambda}_g \leqslant \frac{1}{2}$. This result is interpreted as follows: the low-lying gluonic spectrum vanishes and the glueballs appear only as highly excited states in the high-lying mass spectrum. Fortunately, the existed hadronic mass spectrum agrees with this interpretation.

The logarithm of partition function $\ln Z(\lambda_g)$ for the gas of color-singlet bags of adjoint particles versus the thermal partition parameter $\tilde{\lambda}_g$ with various color numbers $N_c = 2, 3, 4$, and 5 is displayed in Fig. 5. The partition function for the high-lying energy $\tilde{\lambda}_g \geqslant \tilde{\lambda}_0$ is solved using the spectral density method and the GSP method. Both solutions are extrapolated to the low-lying energy range $\tilde{\lambda}_g < \tilde{\lambda}_0$. It is shown that the solution of the GSP method is adjacent and almost parallel to that of the spectral density method, and they are splitting by a tiny additive constant over the high-lying energy domain $\tilde{\lambda}_g \geqslant \frac{1}{2}$. Furthermore, the exact numerical solution is found midway between the two solutions. The tiny split between the exact numerical solution and the asymptotic high-lying energy solution for the two methods becomes less pronounced as N_c increases. The extrapolation of the asymptotic high-lying energy solution found by either method deviates from the exact numerical solution as the thermal running parameter runs over the range $\tilde{\lambda}_g < \frac{1}{2}$. This deviation increases significantly as $\tilde{\lambda}_g$ decreases farther from the critical point. The extrapolation of the high-lying energy solution fails to fit the low-lying energy solution. This characteristic behavior indicates a possible phase transition to another analytic solution. The high-lying energy solution is simply deflected at the Gross-Witten point.

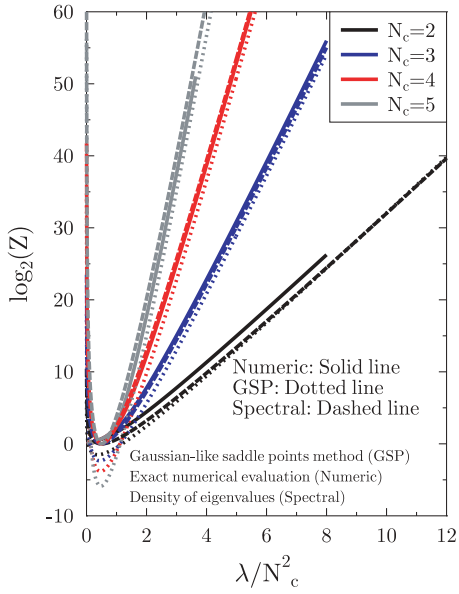

FIG. 5. (Color online) High-lying density of states for the color-singlet bag consisting of only adjoint particles vs the thermal running parameter $\frac{\lambda}{N_c^2}$ for various color numbers N_c. The asymptotic high-lying energy solutions computed using the GSP and spectral density methods over the range $\frac{\lambda}{N_c^2} \geqslant \frac{\lambda_{(\mathrm{II})\min}}{N_c^2} = \frac{1}{2}$ and their extrapolation to the small $\frac{\lambda}{N_c^2}$ are compared with the exact numerical ones.

The asymptotic low-lying energy solution versus $\tilde{\lambda}_g$ in the energy domain $\tilde{\lambda}_g \leqslant \tilde{\lambda}_{g(\mathrm{crit})}$ is displayed in Fig. 6. The asymptotic analytical solution for the low-lying energy states is basically obtained by the power expansion over $\tilde{\lambda}_g$ and the orthogonal relations in the fundamental group representation. The solution for adjoint representation is obtained by using the convolution trick and introducing the Lagrange multiplier. The exact numerical solution coincides with the asymptotic low-lying energy solution in the energy domain $\tilde{\lambda}_g \leqslant \tilde{\lambda}_{g(\mathrm{crit})}$. When the thermal running parameter reaches the Gross-Witten point $\tilde{\lambda}_{g(\mathrm{crit})} \to \tilde{\lambda}_0 = \frac{1}{2}$, it deviates from the exact numerical one, and this deviation grows significantly as $\tilde{\lambda}_g$ increases and exceeds the Gross-Witten point $\tilde{\lambda}_0 = \frac{1}{2}$. The extrapolation of the low-lying energy solution fails to fit the high-lying energy solution, and subsequently this mechanism indicates that the low-lying energy solution is deflected and a phase transition to another analytical solution takes place. To demonstrate that the analytical low-lying energy solution is a correct one, we expand it with respect to the thermal partition parameter $\tilde{\lambda}_g$. The results are displayed in Fig. 7 and show that the asymptotic analytic low-lying energy solution coincides with the exact numerical one, and when the analytical solution is truncated to a lower order it deviates from the exact numerical one significantly.

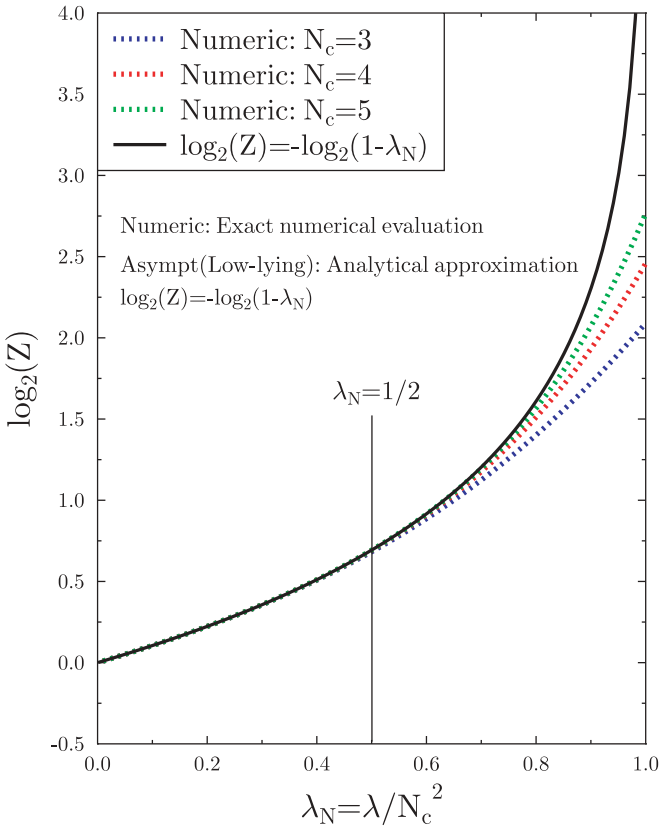

FIG. 6. (Color online) Asymptotic low-lying energy solution for a bag of adjoint particles in the color-singlet state in the limit $N_c \to \infty$ vs the thermal running parameter $\frac{\lambda}{N_c^2}$, compared with the exact numerical one for various color numbers $N_c = 3, 4$, and 5. The exact numerical solution fits the asymptotic low-lying energy solution over the range $\frac{\lambda}{N_c^2} \leqslant \frac{\lambda_{(\mathrm{II})\min}}{N_c^2} = \frac{1}{2} \leqslant \frac{\lambda_{\mathrm{crit}}}{N_c^2}$. The low-lying energy solution vanishes as $\lim_{N_c^2\to\infty} \frac{1}{N_c^2} \ln[Z_{\mathrm{low}}(\lambda/N_c^2)] \to 0$. The asymptotic high-lying energy solution $\lim_{N_c^2\to\infty} \frac{1}{N_c^2} \ln[Z_{\mathrm{high}}(\lambda/N_c^2)]$ vanishes to match the low-lying solution at the point of phase transition.

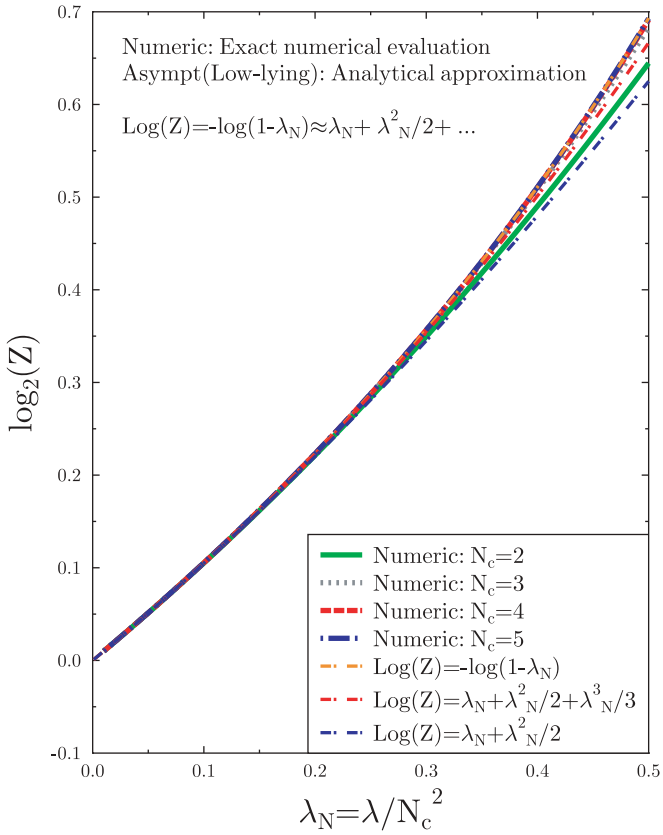

FIG. 7. (Color online) Density of states for the color-singlet fireballs (i.e., the Hagedorn states) vs the thermal running parameter $\frac{\lambda}{N_c^2}$ with various color numbers N_c. It is calculated for color-singlet bags consisting of only adjoint particles. The exact numerical solution is compared with the asymptotic low-lying energy solution with various analytic approximations for the small thermal running parameter $\frac{\lambda}{N_c^2} \leqslant \frac{\lambda_{(\mathrm{II})\min}}{N_c^2} = \frac{1}{2} \leqslant \frac{\lambda_{\mathrm{crit}}}{N_c^2}$. The exact numerical solution is found to fit the asymptotic analytic solution $Z(\lambda) = 1/(1 - \frac{\lambda}{N_c^2})$.

VII. FUNDAMENTAL AND ADJOINT REPRESENTATION FOR SU(3) AND U(3)

In the QCD, the low-lying hadronic states and the fireballs are treated as bags consisting of fundamental quark-antiquark particles and adjoint gluon particles as well. Generally speaking, the adjoint particles are assumed to be the interaction among the fundamental particles, their antiparticles, and the adjoint particles themselves. It will be a reliable approximation to treat the hadronic states as an ideal gas of fundamental and adjoint particles in the color-singlet state. It would be also a good approximation to ignore the interaction among the constituent particles in the present model.

A. Maxwell-Boltzmann statistics

For highly thermal excitations, the Maxwell-Boltzmann statistics becomes a reliable approximation. Fortunately, the Maxwell-Boltzmann statistics is also relatively simple. In the context of this statistics, the partition function for the fundamental and adjoint particles reads

$$Z(\lambda_g, \lambda_{q\bar{q}}) = \int d\mu(g) \exp\left[\lambda_g \frac{1}{\dim_g} \mathrm{tr}_c \mathbf{R}_{\mathrm{adj}}(g) + \lambda_{q\bar{q}} \frac{1}{N_c} \mathrm{tr}_c(\mathbf{R}_{\mathrm{fun}}(g) + \mathbf{R}^*_{\mathrm{fun}}(g))\right]. \quad (123)$$

To simplify our notation, we rescale the thermal running parameters $\tilde{\lambda}_g = \frac{\lambda_g}{\dim_g}$, $\dim_g = N_c^2 - 1$, and $\widetilde{\lambda}_{q\bar{q}} = \frac{\lambda_{q\bar{q}}}{N_c^2}$. With these redefinitions, the canonical ensemble is simplified to

$$Z(\lambda_g, \lambda_{q\bar{q}})|_{\mathrm{SU}(N_c)} = \int d\mu(g) \exp\left[\tilde{\lambda}_g \left\{(N_c^2 - 1) + \sum_{n=1}^{N_c}\sum_{m=1}^{N_c} \cos(\theta_n - \theta_m)\right\} + 2N_c \widetilde{\lambda}_{q\bar{q}} \sum_{n=1}^{N_c} \cos\theta_n\right]. \quad (124)$$

For the large thermal running parameter limit $\tilde{\lambda}_g \geqslant \tilde{\lambda}_{g(\mathrm{II})\mathrm{min}}$ and $\widetilde{\lambda}_{q\bar{q}} \geqslant \widetilde{\lambda}_{q\bar{q}(\mathrm{II})\mathrm{min}}$, it is straightforward to evaluate the partition function using the GSP method. In the asymptotic large $\tilde{\lambda}_g$ and $\widetilde{\lambda}_{q\bar{q}}$, the saddle points are dominated in a narrow interval around the origin. The expansion around the saddle points $\theta_i \approx 0$ reduces the partition function to

$$
\begin{aligned}
Z(\lambda_g, \lambda_{q\bar{q}})|_{\mathrm{SU}(N_c)} &= Z_{(\mathrm{II})}(\lambda_g, \lambda_{q\bar{q}})|_{\mathrm{SU}(N_c)}, \\
Z_{(\mathrm{II})}(\lambda_g, \lambda_{q\bar{q}})|_{\mathrm{SU}(N_c)} &= Z^{(0)}_{\mathrm{SU}(N_c)} \int d\mu(g) \\
&\quad \times \exp\Bigg[- \frac{2N_c\tilde{\lambda}_g}{2} \frac{1}{2N_c} \sum_{n=1}^{N_c} \sum_{m=1}^{N_c} \\
&\quad \times (\theta_n - \theta_m)^2 - \frac{2N_c\widetilde{\lambda}_{q\bar{q}}}{2} \sum_{n=1}^{N_c} \theta_n^2 \Bigg], \\
&\doteq Z^{(0)}_{\mathrm{SU}(N_c)} \int d\mu(g) \exp\Bigg[- (2N_c\widetilde{\lambda}_{q\bar{q}} \\
&\quad + 2N_c\tilde{\lambda}_g) \frac{1}{2} \sum_{n=1}^{N_c} \theta_n^2 \Bigg], \\
&\quad \left(\text{for} \left\{ \begin{array}{c} \tilde{\lambda}_g \\ \widetilde{\lambda}_{q\bar{q}} \end{array} \right\} \text{over the range} \right. \\
&\quad \left. \left\{ \begin{array}{c} \tilde{\lambda}_g \geqslant \tilde{\lambda}_{g(\mathrm{II})\mathrm{min}} \\ \widetilde{\lambda}_{q\bar{q}} \geqslant \widetilde{\lambda}_{q\bar{q}(\mathrm{II})\mathrm{min}} \end{array} \right\} \right), \qquad (125)
\end{aligned}
$$

where

$$
Z^{(0)}_{\mathrm{SU}(N_c)} = \exp\left[\left(N_c^2 - 1\right)\tilde{\lambda}_g + 2N_c^2\widetilde{\lambda}_{q\bar{q}} \right]. \qquad (126)
$$

The invariance measure is approximated to

$$
\frac{1}{2\pi} \int_{\pi}^{\pi} d\mu(g) \to \frac{1}{2\pi} \int_{-\infty}^{\infty} d\mu_{\mathrm{sp}}. \qquad (127)
$$

The Gaussian-like integration over $\mathrm{SU}(N_c)$ leads to

$$
\begin{aligned}
Z_{(\mathrm{II})}(\lambda_g, \lambda_{q\bar{q}})|_{\mathrm{SU}(N_c)} &= \frac{1}{N_c!(2\pi)^{N_c-1}} \frac{(2\pi)^{N_c/2} \prod_{n=1}^{N_c} n!}{\sqrt{2\pi N_c}} \\
&\quad \times \left(\frac{1}{2N_c(\tilde{\lambda}_g + \widetilde{\lambda}_{q\bar{q}})} \right)^{\frac{N_c^2-1}{2}} Z^{(0)}_{\mathrm{SU}(N_c)}. \qquad (128)
\end{aligned}
$$

The same calculation can be carried out in the same manner for the $\mathrm{U}(N_c)$ group. In the asymptotic large thermal running parameters $\widetilde{\lambda}_{q\bar{q}} \geqslant \widetilde{\lambda}_{q\bar{q}(\mathrm{II})\mathrm{min}}$ and $\tilde{\lambda}_g \geqslant \tilde{\lambda}_{g(\mathrm{II})\mathrm{min}}$, the canonical ensemble for $\mathrm{U}(N_c)$ becomes

$$
\begin{aligned}
Z_{(\mathrm{II})}(\lambda_g, \lambda_{q\bar{q}})|_{\mathrm{U}(N_c)} &= \frac{(2\pi)^{N_c/2} \prod_{n=1}^{N_c} n!}{N_c!(2\pi)^{N_c-1}} \frac{1}{\sqrt{2\pi}} \\
&\quad \times \left[\int_{-\pi}^{\pi} \frac{d\theta}{2\pi} e^{-\frac{2N_c\widetilde{\lambda}_{q\bar{q}}}{2}\theta^2} \right] \\
&\quad \times \frac{Z^{(0)}_{\mathrm{U}(N_c)}}{(2N_c(\tilde{\lambda}_g + \widetilde{\lambda}_{q\bar{q}}))^{\frac{N_c^2-1}{2}}}, \\
&= \frac{(2\pi)^{N_c/2} \prod_{n=1}^{N_c} n!}{N_c!(2\pi)^{N_c-1}} \frac{1}{2\pi} \frac{1}{\sqrt{2N_c\widetilde{\lambda}_{q\bar{q}}}} \\
&\quad \times \frac{Z^{(0)}_{\mathrm{U}(N_c)}}{(2N_c(\tilde{\lambda}_g + \widetilde{\lambda}_{q\bar{q}}))^{\frac{N_c^2-1}{2}}}, \qquad (129)
\end{aligned}
$$

where

$$
Z^{(0)}_{\mathrm{U}(N_c)} = \exp\left[N_c^2\tilde{\lambda}_g + 2N_c^2\widetilde{\lambda}_{q\bar{q}} \right]. \qquad (130)
$$

The canonical ensemble is simplified for a further analytical investigation. Using Stirling's approximation in the large $N_c \to \infty$ limit and approximating the summation over n to an integration over n, the canonical ensemble can be approximated to

$$
\begin{aligned}
&\lim_{N_c \to \mathrm{large}} Z(\lambda_g, \lambda_{q\bar{q}})|_{\mathrm{U}(N_c)} \\
&\quad = \lim_{N_c \to \mathrm{large}} Z_{(\mathrm{II})}(\lambda_g, \lambda_{q\bar{q}})|_{\mathrm{U}(N_c)} \\
&\quad = \frac{1}{\sqrt{2\widetilde{\lambda}_{q\bar{q}}}} \frac{\exp\left[N_c^2\tilde{\lambda}_g + 2N_c^2\widetilde{\lambda}_{q\bar{q}} - \frac{3N_c^2}{4} \right]}{(2(\tilde{\lambda}_g + \widetilde{\lambda}_{q\bar{q}}))^{\frac{N_c^2-1}{2}}}, \\
&\qquad \left(\text{for} \left\{ \begin{array}{c} \tilde{\lambda}_g \\ \widetilde{\lambda}_{q\bar{q}} \end{array} \right\} \text{over the range} \left\{ \begin{array}{c} \tilde{\lambda}_g \geqslant \tilde{\lambda}_{g(\mathrm{II})\mathrm{min}} \\ \widetilde{\lambda}_{q\bar{q}} \geqslant \widetilde{\lambda}_{q\bar{q}(\mathrm{II})\mathrm{min}} \end{array} \right\} \right). \qquad (131)
\end{aligned}
$$

In contrast, it is hard to compute the spectral density in the large $\tilde{\lambda}_g$ and $\widetilde{\lambda}_{q\bar{q}}$ limits in the context of the spectral density method. Nonetheless, in that method, the canonical ensemble can be calculated only when the spectral density is known first.

Under certain conditions when both $\tilde{\lambda}_g$ and $\widetilde{\lambda}_{q\bar{q}}$ become small, the color eigenvalues are distributed uniformly over the entire interval $-\pi \leqslant \theta_i \leqslant \pi$. In this case, the partition function in the $U(N_c)$ representation is written as

$$
\begin{aligned}
Z(\lambda_g, \lambda_{q\bar{q}}) &= \int_{-\pi}^{\pi} d\mu(g)\, e^{\lambda_g \frac{1}{\dim_g} \mathrm{tr}\,\mathbf{R}(g) \mathrm{tr}\,\mathbf{R}^*(g)} e^{\lambda_{q\bar{q}} \frac{1}{N_c} \mathrm{tr}(\mathbf{R}(g) + \mathbf{R}^*(g))} \\
&= \int_{-\pi}^{\pi} d\mu(g)\, e^{\tilde{\lambda}_g \mathrm{tr}\,\mathbf{R}(g) \mathrm{tr}\,\mathbf{R}^*(g)} e^{N_c\widetilde{\lambda}_{q\bar{q}} \mathrm{tr}(\mathbf{R}(g) + \mathbf{R}^*(g))} \\
&= \int_{-\pi}^{\pi} d\mu(g) \Bigg\{ \frac{N_c^2}{2\tilde{\lambda}_g} \int_0^{\infty} d\xi\, \xi\, e^{-\frac{N_c^2\xi^2}{4\tilde{\lambda}_g}} \\
&\quad \times e^{\frac{N_c\xi}{2} \mathrm{tr}(\mathbf{R}(g) + \mathbf{R}^*(g))} \Bigg\} e^{N_c\widetilde{\lambda}_{q\bar{q}} \mathrm{tr}(\mathbf{R}(g) + \mathbf{R}^*(g))} \\
&= \frac{N_c^2}{2\tilde{\lambda}_g} \int_0^{\infty} d\xi\, \xi\, e^{-\frac{N_c^2\xi^2}{4\tilde{\lambda}_g}} \\
&\quad \times \int_{-\pi}^{\pi} d\mu(g) \{ e^{N_c[\frac{\xi}{2} + \widetilde{\lambda}_{q\bar{q}}] \mathrm{tr}(\mathbf{R}(g) + \mathbf{R}^*(g))} \}, \qquad (132)
\end{aligned}
$$

where the Lagrange multiplier ξ has been introduced to simplify the equation. By expanding the exponential and evaluating the series term by term using the group bases orthogonality and then finally resumming the resultant terms,

the partition function is reduced to

$$Z(\lambda_g,\lambda_{q\bar{q}}) = \frac{N_c^2}{2\tilde{\lambda}_g}\int_0^{\xi_0} d\xi\xi e^{-\frac{N_c^2\xi^2}{4\tilde{\lambda}_g}} e^{N_c^2(\frac{\xi}{2}+\widetilde{\lambda}_{q\bar{q}})^2} + \frac{N_c^2}{2\tilde{\lambda}_g}\int_{\xi_0}^{\infty} d\xi\xi e^{-\frac{N_c^2\xi^2}{4\tilde{\lambda}_g}} \times\left(\frac{\exp\left[N_c^2(\xi+2\widetilde{\lambda}_{q\bar{q}})-\frac{3N_c^2}{4}\right]}{[\xi+2\widetilde{\lambda}_{q\bar{q}}]^{N_c^2/2}}\right), \quad (133)$$

where ξ_0 is determined by the constraint

$$\left(\frac{\xi_0}{2}+\widetilde{\lambda}_{q\bar{q}}\right)\ll 1 \longrightarrow \xi_0 \ll 2(1-\widetilde{\lambda}_{q\bar{q}}), \quad \text{and} \quad \widetilde{\lambda}_{q\bar{q}} \leqslant \frac{1}{2}. \quad (134)$$

This leads to an additional constraint $\xi_0 \ll 1$. It is possible to approximate Eq. (133) for the energy domain $\widetilde{\lambda}_{q\bar{q}} \leqslant \frac{1}{2}$ in the following way:

$$\begin{aligned} Z(\lambda_g,\lambda_{q\bar{q}}) &\leqslant \frac{N_c^2}{2\tilde{\lambda}_g}\left\{\int_0^{\xi_0} d\xi\xi e^{-\frac{N_c^2\xi^2}{4\tilde{\lambda}_g}}\exp\left[N_c^2\left(\frac{\xi}{2}+\widetilde{\lambda}_{q\bar{q}}\right)^2\right] + \int_{\xi_0}^{\infty} d\xi\xi e^{-\frac{N_c^2\xi^2}{4\tilde{\lambda}_g}}\exp\left[N_c^2(\xi+2\widetilde{\lambda}_{q\bar{q}})-\frac{3N_c^2}{4}\right]\right\} \\ &\leqslant \frac{N_c^2}{2\tilde{\lambda}_g}\left\{\int_0^{\xi_0} d\xi\xi e^{-\frac{N_c^2\xi^2}{4\tilde{\lambda}_g}}\exp\left[N_c^2\left(\frac{\xi}{2}+\widetilde{\lambda}_{q\bar{q}}\right)^2\right] + \int_{\xi_0}^{\infty} d\xi\xi e^{-\frac{N_c^2\xi^2}{4\tilde{\lambda}_g}}\exp\left[N_c^2\left(\frac{\xi}{2}+\widetilde{\lambda}_{q\bar{q}}\right)^2\right]\right\} \\ &= \frac{N_c^2}{2\tilde{\lambda}_g}\int_0^{\infty} d\xi\xi\exp\left[-\frac{N_c^2\xi^2}{4\tilde{\lambda}_g}+N_c^2\left(\frac{\xi}{2}+\widetilde{\lambda}_{q\bar{q}}\right)^2\right]. \end{aligned} \quad (135)$$

After evaluating the integral over the parameter ξ in Eq. (135), the partition function is approximated to

$$Z_{(\mathrm{I})}(\lambda_g,\lambda_{q\bar{q}}) = \frac{1}{1-\tilde{\lambda}_g}\exp\left[\frac{N_c^2\widetilde{\lambda}_{q\bar{q}}^2}{1-\tilde{\lambda}_g}\right] \times\left(2\int_0^{\infty} dx x e^{-(x-b_0)^2}\right), \quad (136)$$

where

$$b_0 = N_c\tilde{\lambda}_{q\bar{q}}\sqrt{\frac{\tilde{\lambda}_g}{1-\tilde{\lambda}_g}}. \quad (137)$$

The integral on the right-hand side of Eq. (136) can be approximated to

$$\begin{aligned} \int_0^{\infty} dx\, x e^{-(x-b_0)^2} &= \frac{1}{2}\left[e^{-b_0^2}+b_0\sqrt{\pi}(1+\mathrm{erf}(b_0))\right] \\ &\approx \frac{1}{2}e^{-b_0^2} \quad (\text{when } b_0 \ll 1). \end{aligned} \quad (138)$$

Using the approximation given by Eq. (138), the partition function is reduced to

$$Z_{(\mathrm{I})}(\lambda_g,\lambda_{q\bar{q}}) \approx \frac{1}{1-\tilde{\lambda}_g}\exp\left[N_c^2\widetilde{\lambda}_{q\bar{q}}^2\right]. \quad (139)$$

To verify the result, we assume that $\tilde{\lambda}_g = 0$ for a system consisting only of fundamental particles. The partition function is reduced to

$$\lim_{\tilde{\lambda}_g\to 0} Z_{(\mathrm{I})}(\lambda_g,\lambda_{q\bar{q}}) = \exp\left[N_c^2\widetilde{\lambda}_{q\bar{q}}^2\right]. \quad (140)$$

On the other hand, in the limit $\widetilde{\lambda}_{q\bar{q}} = 0$, Eq. (139) is converted to

$$\lim_{\widetilde{\lambda}_{q\bar{q}}\to 0} Z_{(\mathrm{I})}(\lambda_g,\lambda_{q\bar{q}}) = \exp[-\ln(1-\tilde{\lambda}_g)], \quad (141)$$

for a system consisting only of adjoint particles.

We are in a position to determine the critical point for the phase transition. This can be done by analyzing the canonical partition function. Solution (II) is given for the thermal running parameters over the ranges $(\tilde{\lambda}_g \geqslant \tilde{\lambda}_{g\mathrm{crit}} \geqslant \tilde{\lambda}_{g(\mathrm{II})\mathrm{min}})$ and $(\widetilde{\lambda}_{q\bar{q}} \geqslant \widetilde{\lambda}_{q\bar{q}\mathrm{crit}} \geqslant \widetilde{\lambda}_{q\bar{q}(\mathrm{II})\mathrm{min}})$. Usually this solution corresponds to the continuous high-lying hadronic mass spectrum. The logarithm of solution (II) is given by Eq. (131), and it reads

$$\lim_{N_c^2\to\mathrm{Large}}\frac{\ln Z_{(\mathrm{II})}(\tilde{\lambda}_g,\widetilde{\lambda}_{q\bar{q}})}{N_c^2} = \tilde{\lambda}_g + 2\widetilde{\lambda}_{q\bar{q}} - \frac{3}{4} - \frac{1}{2}\ln 2(\tilde{\lambda}_g+\widetilde{\lambda}_{q\bar{q}}). \quad (142)$$

This function is concave up where the minimum is located at the points $\tilde{\lambda}_{g(\mathrm{II})\mathrm{min}}$ and $\widetilde{\lambda}_{q\bar{q}(\mathrm{II})\mathrm{min}}$. However, the solution along the thermal running coupling axis in the range less than the minimum points $\tilde{\lambda}_{g(\mathrm{II})\mathrm{min}}$ and $\widetilde{\lambda}_{q\bar{q}(\mathrm{II})\mathrm{min}}$ is excluded, since it will not be physical. Usually, the running thermal parameters $\widetilde{\lambda}_{q\bar{q}}$ and $\tilde{\lambda}_g$ are not strictly independent, but rather they are functions of the variable ζ. They can be written as $\tilde{\lambda}_g(\zeta)$ and $\widetilde{\lambda}_{q\bar{q}}(\zeta)$. The variable ζ could be the hadronic mass m or V/β^3, etc. The extreme left-side threshold of the solution (II) range is determined by finding the solution's minimum location as follows:

$$\lim_{N_c^2\to\mathrm{large}}\left[\left(\frac{\partial}{\partial\tilde{\lambda}_g}\frac{\ln Z_{(\mathrm{II})}(\tilde{\lambda}_g,\widetilde{\lambda}_{q\bar{q}})}{N_c^2}\right)\frac{\partial\tilde{\lambda}_g}{\partial\zeta} + \left(\frac{\partial}{\partial\tilde{\lambda}_{q\bar{q}}}\frac{\ln Z_{(\mathrm{II})}(\tilde{\lambda}_g,\widetilde{\lambda}_{q\bar{q}})}{N_c^2}\right)\frac{\partial\widetilde{\lambda}_{q\bar{q}}}{\partial\zeta}\right]_{\zeta=\zeta_{(\mathrm{II})\mathrm{min}}} = 0. \quad (143)$$

It leads to

$$\tilde{\lambda}_g + \widetilde{\lambda}_{q\bar{q}} \geqslant \frac{1}{2}\left(\frac{\frac{\partial\tilde{\lambda}_g}{\partial\zeta}+\frac{\partial\widetilde{\lambda}_{q\bar{q}}}{\partial\zeta}}{\frac{\partial\tilde{\lambda}_g}{\partial\zeta}+2\frac{\partial\widetilde{\lambda}_{q\bar{q}}}{\partial\zeta}}\right)_{\zeta=\zeta_{(\mathrm{II})\mathrm{min}}}. \quad (144)$$

The minimum thresholds are given by

$$\begin{aligned} \widetilde{\lambda}_{q\bar{q}(\mathrm{II})\mathrm{min}} &= \widetilde{\lambda}_{q\bar{q}}(\zeta_{(\mathrm{II})\mathrm{min}}), \\ \tilde{\lambda}_{g(\mathrm{II})\mathrm{min}} &= \tilde{\lambda}_g(\zeta_{(\mathrm{II})\mathrm{min}}). \end{aligned} \quad (145)$$

However, in the case that $\widetilde{\lambda}_{q\bar{q}}$ and $\tilde{\lambda}_g$ are independent parameters, then the minimum points are determined by the

set of equations

$$\lim_{N_c^2\to\text{large}} \frac{\partial}{\partial\tilde{\lambda}_{q\bar{q}}}\left(\frac{\ln Z_{(\text{II})}(\tilde{\lambda}_g,\widetilde{\lambda}_{q\bar{q}})}{N_c^2}\right)_{\widetilde{\lambda}_{q\bar{q}}=\widetilde{\lambda}_{q\bar{q}(\text{II})\min}} = 0,$$
$$\lim_{N_c^2\to\text{large}} \frac{\partial}{\partial\tilde{\lambda}_{g}}\left(\frac{\ln Z_{(\text{II})}(\tilde{\lambda}_g,\widetilde{\lambda}_{q\bar{q}})}{N_c^2}\right)_{\tilde{\lambda}_{g}=\tilde{\lambda}_{g(\text{II})\min}} = 0. \quad (146)$$

The set of constraints for the solution (II) is given by

$$\widetilde{\lambda}_{q\bar{q}} \geqslant \widetilde{\lambda}_{q\bar{q}(\text{II})\min} = \tfrac{1}{4},$$
or
$$\tilde{\lambda}_{g} \geqslant \tilde{\lambda}_{g(\text{II})\min} = \tfrac{1}{2},$$
[The allowed range for solution (II)]. (147)

However, the number of constraints must be kept to a minimum. When the thermal running parameters $\widetilde{\lambda}_{q\bar{q}}$ and $\tilde{\lambda}_g$ are strictly independent of each other, then the the thermal running parameter $\widetilde{\lambda}_{q\bar{q}}$ for the fundamental particles is adopted as the master constraint for the minimum limit, while the constraint for $\tilde{\lambda}_g$ is restrained in order to obtain a feasible solution. Nevertheless, in the realistic QCD, both parameters $\widetilde{\lambda}_{q\bar{q}}$ and $\tilde{\lambda}_g$ depend on a characteristic variable such as the hadronic mass m or even V/β^3 as mentioned above.

On the other hand, the solution (I) that runs over the range $(0 \leqslant \widetilde{\lambda}_{q\bar{q}} \leqslant \widetilde{\lambda}_{q\bar{q}(\text{I})\max})$ and $(0 \leqslant \tilde{\lambda}_g \leqslant \tilde{\lambda}_{g(\text{I})\max})$ is given by Eq. (139). For both small $\tilde{\lambda}_{q\bar{q}}$ and $\tilde{\lambda}_g$, the solution can be approximated to Eq. (148)

$$\lim_{N_c^2\to\text{Large}} \frac{\ln Z_{(\text{I})}(\tilde{\lambda}_g,\widetilde{\lambda}_{q\bar{q}})}{N_c^2} \approx \widetilde{\lambda}_{q\bar{q}}^2, \quad (148)$$

where $\widetilde{\lambda}_{q\bar{q}}$ and $\tilde{\lambda}_g$ are again assumed to be strictly independent on each other. Solution (I) usually corresponds to the discrete low-lying hadronic mass spectrum. Furthermore, the set of constraints associated with solution (I) reads

$$\widetilde{\lambda}_{q\bar{q}}^2 \ll 1,$$
$$\to \widetilde{\lambda}_{q\bar{q}}^2 \leqslant \widetilde{\lambda}_{q\bar{q}(\text{I})\max}^2 < 1,$$
[The allowed range for solution (I)]. (149)

The critical points $\tilde{\lambda}_{q\bar{q}}$ and $\widetilde{\lambda}_g$ for the phase transition are determined at the point where the two asymptotic solutions match each other, that is,

$$\lim_{N_c^2\to\text{Large}} \frac{\ln Z_{(\text{I})}(\tilde{\lambda}_g,\widetilde{\lambda}_{q\bar{q}})}{N_c^2} = \lim_{N_c^2\to\text{Large}} \frac{\ln Z_{(\text{II})}(\tilde{\lambda}_g,\widetilde{\lambda}_{q\bar{q}})}{N_c^2} \to (\tilde{\lambda}_g,\widetilde{\lambda}_{q\bar{q}})_{\text{crit}}. \quad (150)$$

The solutions are found to match each other at the critical points

$$\widetilde{\lambda}_{q\bar{q}\text{crit}} = \tfrac{1}{2}, \quad \tilde{\lambda}_{g\text{crit}} = 0. \quad (151)$$

This solution is very interesting and is interpreted that the low-lying hadronic mass spectrum does not mix the fundamental particles and the adjoint ones significantly. The hadronic states with the constituent fundamental particles (e.g., quarks) have no significant adjoint components in the low-energy domain. This scenario explains why the low-lying hadronic mass spectrum is likely to consist of mesons and baryons and is unlikely to consist of exotic hadronic states mixed with significant gluonic components (e.g., hybrid: quarks, antiquarks, and glueballs are not common in the low-lying mass spectrum).

The second example is the QCD with $N_c = 3$ $n_{\text{fl}} = 2$. According to Eqs. (157) and (164), we have $\tilde{\lambda}_g = \frac{16}{21}\tilde{\lambda}_{q\bar{q}}$. In this example, we get from the constraint given by Eq. (150) the critical point $\widetilde{\lambda}_{q\bar{q}\text{crit}} \approx 0.6 \geqslant \widetilde{\lambda}_{q\bar{q}(\text{II})\min}$ where $\widetilde{\lambda}_{q\bar{q}(\text{II})\min} \approx 0.18$. It is shown that the low-lying solution given by Eq. (148) has not an adjoint component, and subsequently it leads to an overestimation for $\widetilde{\lambda}_{q\bar{q}\text{crit}}$. However, for a rather large adjoint component, the solution given by Eq. (148) is not appropriate for determining precisely the critical point.

To determine the threshold limit of the (pre-)critical point we can return to Eq. (125). Notice that Eq. (125) can be written as a semifundamental representation as follows:

$$Z_{(\text{II})}(\lambda_g,\lambda_{q\bar{q}})|_{\text{SU}(N_c)} \doteq Z^{(0)}_{\text{SU}(N_c)} \times \int d\mu(g) e^{-(2N_c\widetilde{\lambda}_{q\bar{q}}+2N_c\tilde{\lambda}_g)\frac{1}{2}\sum_{n=1}^{N_c}\theta_n^2},$$
$$\to Z^{(0)}_{\text{SU}(N_c)} \int d\mu(g) e^{-\frac{1}{2}(2N_c\tilde{\lambda})\sum_{n=1}^{N_c}\theta_n^2}. \quad (152)$$

The (pre-)critical point is determined by

$$\tilde{\lambda} \equiv \frac{1}{2N_c}(2N_c\widetilde{\lambda}_{q\bar{q}} + 2N_c\tilde{\lambda}_g)_{\text{crit}} = \frac{1}{2}. \quad (153)$$

This result is analogous to the critical point derived in Sec. VII. The advantage of this method is that the explicit expression for the low-lying solution is not needed and it gives the threshold limit of the critical point $\tilde{\lambda}_{(\text{pre-})\text{crit}} \leqslant \tilde{\lambda}_{\text{crit}}$. Here, we will adopt the above procedure to estimate the location of the critical point and set the correspondence $\tilde{\lambda}_{(\text{pre-})\text{crit}} \to \tilde{\lambda}_{\text{crit}}$.

The grand canonical potential for the color-singlet bags of fundamental and adjoint particles versus the thermal running parameter $\tilde{\lambda}$ with various color numbers $N_c = 2, 3, 4$, and 5 is displayed in Fig. 8. In this toy calculation, we have set $\tilde{\lambda} = \widetilde{\lambda}_{q\bar{q}} = \tilde{\lambda}_g$. The asymptotic analytical high-lying energy solution is displayed for the GSP method. The asymptotic high-lying energy solution is compared with the exact numerical solution. It is shown that the asymptotic analytical solution fits precisely the exact numerical one for the energy domain $\tilde{\lambda} \geqslant \tilde{\lambda}_{\text{crit}}$ even with a small number of colors $N_c = 2$. The extrapolation of the high-lying energy solution to the range $\tilde{\lambda} < \tilde{\lambda}_{\text{crit}}$ deviates from the exact numerical solution. This deviation becomes significant as $\tilde{\lambda}$ decreases. It is evident that the extrapolation of the high-lying energy solution to the low-lying solution is unphysical. Moreover, it is evident that the grand potential is deflected at the Gross-Witten point. Hence, the high-lying energy solution undergoes a phase transition to another analytical function that describes the low-lying energy solution more successfully.

The asymptotic analytical low-lying energy solution is displayed in Fig. 9. The low-lying energy solution is approximated by expanding the canonical ensemble as a power expansion over $\tilde{\lambda}$ and then integrating it over the entire color circle and using the Lagrange multiplier and the convolution for the adjoint particles. The low-lying energy solution fits the exact numerical one over the range $\tilde{\lambda} < \tilde{\lambda}_{\text{crit}}$ even with

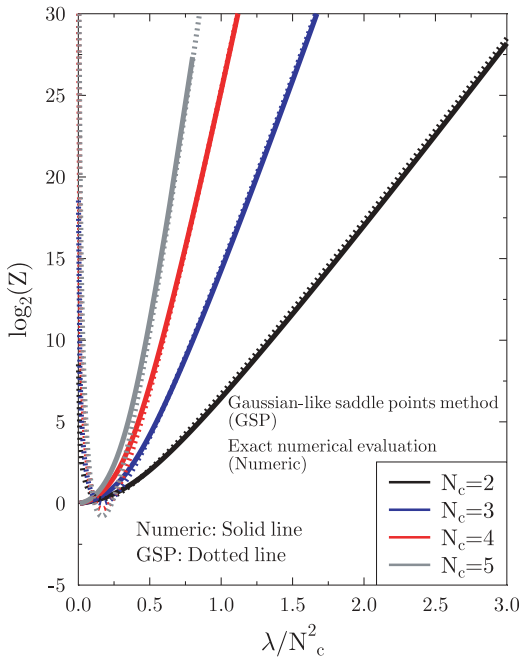

FIG. 8. (Color online) High-lying density of states and its extrapolation for the color-singlet bag consisting of fundamental and adjoint particles with the same thermal running parameter vs the thermal running parameter $\frac{\lambda}{N_c^2}$ with various color numbers N_c. The high-lying energy solution is the asymptotic solution for the thermal running parameter over the range $\frac{\lambda}{N_c^2} \geqslant \frac{\lambda_{\text{crit}}}{N_c^2} \geqslant \frac{\lambda_{(\text{pre-})\text{crit}}}{N_c^2} \geqslant \frac{\lambda_{(\text{II})\min}}{N_c^2}$. The asymptotic high-lying energy solutions are computed using the GSP and spectral density methods and compared with the exact numerical one.

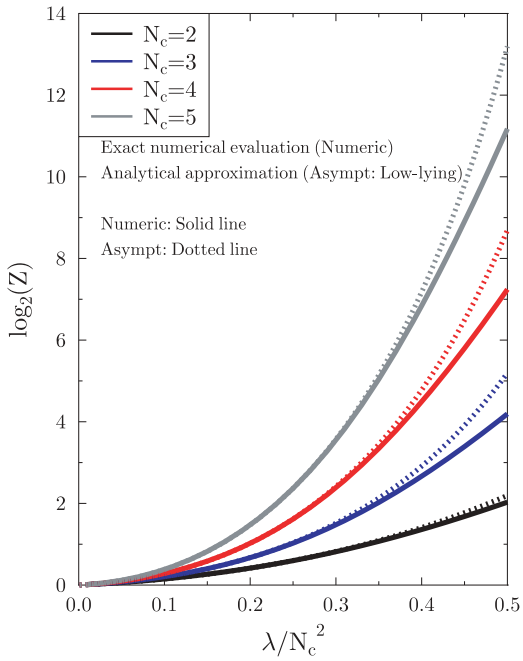

FIG. 9. (Color online) Asymptotic low-lying energy solution for color-singlet bags consisting of fundamental and adjoint particles with the same thermal running parameter $\frac{\lambda}{N_c^2}$ for both fundamental and adjoint particles vs $\frac{\lambda}{N_c^2}$ with various color numbers N_c. The exact numerical solution is compared with the analytic approximation of the low-lying energy solution for the thermal running parameter over the range $\frac{\lambda}{N_c^2} \leqslant \frac{1}{2}$. The exact numerical solution fits the approximate analytical one for small values of $\frac{\lambda}{N_c^2}$. When the thermal running parameter exceeds the (pre-)critical one $\frac{\lambda}{N_c^2} \geqslant (\frac{\lambda}{N_c^2})_{(\text{pre-})\text{crit}}$, the exact numerical solution starts to deviate slightly from the approximate analytical solution; this deviation becomes noticeable beyond the point $\frac{\lambda_{\text{crit}}}{N_c^2} = (\frac{\lambda}{N_c^2})_{\text{match}} = 0.34$.

a small number of colors $N_c = 2$. It deviates from the exact numerical solution when $\tilde{\lambda}$ increases and exceeds the critical point $\tilde{\lambda}_{q\bar{q}} + \tilde{\lambda}_g = 2\tilde{\lambda} \geqslant 2\tilde{\lambda}_{\text{crit}}$. The numerical calculations show that the split between the exact numerical solution and the low-lying energy solution [i.e., solution (I)] becomes noticeable at the point $\tilde{\lambda} = \frac{\lambda}{N_c^2} \approx 0.34 \geqslant \tilde{\lambda}_{(\text{pre-})\text{crit}} = \frac{1}{4}$ in agreement with the result of Eq. (150). Furthermore, the extrapolation of the low-lying energy solution to a larger thermal running parameter $\tilde{\lambda} > \tilde{\lambda}_{\text{crit}}$ deviates from the exact numerical solution significantly. This failure of the low-energy extrapolation indicates that the analytic solution is deflected in the middle between the low-lying and high-lying energy solutions and proves the existence of the phase transition.

To demonstrate the phase transition and the deflection point for the analytic solution, we display the low- and high-lying energy solutions and their extrapolations in Fig. 10. The asymptotic analytical solutions and their extrapolations for the entire energy domain are compared with the exact numerical one. It is shown that the low-lying energy solution fits the numerical one for the small thermal running parameter $\tilde{\lambda} \leqslant \tilde{\lambda}_{\text{crit}}$. But when the thermal running parameter $\tilde{\lambda}$ reaches the Gross-Witten critical point, the solution starts to deviate significantly from the exact numerical one as $\tilde{\lambda}$ increases and runs far from that point. On the other hand, the high-lying energy solution fits the exact numerical one for the large thermal running parameter over the range $\tilde{\lambda} \geqslant \tilde{\lambda}_{\text{crit}}$, whereas its extrapolation to small values deviates from the exact numerical one, and this deviation increases significantly as the thermal running parameter $\tilde{\lambda}$ decreases below the Gross-Witten point and approaches the origin. Evidently, the extrapolations of both solutions fail to fit the exact numerical one when they go far beyond the critical point in the opposite directions. This demonstrates how the analytical solution is smoothly deflected at the critical point. This soft deflection causes the asymptotic analytic low- and high-lying solutions to lie just above each other and reduces the intersection possibility to the minimum in any realistic rough approximations. Therefore, the Gross-Witten point is then determined midway between the smooth interpolation from the low- to high-lying energy domain or from a small to the large thermal running parameter $\tilde{\lambda}$. The exact numerical solution matches the asymptotic low-lying energy solution from the left, and then it matches the asymptotic high-lying energy solution from the right beneath this small interval around the Gross-Witten point. However, when the low-lying energy solution is not known, the extreme left-hand critical point is determined by the minimum point of the high-lying energy solution extrapolation. This point is the extreme left-hand threshold of the high-lying energy solution. This threshold point can shed light on the existence of the phase transition even for a complicated realistic physical situation

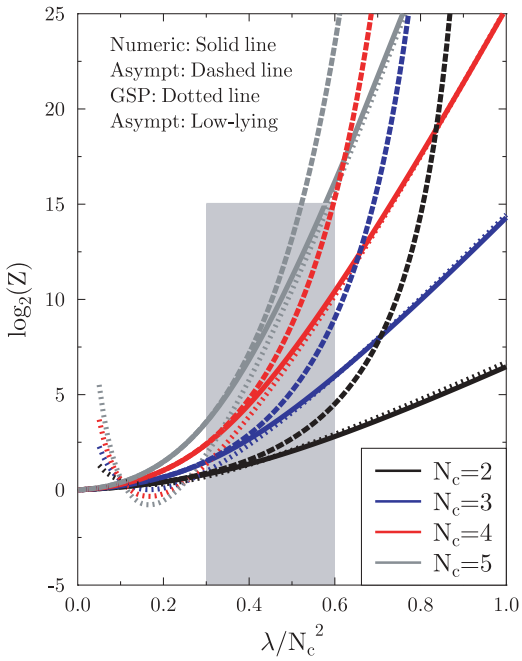

FIG. 10. (Color online) Asymptotic low- and high-lying energy solutions and their extrapolations for the color-singlet bag of fundamental and adjoint particles with the same thermal running parameter vs $\frac{\lambda}{N_c^2}$ for various color numbers N_c. The exact numerical solution fits the asymptotic low-lying energy solution over the range $\frac{\lambda}{N_c^2} \leqslant \frac{\lambda_{\rm crit}}{N_c^2}$ and fits the high-lying energy solution over the range $\frac{\lambda}{N_c^2} \geqslant \frac{\lambda_{\rm crit}}{N_c^2}$. The two solutions split by a small redundant constant at the critical point of the phase transition. This redundant small constant emerges because of the kind of approximations considered.

that cannot be solved using the spectral density method. The characteristic solutions of the low-lying and high-lying energy domains are found to be not restricted to the large $N_c \to \infty$ limit and are satisfactory even for a small number of colors $N_c = 2$.

B. Quark and gluon fireball

The hadronic states are bound states of quarks and gluons confined by a color-singlet state. The excited hadronic states are assumed to be Hagedorn states. The Hagedorn states are approximated as bags of ideal quark and gluon gases, and each bag is in the color-singlet state. In the realistic QCD, quarks are fundamental particles that satisfy the Fermi-Dirac statistics, while gluons are adjoint particles that satisfy the Bose-Einstein statistics. The canonical potential in the Fock space for quark and antiquark with an internal color structure is formalized as follows:

$$\begin{aligned}\ln Z_{q\bar{q}}(\beta, V) &= \frac{1}{N_c}\mathrm{tr}_c \sum_{\rm fl}\left(\sum_{\alpha}\ln[1+\mathbf{R}(g)e^{-\beta E_{q\alpha}}]\right.\\ &\quad\left.+\sum_{\alpha}\ln[1+\mathbf{R}^*(g)e^{-\beta E_{q\alpha}}]\right)\\ &= \frac{1}{N_c}\mathrm{tr}_c \sum_{\rm fl}\sum_{\alpha}\ln[1+(\mathbf{R}(g)\\ &\quad+\mathbf{R}^*(g))e^{-\beta E_{q\alpha}}+e^{-2\beta E_{q\alpha}}]. \end{aligned} \tag{154}$$

For the highly thermal excited hadronic states, the color saddle points become dominant over a tiny interval around the origin. These highly thermal excited states correspond to the energy domain $\lambda \geqslant \lambda_{\rm crit} \geqslant \lambda_{\rm (II)min}$ and the analog solution $Z_{\rm (II)}(\beta, V)$. In the Hagedorn Hilbert space, the quark-antiquark canonical potential is approximated to

$$\begin{aligned}\ln Z_{q\bar{q}}(\beta, V) &\approx \sum_{\rm fl}\sum_{\alpha}\ln[1+2e^{-\beta E_{q\alpha}}+e^{-2\beta E_{q\alpha}}] - \frac{1}{2}\frac{1}{N_c}\\ &\quad\times\sum_{i}^{N_c}\theta_i^2\left[\sum_{\rm fl}\sum_{\alpha}\frac{2e^{-\beta E_{q\alpha}}}{[1+2e^{-\beta E_{q\alpha}}+e^{-2\beta E_{q\alpha}}]}\right]\\ &= \Phi^{(0)}_{q\bar{q}} - \frac{1}{2}\Phi^{(2)}_{q\bar{q}}\sum_{i}^{N_c}\theta_i^2, \end{aligned} \tag{155}$$

where the following parameters are introduced to simplify our notation:

$$\begin{aligned}\Phi^{(0)}_{q\bar{q}} &= \sum_{\rm fl}\sum_{\alpha}\ln[1+2e^{-\beta E_{q\alpha}}+e^{-2\beta E_{q\alpha}}],\\ \Phi^{(2)}_{q\bar{q}} &= \frac{1}{N_c}\sum_{\rm fl}\sum_{\alpha}\frac{2e^{-\beta E_{q\alpha}}}{[1+2e^{-\beta E_{q\alpha}}+e^{-2\beta E_{q\alpha}}]}. \end{aligned} \tag{156}$$

The sum over states for an ideal gas of massless quarks and antiquarks confined in a cavity with a sharp boundary is approximated by the integration over the density of states:

$$\begin{aligned}\Phi^{(0)}_{q\bar{q}} &= (2j+1)\cdot N_c n_{\rm fl}\int\frac{Vd^3k}{(2\pi)^3}2\ln[1+e^{-\beta p}]\\ &= \frac{7\pi^2}{360}(2j+1)N_c n_{\rm fl}\frac{V}{\beta^3}, \end{aligned} \tag{157}$$

and

$$\begin{aligned}\Phi^{(2)}_{q\bar{q}} &= (2j+1)\cdot N_c n_{\rm fl}\frac{1}{N_c}\int\frac{Vd^3p}{(2\pi)^3}\frac{2e^{-\beta p}}{(1+e^{-\beta p})^2}\\ &= \frac{1}{6}(2j+1)n_{\rm fl}\frac{V}{\beta^3}, \end{aligned} \tag{158}$$

where V is the bag volume, and $(2j+1)$ comes from the spin degeneracy. Since the constituent adjoint gluons satisfy the Bose-Einstein statistics, the canonical potential for the gas of gluons reads

$$\ln Z_g(\beta, V) = -\frac{1}{\dim_g}\mathrm{tr}_c\sum_{\alpha}\ln[1-\mathbf{R}_{\rm adj}(g)e^{-\beta E_{g\alpha}}]. \tag{159}$$

The internal color structure for the SU(N_c) [or U(N_c)] symmetry group is separated and evaluated as follows

$$\begin{aligned}&\mathrm{tr}_c\{\ln[1-\lambda\mathbf{R}_{\rm adj}(g)]\}\\ &= \sum_{k=1}^{\infty}\lambda^k\mathrm{tr}_c\mathbf{R}_{\rm adj}(g^k)\\ &= \sum_{k=1}^{\infty}\lambda^k\left\{\left[\sum_{i\neq j}^{N_c}\cos k(\theta_i-\theta_j)\right]+(N_c-1)\right\}\end{aligned}$$

$$= \Re \sum_{k=1}^{\infty} \lambda^k \left\{ \left[\sum_{i \neq j}^{N_c} e^{ik(\theta_i - \theta_j)} \right] + (N_c - 1) \right\}$$
$$= \Re \left(\sum_{i \neq j}^{N_c} \ln[1 - \lambda e^{i(\theta_i - \theta_j)}] \right) + (N_c - 1) \ln[1 - \lambda]. \tag{160}$$

The approximation of the gluon canonical potential around the color saddle points, which are dominant near the origin, becomes

$$\ln Z_g(\beta, V) \approx - \sum_{\alpha} \ln[1 - e^{-\beta E_{g\alpha}}] - \frac{1}{2} \sum_{n=1}^{N_c} \sum_{m=1}^{N_c} (\theta_n - \theta_m)^2 \times \left[\frac{1}{\dim_g} \sum_{\alpha} \frac{e^{-\beta E_{g\alpha}}}{[1 - e^{-\beta E_{g\alpha}}]^2} \right],$$
$$= \Phi_g^{(0)} - \frac{1}{2} \Phi_g^{(2)} \sum_{n=1}^{N_c} \sum_{m=1}^{N_c} (\theta_n - \theta_m)^2. \tag{161}$$

The terms

$$\Phi_g^{(0)} = \sum_{\alpha} \ln[1 - e^{-\beta E_{g\alpha}}], \tag{162}$$

and

$$\Phi_g^{(2)} = \frac{1}{\dim_g} \sum_{\alpha} \frac{e^{-\beta E_{g\alpha}}}{[1 - e^{-\beta E_{g\alpha}}]^2}, \tag{163}$$

are introduced for our convenience to simplify our notation. Furthermore, we have the dimension $\dim_g = (N_c^2 - 1)$ and the color constraint $\theta_{N_c} = -\sum_{i=1}^{N_c - 1} \theta_i$ for the SU(N_c) group representation. Since the quarks and gluons are assumed to be confined in a cavity with a sharp boundary, then the summation over the energy states is performed as follows:

$$\Phi_g^{(0)} = (2j + 1) \dim_g \int \frac{V d^3k}{(2\pi)^3} \ln[1 - e^{-\beta p}]$$
$$= \frac{\pi^2}{90} (2j + 1) \dim_g \frac{V}{\beta^3}, \tag{164}$$

and

$$\Phi_g^{(2)} = (2j + 1) \int \frac{V d^3k}{(2\pi)^3} \frac{e^{-\beta k}}{[1 - e^{-\beta k}]^2}$$
$$= \frac{1}{6} (2j + 1) \frac{V}{\beta^3}. \tag{165}$$

The partition function for an ideal quark and gluon gas, which is in the color-singlet state in the Hilbert space of the Hagedorn state, is the tensor product of Fock spaces for the quark and gluon partition functions. The resultant tensor product is then projected into a color-singlet state as

$$Z_{q\bar{q}g}(\beta, V) = \int d\mu(g) Z_g(\beta, V) Z_{q\bar{q}}(\beta, V). \tag{166}$$

The integration over the Fourier color variables is evaluated by the Gaussian quadrature integration around the saddle points. In the extreme condition in the limit $\beta \to 0$, the color saddle points become dominant in a tiny range around the origin. Hence, the canonical ensemble for the highly thermal excited states is then approximated by the quadratic expansion around the saddle points as follows:

$$Z_{q\bar{q}g}(\beta, V) \approx Z_{q\bar{q}g(\mathrm{II})}(\beta, V)$$
$$Z_{q\bar{q}g(\mathrm{II})}(\beta, V) = \exp\left[\Phi_{q\bar{q}}^{(0)} + \Phi_g^{(0)}\right] \times \int d\mu(g)_{\mathrm{sp}} \exp\left[-\frac{1}{2} \Phi_{q\bar{q}}^{(2)} \sum_i^{N_c} \theta_i^2 - \frac{1}{2} \frac{\left(2N_c \Phi_g^{(2)}\right)}{2N_c} \sum_{n=1}^{N_c} \sum_{m=1}^{N_c} (\theta_n - \theta_m)^2 \right], \tag{167}$$

where the approximate Haar measure near the saddle points is embedded in the Gaussian integration. After evaluating the Gaussian-like integral over the Fourier color variables, the canonical ensemble becomes

$$Z_{q\bar{q}g(\mathrm{II})}(\beta, V) = \mathcal{N}_{q\bar{q}g} \left(\frac{1}{2N_c \Phi_g^{(2)} + \Phi_{q\bar{q}}^{(2)}} \right)^{\frac{N_c^2 - 1}{2}} \exp\left[\Phi_{q\bar{q}}^{(0)} + \Phi_g^{(0)}\right], \tag{168}$$

where the prefactor normalization is given by

$$\mathcal{N}_{q\bar{q}g} = \frac{1}{N_c! (2\pi)^{N_c - 1}} \frac{(2\pi)^{N_c/2} \prod_{k=1}^{N_c} k!}{\sqrt{2\pi N_c}}. \tag{169}$$

To be in a position to compute the microcanonical ensemble, it is appropriate to extract the thermodynamic ensembles (V, β^3) in the following way:

$$Z_{q\bar{q}g(\mathrm{II})}(\beta, V) = \mathcal{N}_{q\bar{q}g} \left(\frac{\beta^3 / V}{2N_c \tilde{\Phi}_g^{(2)} + \tilde{\Phi}_{q\bar{q}}^{(2)}} \right)^{\frac{N_c^2 - 1}{2}} \times \exp\left[\frac{V}{\beta^3} \left(\tilde{\Phi}_{q\bar{q}}^{(0)} + \tilde{\Phi}_g^{(0)} \right) \right]. \tag{170}$$

The functions $\tilde{\Phi}_{q\bar{q}}^{(0)}$, $\tilde{\Phi}_g^{(0)}$, $\tilde{\Phi}_{q\bar{q}}^{(2)}$, and $\tilde{\Phi}_g^{(2)}$ are independent of V and β and calculated by dividing the un-tilde terms by $\frac{V}{\beta^3}$,

$$\tilde{\Phi}_{q\bar{q}}^{(0)} = \Phi_{q\bar{q}}^{(0)} \Big/ \frac{V}{\beta^3},$$
$$\tilde{\Phi}_{q\bar{q}}^{(2)} = \Phi_{q\bar{q}}^{(2)} \Big/ \frac{V}{\beta^3},$$
$$\tilde{\Phi}_g^{(0)} = \Phi_g^{(0)} \Big/ \frac{V}{\beta^3}, \tag{171}$$
$$\tilde{\Phi}_g^{(2)} = \Phi_g^{(2)} \Big/ \frac{V}{\beta^3}.$$

The microcanonical ensemble is found by calculating the inverse Laplace transformation as

$$Z_{q\bar{q}g(\mathrm{II})}(W,V) = \frac{1}{2\pi i}\int_{\beta_c-i\infty}^{\beta_c+i\infty} d\beta e^{\beta W} Z_{q\bar{q}g(\mathrm{II})}(\beta,V) = \frac{\mathcal{N}_{q\bar{q}g}}{2\pi i}\int_{\beta_c-i\infty}^{\beta_c+i\infty} d\beta e^{\beta W}\beta^{\frac{3}{2}(N_c^2-1)} \times \frac{\exp\left[\frac{V}{\beta^3}\left(\tilde{\Phi}^{(0)}_{q\bar{q}}+\tilde{\Phi}^{(0)}_{g}\right)\right]}{V^{\frac{N_c^2-1}{2}}\left(2N_c\tilde{\Phi}^{(2)}_{g}+\tilde{\Phi}^{(2)}_{q\bar{q}}\right)^{\frac{N_c^2-1}{2}}}. \quad (172)$$

It is appropriate to define explicitly the following constants which are independent of β and V,

$$\tilde{\Phi}^{(0)}_{q\bar{q}g} = \left[\tilde{\Phi}^{(0)}_{q\bar{q}}+\tilde{\Phi}^{(0)}_{g}\right] = (2j+1)\left[\frac{7\pi^2}{360}N_c n_{\mathrm{fl}}+\frac{\pi^2}{90}\left(N_c^2-1\right)\right], \quad (173)$$

and

$$\tilde{\Phi}^{(2)}_{q\bar{q}}+2N_c\tilde{\Phi}^{(2)}_{g} = \tfrac{1}{6}(2j+1)[n_{\mathrm{fl}}+N_c]. \quad (174)$$

The Laplace transform is evaluated using the steepest-descent method. The Laplace saddle point is determined at the following point

$$\beta_0 = \left[\frac{3V}{W}\tilde{\Phi}^{(0)}_{q\bar{q}g}\right]^{\frac{1}{4}}. \quad (175)$$

The microcanonical ensemble for the Hagedorn states corresponds to the high-lying energy solution as follows:

$$Z_{\mathrm{Hagedorn}}(W,V) \to Z_{q\bar{q}g(\mathrm{II})}(W,V). \quad (176)$$

The microcanonical ensemble for quark and gluon bag in the color-singlet state reads

$$Z_{q\bar{q}g(\mathrm{II})}(W,V) \approx \frac{1}{2\sqrt{2\pi}}\mathcal{N}_{q\bar{q}g}N_{\tilde{\Phi}}\frac{1}{W}\left(\frac{1}{VW^3}\right)^{\frac{N_c^2-2}{8}} \times \exp\left[\frac{4}{3}\left(3\tilde{\Phi}^{(0)}_{q\bar{q}g}\right)^{\frac{1}{4}}W^{3/4}V^{1/4}\right], \quad (177)$$

where the prefactor constant $N_{\tilde{\Phi}}$ is given by

$$N_{\tilde{\Phi}} = \frac{\left(3\tilde{\Phi}^{(0)}_{q\bar{q}g}\right)^{\frac{3N_c^2-2}{8}}}{\left(2N_c\tilde{\Phi}^{(2)}_{g}+\tilde{\Phi}^{(2)}_{q\bar{q}}\right)^{\frac{N_c^2-1}{2}}}. \quad (178)$$

After scaling the bag energy with respect to its volume $x = W/V$, which is denoted as the bag energy density, the microcanonical ensemble becomes

$$Z_{q\bar{q}g(\mathrm{II})}(x,V) \equiv \frac{1}{2\sqrt{2\pi}}\mathcal{N}_{q\bar{q}g}N_{\tilde{\Phi}}V^{-\frac{N_c^2}{2}}x^{-\frac{3N_c^2+2}{8}} \times \exp\left[\frac{4}{3}\left(3\tilde{\Phi}^{(0)}_{q\bar{q}g}\right)^{\frac{1}{4}}x^{3/4}V\right]. \quad (179)$$

In the real world of the relativistic heavy ion collisions, the story is more complicated. The masses for the constituent quarks even for the light flavors do not identically vanish to zero under the Gross-Witten phase transition line to the Hagedorn phase due the chiral bound interaction. Although the constituent zero mass approximation for the light flavors is satisfactory, in particular for the hadronic phase just below the deconfinement phase transition point, the constituent strange flavor mass still deviates significantly from zero. Therefore, the inclusion of massive flavors such as strangeness degrees of freedom will drastically modify the numerical results quantitatively. The calculation of the microcanonical ensemble becomes more complicated for the massive flavors. The major trouble comes from the analytical calculation for the location of the Laplace saddle point in the steepest-descent method. In this case, after integration by parts, the quark and antiquark partition function, namely,

$$\Phi^{(0)}_{q\bar{q}} \equiv \Phi^{(0)}_{q\bar{q}}(\beta,V), \quad \Phi^{(0)}_{q\bar{q}}(\beta,V) = (2j+1)N_c n_{\mathrm{fl}}\int\frac{Vd^3k}{(2\pi)^3}2\ln\left[1+e^{-\beta\sqrt{k^2+m^2}}\right], \quad (180)$$

is reduced to

$$\Phi^{(0)}_{q\bar{q}}(\beta,V) = (2j+1)N_c n_{\mathrm{fl}}\frac{V}{\beta^3}\frac{1}{\pi^2} \times\int_0^\infty dk\frac{1}{3}\frac{\beta^4k^3}{\sqrt{\beta^2k^2+\beta^2m^2}}\frac{1}{\left[e^{\sqrt{\beta^2k^2+\beta^2m^2}}+1\right]} = (2j+1)N_c n_{\mathrm{fl}}\frac{V}{\beta^3}\frac{1}{\pi^2}I_{\Phi^{(0)}_{q\bar{q}}}(m\beta), \quad (181)$$

where the integration term reads

$$I_{\Phi^{(0)}_{q\bar{q}}}(m\beta) = \int_0^\infty dx\frac{1}{3}\frac{x^3}{\sqrt{x^2+\beta^2m^2}}\frac{1}{\left[e^{\sqrt{x^2+\beta^2m^2}}+1\right]}. \quad (182)$$

The same thing can also be done for the second-order function $\Phi^{(2)}_{q\bar{q}}$. When the mixed-grand canonical ensemble is transformed to the microcanonical ensemble, the massive flavor produces a complicated transcendental function for the stationary Laplace saddle point solution. Generally speaking, it is possible to solve the transcendental equation by the iteration. At first, the solution for the zeroth iteration is assumed to be $\beta^{(0)}_0 m = 0$. Then in the first iteration, we solve the stationary saddle point $\beta_0 = \beta^{(1)}_0$. In the second iteration, the massive flavor is considered explicitly, and then we repeat the iteration to the higher order until the convergence is achieved. This procedure is summarized as

$$\begin{aligned}&\beta m \to 0,\\ &\beta m \to \beta^{(0)}_0 m,\\ &\beta m \to \beta^{(1)}_0 m,\\ &\vdots\end{aligned} \quad (183)$$

Nonetheless, it is expected that the convergence is achieved very rapidly, and subsequently the first-order iteration is an adequate and sufficient approximation for light flavors including the strangeness. Therefore, the first-order iteration truncation $\beta m \to \beta^{(1)}_0 m$ is an appropriate one for the relativistic heavy ion collisions

$$\Phi^{(0)}_{q\bar{q}}(\beta,V) = (2j+1)N_c n_{\mathrm{fl}}\frac{V}{\beta^3}\frac{1}{\pi^2}I_{\Phi^{(0)}_{q\bar{q}}}\left(\beta^{(0)}_0 m\right). \quad (184)$$

The value of the point $\beta_0^{(0)}$ can be simplified in the context of the standard MIT bag model. After considering the bag's total energy $m = W + BV$ and the volume $V = m/4B$ constraints, the stationary point becomes

$$\beta_0^{(0)} = \left[\left(\tilde{\Phi}_{q\bar{q}}^{(0)} + \tilde{\Phi}_g^{(0)}\right)/B\right]^{\frac{1}{4}} = \frac{1}{T_\beta}. \tag{185}$$

The term T_β can be interpreted as an effective temperature for the screening mass. Alternatively, to overcome any possible complication in the microcanonical ensemble, it is possible to assume the ansatz

$$\beta m \to \frac{m}{T}, \quad \text{and} \quad T\beta \sim \mathcal{O}(1), \tag{186}$$

for the high-temperature approximation. This assumption simplifies the mixed-grand canonical ensemble significantly,

$$\Phi_{q\bar{q}}^{(0)}(\beta, V) = (2j+1)N_c n_{\text{fl}} \frac{V}{\beta^3}\frac{1}{\pi^2} I_{\Phi_{q\bar{q}}^{(0)}}\left(\frac{m}{T}\right). \tag{187}$$

An alternative assumption regarding the highly compressed hadronic matter reads

$$\beta m \propto \frac{1}{\mu} m. \tag{188}$$

Nonetheless, the density of states for the highly compressed matter at low temperature needs more consideration. In this regime, the physics is rich due to the configuration space, flavor, and/or flavor-color correlations. Furthermore, a new equation of state is expected to emerge due to the formation of the color superconductivity.

On the other hand, in the limit of low-lying energy $\beta \gg 1$ (i.e., the diluted and relatively cold matter which is analogous to the $Z_{(\text{I})}(\lambda)$ solution where $\lambda \leqslant \lambda_{\text{crit}} \leqslant \lambda_{(\text{I})\text{max}}$), the partition function for an ideal gas of quarks and antiquarks can be approximated to

$$\begin{aligned}
\ln Z_{q\bar{q}}(\beta, V) &= \text{tr}_c \sum_{\text{fl}} \sum_{\alpha} \ln[1 + \mathbf{R}(g) e^{-\beta E_{q\alpha}}] \\
&\quad + \text{tr}_c \sum_{\text{fl}} \sum_{\alpha} \ln[1 + \mathbf{R}^*(g) e^{-\beta E_{q\alpha}}] \\
&\approx \sum_{\text{fl}} \left[\text{tr}_c \mathbf{R}(g) \sum_{\alpha} e^{-\beta E_{q\alpha}} \right. \\
&\quad \left. + \text{tr}_c \mathbf{R}^*(g) \sum_{\alpha} e^{-\beta E_{q\alpha}} \right] \\
&= \sum_{\text{fl}} \left(\sum_{\alpha} e^{-\beta E_{q\alpha}} \right) \text{tr}_c[\mathbf{R}(g) + \mathbf{R}^*(g)].
\end{aligned} \tag{189}$$

The low-lying energy limit for the gluon gas reads

$$\begin{aligned}
\ln Z_g(\beta, V) &= -\text{tr}_c \sum_{\alpha} \ln[1 - \mathbf{R}_{\text{adj}}(g) e^{-\beta E_{g\alpha}}] \\
&\approx \text{tr}_c \sum_{\alpha} \mathbf{R}_{\text{adj}}(g) e^{-\beta E_{g\alpha}} \\
&= \left(\sum_{\alpha} e^{-\beta E_{g\alpha}} \right) \text{tr}_c \mathbf{R}_{\text{adj}}(g).
\end{aligned} \tag{190}$$

By substituting the following thermal running parameters

$$\begin{aligned}
\lambda_{q\bar{q}} &= \sum_{\text{fl}} \sum_{\alpha} e^{-\beta E_{q\alpha}}, \\
\lambda_g &= \sum_{\alpha} e^{-\beta E_{g\alpha}},
\end{aligned} \tag{191}$$

we get the partition function

$$\begin{aligned}
&Z_{q\bar{q}g(\text{I})}(\lambda_{q\bar{q}}, \lambda_g) \\
&= \int_{-\pi}^{\pi} d\mu(g)\, e^{\lambda_g \frac{1}{\dim g} \text{tr}_c \mathbf{R}(g) \text{tr}_c \mathbf{R}^*(g)} e^{\lambda_{q\bar{q}} \frac{1}{N_c} \text{tr}_c (\mathbf{R}(g) + \mathbf{R}^*(g))},
\end{aligned} \tag{192}$$

for the SU(N_c) group representation. This equation is similar to Eq. (132). The result reads

$$Z_{q\bar{q}g(\text{I})}(\lambda_{q\bar{q}}, \lambda_g) = \frac{1}{1 - \frac{\lambda_g}{(N_c^2 - 1)}} \exp\left[\lambda_{q\bar{q}}^2 / N_c^2\right], \tag{193}$$

where $\lambda_{q\bar{q}} = \frac{N_c}{\pi^2}\frac{(2j+1)V}{\beta^3} n_{\text{fl}}$ for massless flavors and $\lambda_g = \frac{(N_c^2-1)}{\pi^2}\frac{(2j+1)V}{\beta^3}$. This approximation is an appropriate solution over the energy domain $\lambda_{q\bar{q}} \leqslant \lambda_{q\bar{q}\text{crit}} \leqslant \lambda_{q\bar{q}(\text{I})\text{max}}$ and $\lambda_g \leqslant \lambda_{g\text{crit}} \leqslant \lambda_{g(\text{I})\text{max}}$. This result is analogous to the result given in Eq. (139). Furthermore, we have for massive flavors, the following thermal $q\bar{q}$-running parameter

$$\lambda_{q\bar{q}} = N_c n_{\text{fl}} \frac{(2j+1)V}{\beta^3} \frac{m_q^2 \beta^2}{2\pi^2} K_2(m_q \beta), \tag{194}$$

where $K_2(x)$ is a Bessel function of the second kind. For the low-lying energy with massive flavors in the limit $\beta m_q \gg 1$, the $q\bar{q}$-running parameter becomes

$$\lambda_{q\bar{q}} \approx N_c n_{\text{fl}} \frac{(2j+1)V}{\beta^3} \left(\frac{m_q \beta}{2\pi}\right)^{3/2} e^{-\beta m_q}. \tag{195}$$

Nonetheless, in the realistic case, the density of states derived from the microcanonical transformation of the low-lying mixed-canonical ensemble given by Eq. (193) will be found in Sec. VIII to be replaced by the discrete low-lying mass spectrum.

VIII. MICROCANONICAL ENSEMBLE AS A DENSITY OF STATES

The microcanonical ensemble becomes known after calculating the inverse Laplace transform of the mixed-canonical ensemble,

$$\begin{aligned}
Z(W, V) &= \frac{1}{2\pi i} \int_{\beta_c - i\infty}^{\beta_c + i\infty} d\beta e^{\beta W} Z(\beta, V), \\
&= \frac{1}{2\pi i} \int_{\beta_c - i\infty}^{\beta_c + i\infty} d\beta \exp[\beta W + \ln Z(\beta, V)].
\end{aligned} \tag{196}$$

The above integral can be computed by the steepest-descent method. In this method the integral is approximated to the Gaussian-like integral around the saddle point. The general

result reads

$$Z(W,V)=\frac{1}{2}\frac{1}{\sqrt{2\pi}}\frac{\exp[\overline{\beta}W+\ln Z(\overline{\beta},V)]}{\left[\left(\frac{1}{Z(\beta,V)}\frac{\partial Z(\beta,V)}{\partial\beta}\right)^2-\frac{1}{Z(\beta,V)}\frac{\partial^2 Z(\beta,V)}{\partial\beta^2}\right]^{1/2}_{\beta=\overline{\beta}}}, \tag{197}$$

where the saddle point $\overline{\beta}$ of the stationary condition is determined at the extremum point

$$W+\frac{1}{Z(\overline{\beta},V)}\frac{\partial Z(\beta,V)}{\partial\beta}\bigg|_{\beta=\overline{\beta}}=0. \tag{198}$$

In the standard MIT bag model, the density of states is determined for constituent particles confined in a cavity with a sharp boundary. In a realistic model, it is possible to deform the cavity's boundary. The δ function for the sharp boundary in the standard MIT bag model can be smeared by the Gaussian smoothing function. The extreme conditions in the relativistic heavy ion collisions may smooth the sharp boundary for the quark and gluon bag. Therefore, the microcanonical ensemble for the gas of bags with extended boundaries is approximated to

$$\begin{aligned}Z(W,V)&=\int dv\delta(v-V)Z(W,v)\\&=\int dv f_{\rm sm}(v-V)Z(W,v),\end{aligned} \tag{199}$$

where the boundary surface is extended by the Gaussian smoothing function

$$f_{\rm sm}(v)=\sqrt{\frac{\pi}{\Delta/W}}e^{-\frac{\Delta}{W}v^2(1-\frac{v_0}{v})^2}. \tag{200}$$

The bag's boundary becomes more extended with respect to the energy when the bag's energy increases with respect to temperature, while on the contrary, the surface turns out to be sharper for the low energy. The bag volume is proportional to its energy $v_0\propto W$. In the low-energy limit, the bag's boundary is reduced to a δ function

$$\lim_{W\to 0}f_{\rm sm}(v)=\delta(v-v_0). \tag{201}$$

Hence, the Hagedorn's density of states for the standard MIT bag with a sharp surface boundary reads

$$\rho_{\rm (II)}(m,v)=\delta\left(v-\frac{m}{4B}\right)Z(W,v), \tag{202}$$

where $W=m-Bv$. The microcanonical ensemble $Z(W,v)$ is given by Eq. (177). The density of states can be rewritten as

$$\rho_{\rm (II)}(m,v)=\delta(m-4Bv)Z(m,v). \tag{203}$$

The generalization of the microcanonical ensemble to take into account the inclusion of volume variation reads

$$\rho_{\rm (II)}(W,v)=f_{\rm sm}(v)Z(W,v). \tag{204}$$

The volume fluctuation effect is studied in detail in Ref. [28], and the bag stability needs further investigation.

A. Critical mass for the bag consisting of fundamental particles obeying Maxwell-Boltzmann statistics

The canonical ensemble for a gas with the internal color symmetry U(N_c) reads

$$\begin{aligned}Z(\beta,V)&\approx Z_{\rm (I)}(\beta,V),\\Z_{\rm (I)}(\beta,V)&=e^{N_c^2\widetilde{\lambda}^2},\\\widetilde{\lambda}&\leqslant\frac{1}{2}\leqslant\lambda_{\rm (I)max}\ll 1,\end{aligned} \tag{205}$$

and

$$\begin{aligned}Z(\beta,V)&\approx Z_{\rm (II)}(\beta,V),\\Z_{\rm (II)}(\beta,V)&=\left(\frac{1}{2\widetilde{\lambda}}\right)^{\frac{N_c^2}{2}}e^{(2N_c^2\widetilde{\lambda}-\frac{3}{4}N_c^2)},\\\widetilde{\lambda}&\geqslant\frac{1}{2}\geqslant\widetilde{\lambda}_{\rm (II)min},\end{aligned} \tag{206}$$

for the low- and high-lying energy solutions, respectively. The effective thermal running parameter $\widetilde{\lambda}$ for an ideal gas of fundamental particles embedded in the thermal bath and satisfying Maxwell-Boltzmann statistics reads

$$\begin{aligned}\widetilde{\lambda}&=\lambda/N_c^2,\\&=\frac{1}{N_c}(2j+1)\int\frac{Vd^3p}{(2\pi)^3}e^{-\beta\sqrt{p^2+m^2}}\bigg|_{m=0},\\&=\frac{1}{\pi^2}\frac{(2j+1)}{N_c}\frac{V}{\beta^3}.\end{aligned} \tag{207}$$

The low-temperature $1/\beta$ phase has a free energy of order $O(N_c^0)$. The high-temperature phase has a free energy of order $O(N_c^2)$. It is characterized by the Hagedorn growth in its density of states.

The microcanonical ensemble is computed by calculating the inverse Laplace transform as follows:

$$\begin{aligned}Z_{\rm (II)}(W,V)&=\lim_{W\to\infty}\frac{1}{2\pi i}\int_{\beta_c-i\infty}^{\beta_c+i\infty}d\beta e^{\beta W}Z_{\rm (II)}(\beta,V),\\&\qquad\left(\text{for }\widetilde{\lambda}\geqslant\frac{1}{2}\geqslant\widetilde{\lambda}_{\rm (II)min}\right),\\&=\frac{1}{2\sqrt{2\pi}}\frac{1}{\sqrt{12}N_c}\left[\frac{\pi^2N_c}{2(2j+1)}\right]^{\frac{N_c^2+1}{2}}\\&\quad\times\beta_0^{(3N_c^2+5)/2}V^{-(N_c^2+1)/2}\\&\quad\times\exp\left[\frac{4}{3}\left(\frac{6(2j+1)N_c}{\pi^2}\right)^{1/4}\right.\\&\quad\left.\times V^{1/4}W^{3/4}-\frac{3}{4}N_c^2\right].\end{aligned} \tag{208}$$

The stationary point for the steepest-descent method is found at

$$\beta_0=\left(\frac{6(2j+1)N_c}{\pi^2}\frac{V}{W}\right)^{\frac{1}{4}}. \tag{209}$$

In the microcanonical representation, the effective thermal running parameter and the energy constraint for the highly excited states are reduced to

$$\widetilde{\lambda} = \frac{1}{6N_c^2}\left(\frac{6(2j+1)N_c}{\pi^2}\right)^{1/4} W^{3/4}V^{1/4}, \\ \geqslant \frac{1}{2} \geqslant \widetilde{\lambda}_{(\mathrm{II})\min}. \tag{210}$$

In the standard MIT bag model, the effective bag mass and volume are given by the relations

$$m = W + BV, \tag{211}$$
$$m = 4BV, \tag{212}$$
$$W = \frac{3}{4}m, \tag{213}$$
$$V = \frac{m}{4B}. \tag{214}$$

In the present model, the Hagedorn states appear in the hadronic mass spectrum when the energy reaches the threshold $\widetilde{\lambda} \geqslant \widetilde{\lambda}_{(\text{pre-})\mathrm{crit}} = \frac{1}{2} \geqslant \widetilde{\lambda}_{(\mathrm{II})\min}$ and subsequently the Hagedorn mass threshold exceeds the limit

$$m \geqslant 2\sqrt{2\pi}N_c^{(1+3/4)}\left[\frac{2B}{(2j+1)}\right]^{1/4} \\ \geqslant 6.2\ \mathrm{GeV} \quad \text{with} \quad B^{1/4} = 180\ \mathrm{MeV}. \tag{215}$$

This threshold mass is relatively large due to the classical Maxwell-Boltzmann statistics considered in the present scenario.

On the other hand, the situation is rather different for the low-lying energy for the small thermal running parameter $\widetilde{\lambda} \leqslant \frac{1}{2} \leqslant \widetilde{\lambda}_{(\mathrm{I})\max}$ (usually $\widetilde{\lambda}_{(\mathrm{I})\max} < 1$), where the microcanonical ensemble is evaluated as

$$Z_{(\mathrm{I})}(W,V) = \frac{1}{2\pi\imath}\int_{\beta_c-i\infty}^{\beta_c+i\infty} d\beta e^{\beta W} Z_{(\mathrm{I})}(\beta,V) \\ = \frac{1}{2\pi\imath}\int_{\beta_c-i\infty}^{\beta_c+i\infty} d\beta e^{\beta W} e^{[d_q^2\frac{V^2}{\beta^6}]}, \tag{216}$$

where $d_q = \frac{(2j+1)}{\pi^2}$. In the standard MIT bag, we have the effective bag energy $W \approx \frac{3}{4}m$. For the energy excitation less than the threshold $\widetilde{\lambda} \leqslant \frac{1}{2} \leqslant \widetilde{\lambda}_{(\mathrm{I})\max}$, we have the low-lying hadronic mass spectrum, which ends when the energy scale reaches the critical point

$$m \leqslant m(\widetilde{\lambda}_{(\text{pre-})\mathrm{crit}}) : 6.2\ \mathrm{GeV}, \quad \text{with} \quad B^{1/4} = 180\ \mathrm{MeV}, \\ \ll m_{(\mathrm{I})\max} : 10\ \mathrm{GeV}, \tag{217}$$

where the upper limit $m_{(\mathrm{I})\max}$ will be given by Eq. (251). When the energy scale exceeds this point, the microcanonical ensemble for the low-lying hadronic states becomes inappropriate. The extrapolation of the steepest-descent approximation leads to the density of states, i.e.,

$$Z_{(\mathrm{I})}(W,V) = \frac{1}{2\sqrt{2\pi}}\frac{\left[6d_q^2\right]^{1/14}}{\sqrt{7}V^{-1/7}W^{4/7}} \\ \times \exp\left[\frac{7}{6}\left[6d_q^2\right]^{1/7}V^{2/7}W^{6/7}\right] \\ \sim (\cdots)V^{1/7}W^{-4/7}\exp[(\cdots)V^{2/7}W^{6/7}], \\ (\text{for } m \leqslant m_{(\mathrm{I})\max}). \tag{218}$$

This approximation is not valid for small W or $m \leqslant m_{(\mathrm{I})\max}$ if the low-lying spectrum is a discrete one, as will be found in the realistic physical situation in Sec. VIII B. We will assume that $m_{(\mathrm{I})\max} \geqslant m_{\mathrm{crit}} \sim m_{\mathrm{physical}}$, where $m_{\mathrm{physical}} \approx 2.0$ GeV is the maximum mass for the known physical particles found experimentally without strangeness [45]. For the low-lying hadronic mass spectrum, we have considered the density of states for the known mass spectrum particles

$$Z_{\mathrm{low}}(W,V) \to Z_{(\mathrm{I})}(W,V), \\ \rho_{\mathrm{low}}(W,V) \propto Z_{\mathrm{low}}(W,V), \\ \approx \sum_{m_i,v_i}^{m_{\mathrm{crit}}} \delta(m-m_i)\delta(v-v_i). \tag{219}$$

Nonetheless, the microcanonical extrapolation given in Eq. (218) is useful to show that the discrete hadronic low-lying mass spectrum is essential. If the standard MIT bag model with a sharp surface boundary is applied to Eq. (218), no phase transition to an explosive QGP takes place. To see this, let us adopt the standard MIT bag approximation where $W \propto V$. This consideration leads to a continuous density of states $\rho \sim (\ldots)v^{-3/7}e^{(\ldots)v^{8/7}}$. This density leads to a divergence in the isobaric partition function, and this standard approximation of the MIT bag for the low-lying mass spectrum fails. It is evident that the Hagedorn states do not appear in the low-lying mass spectrum limit. Furthermore, if we argue that the continuous density of states grows exponentially as a linear exponential growth with respect to the hadron's excluded volume, it is possible to extrapolate $V^{2/7}W^{6/7} \propto V$ or $W \propto V^{5/6}$. With this approximation, the density of states is reduced roughly speaking to $\rho \sim (\ldots)v^{-1/3}e^{(\ldots)v}$. This density gives no phase transition to the QGP. Both of the above approximations show that a continuous low-lying mass spectrum cannot generate explosive bags.

B. Critical mass for the quark and gluon fireball (e.g., Hagedorn state threshold)

In QCD, the Hagedorn state is assumed to be a bag of weakly interacting quarks and gluons confined in a color-singlet state. The canonical ensemble for a quark and gluon gas in the color-singlet state is given by Eq. (170). The logarithm of the canonical partition function is simified as follows:

$$\ln(Z_{q\bar{q}g}(V/\beta^3)) \approx \ln(Z_{q\bar{q}g(\mathrm{II})}(V/\beta^3)), \\ \ln(Z_{q\bar{q}g(\mathrm{II})}(V/\beta^3)) = \frac{V}{\beta^3}\left[\tilde{\Phi}_{q\bar{q}}^{(0)} + \tilde{\Phi}_g^{(0)}\right] \\ - \frac{N_c^2-1}{2}\ln\frac{V}{\beta^3} + \mathrm{const.}, \tag{220}$$

for the energy domain $\lambda_{q\bar{q}g} \geqslant \lambda_{q\bar{q}g(\mathrm{II})\min}$, where $\lambda_{q\bar{q}g} \propto V/\beta^3$. The critical point for the phase transition is determined by

finding the extremum left-hand point as

$$\frac{\partial}{\partial\left(\frac{V}{\beta^3}\right)} \ln Z_{q\bar{q}g(\mathrm{II})}(V/\beta^3) = 0. \tag{221}$$

The parameter $\frac{V}{\beta^3}$ is related to the running coupling parameter λ, and it determines the threshold point of a possible phase transition to the Hagedorn phase. The extreme left-hand side location for the prospective phase transition is located at

$$\frac{1}{N_c^2-1}\left(\frac{V}{\beta^3}\right)\left[\tilde{\Phi}^{(0)}_{q\bar{q}} + \tilde{\Phi}^{(0)}_{g}\right] \geqslant \frac{1}{2}. \tag{222}$$

Below the minimum left-hand side point, the solution must be already deflected to another analytical solution, and in this sense the critical point is bounded from below by the extreme left-hand side point. The minimum limit for the threshold Hagedorn mass (i.e., $m_{(\mathrm{II})\mathrm{min}}$ where $m_{\mathrm{crit}} \geqslant m_{(\mathrm{II})\mathrm{min}}$) for the phase transition from the low-lying mass spectrum to the highly excited spectrum of fireballs or more precisely the continuous Hagedorn states in the context of the microcanonical ensemble is given by the condition

$$\frac{1}{3\left(N_c^2-1\right)}\left[3\left(\tilde{\Phi}^{(0)}_{q\bar{q}} + \tilde{\Phi}^{(0)}_{g}\right) V W^3\right]^{\frac{1}{4}} \geqslant \frac{1}{2}. \tag{223}$$

The stationary point of the steepest-descent method for the inverse Laplace transform to the microcanonical ensemble is determined by Eq. (175). In the context of the standard MIT bag model with a sharp boundary surface, the point of the critical point is determined by the constraint

$$[3VW^3]^{1/4} = \frac{3m}{4B^{1/4}}. \tag{224}$$

The minimum limit for the threshold Hagedorn mass production in the context of the MIT bag with the sharp surface boundary approximation is given by the constraint

$$\begin{aligned} &\frac{(2j+1)^{1/4}}{2(N_c^2-1)}\left[\frac{7\pi^2}{360}N_c n_{\mathrm{fl}} + \frac{\pi^2}{90}(N_c^2-1)\right]^{1/4}\frac{m}{B^{1/4}} \geqslant 1, \\ &\quad \rightarrow m \geqslant m_{(\mathrm{II})\mathrm{min}} \text{ (the resultant constraint).} \end{aligned} \tag{225}$$

Hence, the threshold Hagedorn mass production for $N_c = 3$ and $B^{1/4} = 180$ MeV is given by

$$\begin{aligned} m &\geqslant m_{(\mathrm{II})\mathrm{min}}, \\ m &\geqslant 2206 \text{ MeV (one massless flavor)}, \\ &\geqslant 2029 \text{ MeV (two massless flavors)}, \\ &\geqslant 1906 \text{ MeV (three massless flavors).} \end{aligned} \tag{226}$$

The critical point for the phase transition from the discrete low-lying mass spectrum to the continuous Hagedorn density of states is located just above the maximum mass of the known hadronic particles found in the Data book [45]. The highest experimental nonstrange hadron state is roughly estimated to be $m_{\mathrm{max}} \sim 2.0$–$2.3$ GeV. The critical point exists above the minimum point solution of the Hagedorn threshold $m_{\mathrm{crit}} \geqslant m_{(\mathrm{II})\mathrm{min}}$. The estimation of the Hagedorn critical mass threshold will be given in Eqs. (270) and (271).

The low-lying mass spectrum is considered a discrete density of states that includes all the known mass spectrum particles

$$\begin{aligned} Z_{\mathrm{low}}(W,V) &= Z_{q\bar{q}g(\mathrm{I})}(W,V), \\ \rho_{\mathrm{low}}(m,v) &\sim \sum_{m_i,v_i}^{m_{\mathrm{max}}} \delta(m-m_i)\delta(v-v_i). \end{aligned} \tag{227}$$

Using the following connections between the canonical ensemble and the density of the states

$$\begin{aligned} \rho(W,V) &\propto Z_{q\bar{q}g(\mathrm{I})}(W,V) + Z_{q\bar{q}g(\mathrm{II})}(W,V), \\ &\propto Z_{\mathrm{low}}(W,V) + Z_{\mathrm{fireballs}}(W,V), \end{aligned} \tag{228}$$

the density of states for the entire hadronic states is approximated to

$$\begin{aligned} \rho(m,v) \approx &\sum_{m_i,v_i}^{m_{\mathrm{max}}} \delta(m-m_i)\delta(v-v_i) + Z_{\mathrm{fireballs}}(W,v) \\ &\times (\text{volume-mass fluctuation}), \end{aligned} \tag{229}$$

where the microcanonical ensemble $Z_{q\bar{q}g(\mathrm{II})}(W,V)$ is the continuous mass spectrum for the Hagedorn states [i.e., $Z_{\mathrm{fireballs}}(W,V)$]. In the standard MIT bag model with the sharp surface boundary, the volume-mass fluctuation is determined by the relation $\delta(m-4BV)$. For any fuzzy bag model, the volume-mass fluctuation becomes nontrivial and may change the order of the phase transition.

IX. DENSITY OF STATES

The density of states can be evaluated by using the phase-space integral. The calculation for an ideal gas of particles in finite size has been evaluated and studied without the internal color structure [3]. We use the same procedure to re-derive the density of states reached in the previous sections, in particular Sec. VII B. The density of states from the phase-space integral reads

$$\begin{aligned} \rho(W,V) = &\sum_{n=2}^{\infty} \frac{N_c^n (2j+1)^n}{n!} \\ &\times \left[\prod_{i=1}^{n} \int \frac{V d^3 p_i}{(2\pi)^3}\right] \delta\left(W - \sum_{i=1}^{n} \epsilon(\vec{p}_i)\right), \end{aligned} \tag{230}$$

where the constituent particle energy $\epsilon(\vec{p}_i) = \sqrt{\vec{p}_i^{\,2} + m^2}$, and it is reduced to $\epsilon(\vec{p}_i) \doteq |\vec{p}|$ for the massless one. Here j is the particle quantum number, and V and W are the bag volume and energy, respectively. The internal color symmetry is embedded in the phase-space integral as follows:

$$\begin{aligned} \rho(W,V) &= \sum_{n=2}^{\infty} \frac{(2j+1)^n}{n!}\left[\prod_{i=1}^{n} \mathrm{tr}[\mathbf{R}(g) + \mathbf{R}^*(g)] \int \frac{V d^3 p_i}{(2\pi)^3}\right] \\ &\quad \times \delta\left(W - \sum_{i=1}^{n} |\vec{p}_i|\right) \\ &= \sum_{n=2}^{\infty} \frac{(2j+1)^n}{n!} (\mathrm{tr}[\mathbf{R}(g) + \mathbf{R}^*(g)])^n \end{aligned}$$

$$\times \left(\frac{V}{2\pi^2}\right)^n \frac{2^n W^{3n-1}}{(3n-1)!}$$
$$= \frac{1}{W}\sum_{n=2}^{\infty} \frac{1}{n!(3n-1)!}(a_{\{W^3V\}}(\mathbf{R}))^n. \quad (231)$$

In Eq. (231), the following function has been introduced:

$$a_{\{W^3V\}}(\mathbf{R}) = \tilde{a}_{\{W^3V\}}\mathrm{tr}[\mathbf{R}(g) + \mathbf{R}^*(g)]$$
$$= \pi^2 \tilde{a}_{\{W^3V\}}\mathrm{tr}\left(\mathbf{R}(g)\int \frac{dx}{2\pi^2}x^2 e^{-x} + \mathbf{R}^*(g)\int \frac{dx}{2\pi^2}x^2 e^{-x}\right), \quad (232)$$

where

$$\tilde{a}_{\{W^3V\}} = \frac{(2j+1)}{\pi^2}[W^3V]. \quad (233)$$

The summation over the number n is approximated with the help of Stirling's formula to an integration over the variable n

$$\rho(W,V) = \frac{1}{W}\int_0^{\infty} dn \exp[n\ln(a_{\{W^3V\}}(\mathbf{R})) - \ln n! - \ln(3n-1)!]. \quad (234)$$

The above integration is evaluated using the saddle point approximation. The saddle point is found as follows

$$n \approx \left(\frac{a_{\{W^3V\}}(\mathbf{R})}{27}\right)^{\frac{1}{4}}. \quad (235)$$

In this approximation, the density of states is reduced to

$$\rho(W,V) = \frac{\sqrt{3}}{2\pi}\frac{1}{W}\exp\left[\left(\frac{256}{27}a_{\{W^3V\}}(\mathbf{R})\right)^{1/4}\right] \times C_n(W,V), \quad (236)$$

where

$$C_n(W,V) = \int_0^{\infty} dn \exp\left[-\frac{1}{2}\left(\frac{256\times 27}{a_{\{W^3V\}}(\mathbf{R})}\right)^{1/4} n^2\right]$$
$$= \frac{1}{2}\sqrt{2\pi}\left(\frac{a_{\{W^3V\}}(\mathbf{R})}{256\times 27}\right)^{1/8}. \quad (237)$$

Hence the density of states reads

$$\rho(W,V) = \frac{1}{4\sqrt{2\pi}}(3a_{\{W^3V\}}(\mathbf{R}))^{\frac{1}{8}}\frac{1}{W} \times \exp\left[\frac{4}{3}(3a_{\{W^3V\}}(\mathbf{R}))^{1/4}\right]. \quad (238)$$

After tracing over the color index for $\mathrm{U}(N_c)$ [or $\mathrm{SU}(N_c)$], Eq. (232) becomes

$$a_{\{W^3V\}}(\mathbf{R}) = 2\tilde{a}_{\{W^3V\}}\sum_{i=1}^{N_c}\cos\theta_i. \quad (239)$$

The projection over the color-singlet state reduces the density of states to

$$\rho_{\mathrm{singlet}} = \int_{-\pi}^{\pi} d\mu(g)\rho(W). \quad (240)$$

The density of states under the integral is approximated to the Gaussian-like integral over the color variables, since it dominates a tiny range around the origin along the real axis of Fourier color variables, that is,

$$\rho(W,V) = \frac{1}{4\sqrt{2\pi}}\left(6\tilde{a}_{\{W^3V\}}\sum_i^{N_c}\cos\theta_i\right)^{\frac{1}{8}}\frac{1}{W} \times \exp\left[\frac{4}{3}\left(6\tilde{a}_{\{W^3V\}}\sum_{i=1}^{N_c}\cos\theta_i\right)^{1/4}\right]$$
$$= \mathcal{C}_\rho \times \exp\left[-\frac{1}{2}\mathcal{D}_\rho\sum_{i=1}^{N_c}\theta_i^2\right], \quad (241)$$

where the preexponential coefficient reads

$$\mathcal{C}_\rho = \frac{1}{4\sqrt{2\pi}}(6N_c\tilde{a}_{\{W^3V\}})^{\frac{1}{8}}\frac{1}{W}\exp\left[\frac{4}{3}(6N_c\tilde{a}_{\{W^3V\}})^{1/4}\right]. \quad (242)$$

The exponential term is given by

$$\mathcal{D}_\rho = \frac{4}{3}\frac{1}{4N_c^{3/4}}(6\tilde{a}_{\{W^3V\}})^{1/4} = \frac{1}{3N_c}\left[\frac{6(2j+1)N_c}{\pi^2}W^3V\right]^{1/4}. \quad (243)$$

The color-singlet density of states for the groups $\mathrm{U}(N_c)$ and $\mathrm{SU}(N_c)$ is, respectively, approximated to

$$\rho_{\mathrm{singlet}}(W,V) = \mathcal{C}_\rho\int_{-\theta_c}^{\theta_c} d\mu \exp\left[-\frac{1}{2}\mathcal{D}_\rho\sum_{i=1}^{N_c}\theta_i^2\right],$$
$$\approx \frac{\prod_{n=1}^{N_c} n!}{N_c!(2\pi)^{N_c/2}} \times \left(\frac{1}{\mathcal{D}_\rho}\right)^{N_c^2/2} \times \mathcal{C}_\rho, \quad \text{for } \mathrm{U}(N_c),$$
$$\approx \frac{\prod_{n=1}^{N_c} n!}{N_c!(2\pi)^{N_c/2}}\sqrt{\frac{2\pi}{N_c}} \times \left(\frac{1}{\mathcal{D}_\rho}\right)^{(N_c^2-1)/2} \times \mathcal{C}_\rho, \quad \text{for } \mathrm{SU}(N_c), \quad (244)$$

where $\mathcal{D}_\rho/N_c \geqslant 1$. Furthermore, the approximation carried out in Eqs. (241) and (244) requires the constraint $\mathcal{D}_\rho/N_c \geqslant 1$. This is derived trivially using the analogous behavior $\rho(\tilde{\lambda}) \propto e^{2N_c^2\tilde{\lambda}}\int d\mu(g)\exp[-\frac{1}{2}(2N_c\tilde{\lambda})\sum_i\theta_i^2]$, where $\tilde{\lambda} \geqslant 1/2$. The constraint $\mathcal{D}_\rho/N_c \geqslant 1$ is exactly the same constraint given by Eq. (210). The asymptotic color-singlet density of states for the $\mathrm{U}(N_c)$ and $\mathrm{SU}(N_c)$ group representations behaves as follows

$$\rho_{\mathrm{singlet}}(W,V) \propto \frac{1}{W}\left[\frac{1}{W^3V}\right]^{\frac{N_c^2-1}{8}} \times \exp\left[\text{const.}\,(W^3V)^{1/4}\right], \quad \text{for } \mathrm{U}(N_c),$$
$$\propto \frac{1}{W}\left[\frac{1}{W^3V}\right]^{\frac{N_c^2-2}{8}} \times \exp\left[\text{const.}\,(W^3V)^{1/4}\right], \quad \text{for } \mathrm{SU}(N_c), \text{ (with constraint } \mathcal{D}_\rho/N_c \geqslant 1). \quad (245)$$

To analyze the results for the low-energy limit, it would be worthy to perform the analysis in the language of the canonical-like ensemble rather than the microcanonical ensemble. The density of states in term of the canonical-like ensemble can be defined as

$$\begin{aligned}\rho_{\text{singlet}}(W,V) &= \frac{1}{2}\frac{1}{W}\frac{1}{2\sqrt{2\pi}}(3a_{\{W^3V\}}(\mathbf{R}))^{\frac{1}{8}} \\ &\quad\times\exp\left[\frac{4}{3}(3a_{\{W^3V\}}(\mathbf{R}))^{1/4}\right] \\ &\sim \frac{1}{2}\frac{1}{W}\frac{1}{2\pi i}\int_{\zeta_0-i\infty}^{\zeta_0+i\infty} d\zeta\, e^{\zeta y} \\ &\quad\times\exp\left[\frac{1}{\zeta^3}(a_{\{W^3V\}}(\mathbf{R}))\right]_{y=1}. \quad (246)\end{aligned}$$

The projection of the color-singlet state reduces the density of states to

$$\begin{aligned}\rho_{\text{singlet}}(W,V) &\cong \frac{1}{2}\frac{1}{W}\int d\mu(g)\frac{1}{2\pi i}\int_{\zeta_0-i\infty}^{\zeta_0+i\infty} d\zeta\, e^{\zeta y} \\ &\quad\times\exp\left[\frac{1}{\zeta^3}(a_{\{W^3V\}}(\mathbf{R}))\right]_{y=1} \\ &\cong \frac{1}{2}\frac{1}{W}\frac{1}{2\pi i}\int_{\zeta_0-i\infty}^{\zeta_0+i\infty} d\zeta e^{\zeta y}\int d\mu(g) \\ &\quad\times\exp\left[\frac{1}{\zeta^3}(a_{\{W^3V\}}(\mathbf{R}))\right]_{y=1}. \quad (247)\end{aligned}$$

Hence, the analysis of the above equation becomes similar to the Gross-Witten critical point solution. For $\frac{\tilde{a}_{\{W^3V\}}}{N_c\zeta^3} \ll 1$, the color saddle points will be distributed uniformly over the invariance measure $\int_{-\pi}^{\pi} d\mu(g)$. It is evaluated as follows

$$\begin{aligned}\rho_{\text{low}}(W,V) &\cong \frac{1}{2}\frac{1}{W}\frac{1}{2\pi i}\int_{\zeta_0-i\infty}^{\zeta_0+i\infty} d\zeta\, e^{\zeta y}\int_{-\pi}^{\pi} d\mu(g) \\ &\quad\times\exp\left[\frac{\tilde{a}_{\{W^3V\}}}{\zeta^3}(\operatorname{tr}\mathbf{R}(g)+\operatorname{tr}\mathbf{R}^*(g))\right]_{y=1} \\ &= \frac{1}{2}\frac{1}{W}\frac{1}{2\pi i}\int_{\zeta_0-i\infty}^{\zeta_0+i\infty} d\zeta\, e^{\zeta y}\exp\left[\left(\frac{\tilde{a}_{\{W^3V\}}}{\zeta^3}\right)^2\right]_{y=1}, \\ &\quad\text{(i.e., continuous low-lying spectrum).} \quad (248)\end{aligned}$$

Under the constraint $\frac{\tilde{a}_{\{W^3V\}}}{N_c\zeta^3} \ll 1$, the integration over the Laplace transform is evaluated using the steepest-descent method. It is reduced to

$$\begin{aligned}\rho_{(\text{I})}(W,V) &= \rho_{\text{low}}(W,V) \\ &= \frac{1}{2}\frac{1}{W}\frac{1}{\sqrt{2\pi}}\frac{1}{\sqrt{7}}\left(6\tilde{a}^2_{\{W^3V\}}\right)^{1/14} \\ &\quad\times\exp\left[\frac{7}{6}\left(6\tilde{a}^2_{\{W^3V\}}\right)^{1/7}\right] \\ &\propto \frac{1}{2}\frac{1}{W}(W^3V)^{1/7}\exp\left[\text{const.}\,(W^3V)^{2/7}\right], \quad (249)\end{aligned}$$

where the saddle point of the stationary condition is found at

$$\bar{\zeta} = \left[6\tilde{a}^2_{\{W^3V\}}\right]^{1/7}. \quad (250)$$

The location of the saddle point must satisfy the energy constraint

$$\begin{aligned}\frac{\tilde{a}_{\{W^3V\}}}{N_c\bar{\zeta}^3} &= \frac{1}{6^{4/7}N_c^{8/7}}(6N_c\tilde{a}_{\{W^3V\}})^{1/7} \ll 1, \\ &\to \frac{1}{6N_c^2}(6N_c\tilde{a}_{\{W^3V\}})^{1/4} \ll 1, \\ &\to \frac{1}{6N_c^2}\left(\frac{6(2j+1)N_c}{\pi^2}\right)^{1/4}[W^{3/4}V^{1/4}] \ll 1, \\ &\to \left[\frac{1}{6N_c^2}\left(\frac{6(2j+1)N_cn_{\text{fl}}}{\pi^2}\right)^{1/4}[W^{3/4}V^{1/4}]\right] \ll 1, \\ &\to m \ll 10\ \text{GeV (for two flavors).} \quad (251)\end{aligned}$$

In the realistic QCD, the quarks obey Fermi-Dirac statistics, while the gluons obey Bose-Einstein statistics. The partition-like function for a gas of massless quarks and antiquarks confined in a finite size cavity with the internal color structure SU(N_c) [or U(N_c)] reads

$$\begin{aligned}a_{q\bar{q}}(\mathbf{R}) &= \frac{(2j+1)}{\pi^2}(W^3V)n_{\text{fl}}\operatorname{tr}\Bigg(\int_0^\infty dx\, x^2\ln[1+\mathbf{R}_{\text{fun}}(g)e^{-x}] \\ &\quad+\int_0^\infty dx x^2\ln[1+\mathbf{R}^*_{\text{fun}}(g)e^{-x}]\Bigg). \quad (252)\end{aligned}$$

Similarly, the partition-like function for a gas of gluons is reduced to

$$\begin{aligned}a_g(\mathbf{R}) &= -\frac{(2j+1)}{\pi^2}(W^3V) \\ &\quad\times\operatorname{tr}\left(\int_0^\infty dx\, x^2\ln[1-\mathbf{R}_{\text{adj}}(g)e^{-x}]\right). \quad (253)\end{aligned}$$

It is interesting to note here that when $\tilde{a}_{q\bar{q}}/\zeta^3 \leqslant O(1)_{\text{crit}}$ and $\tilde{a}_g/\zeta^3 \leqslant O(1)_{\text{crit}}$, the color saddle points are distributed uniformly over the entire circle. In this case, the Maxwell-Boltzmann statistics can be produced as follows:

$$\begin{aligned}\ln[1+\mathbf{R}^*_{\text{fun}}(g)e^{-x}] &\approx \mathbf{R}^*_{\text{fun}}(g)e^{-x}, \\ -\ln[1-\mathbf{R}_{\text{adj}}(g)e^{-x}] &\approx \mathbf{R}_{\text{adj}}(g)e^{-x}.\end{aligned} \quad (254)$$

On the other hand, in the case of $\tilde{a}_{q\bar{q}}/\zeta^3 > O(1)_{\text{crit}}$ and $\tilde{a}_g/\zeta^3 > O(1)_{\text{crit}}$, the color saddle points become more dominant in a narrow domain around the origin. In this domain, the partition-like function is expanded around the color saddle points. The coefficients of the expansion around the saddle points for the quark and antiquark partition-like function read

$$\begin{aligned}a_{q\bar{q}}(\mathbf{R})|_{\{\theta\}=0} &= \frac{7\pi^2}{360}N_cn_{\text{fl}}(2j+1)(W^3V), \\ \left.\frac{\partial^2 a_{q\bar{q}}(\mathbf{R})}{\partial\theta_i^2}\right|_{\{\theta\}=0} &= -\frac{1}{6}n_{\text{fl}}(2j+1)(W^3V).\end{aligned} \quad (255)$$

Moreover, the same thing can be calculated for the gluons:

$$\begin{aligned}a_g(\mathbf{R})|_{\{\theta\}=0} &= \frac{\pi^2}{90}\left(N_c^2-1\right)(2j+1)(W^3V), \\ \left.\frac{\partial^2 a_g(\mathbf{R})}{\partial(\theta_i-\theta_j)^2}\right|_{\{\theta\}=0} &= -\frac{1}{6}(2j+1)(W^3V).\end{aligned} \quad (256)$$

The coefficient of the quark, antiquark, and gluon gas is reduced to

$$a_{\{W^3V\}}(\mathbf{R}) = a_{q\bar{q}}(\mathbf{R}) + a_g(\mathbf{R}). \tag{257}$$

The coefficient of the zeroth approximation reads

$$a_{\{W^3V\}}(\mathbf{R})|_{\{\theta\}=0} = d_{q\bar{q}g} W^3 V, \tag{258}$$

where

$$d_{q\bar{q}g} = (2j+1)\left(\frac{7\pi^2}{360} N_c n_{\mathrm{fl}} + \frac{\pi^2}{90}\left(N_c^2 - 1\right)\right). \tag{259}$$

The density of states is approximated to the Gaussian-like function around the saddle points as follows:

$$\begin{aligned}\rho_{(\mathrm{II})}(W,V) &= \rho_{\mathrm{high}}(W,V) \\ &= \frac{1}{4\sqrt{2\pi}}\frac{1}{W}(3a_{\{W^3V\}}(\mathbf{R}))^{1/8} \\ &\quad \times \exp\left[\frac{4}{3}(3a_{\{W^3V\}}(\mathbf{R}))^{1/4}\right] \\ &\approx \mathcal{C}_{q\bar{q}g}(W,V)\exp\left[-\frac{1}{2}\lambda_{q\bar{q}}^{(2)}\sum_{i=1}^{N_c}\theta_i^2\right. \\ &\quad \left. -\frac{1}{2}\frac{2N_c\lambda_g^{(2)}}{2N_c}\sum_{i=1}^{N_c}\sum_{j=1}^{N_c}(\theta_i-\theta_j)^2\right],\end{aligned} \tag{260}$$

where the preexponential coefficient reads

$$\begin{aligned}\mathcal{C}_{q\bar{q}g}(W,V) &= \frac{1}{4\sqrt{2\pi}}\frac{1}{W}(3d_{q\bar{q}g}W^3V)^{1/8} \\ &\quad \times \exp\left[\frac{4}{3}(3d_{q\bar{q}g}W^3V)^{1/4}\right].\end{aligned} \tag{261}$$

The quadratic terms in the exponential read

$$\begin{aligned}\lambda_{q\bar{q}}^{(2)} &= -\left(\frac{1}{3d_{q\bar{q}g}W^3V}\right)^{3/4}\left.\frac{\partial^2 a_{q\bar{q}}(\mathbf{R})}{\partial\theta_i^2}\right|_0 \\ &= \frac{1}{(3d_{q\bar{q}g})^{3/4}}\frac{1}{6}(2j+1)n_{\mathrm{fl}}(W^3V)^{1/4},\end{aligned} \tag{262}$$

and

$$\begin{aligned}\lambda_g^{(2)} &= \left(\frac{1}{3d_{q\bar{q}g}W^3V}\right)^{3/4}\left.\frac{\partial^2 a_g(\mathbf{R})}{\partial(\theta_i-\theta_j)^2}\right|_0 \\ &= \frac{1}{(3d_{q\bar{q}g})^{3/4}}\frac{1}{6}(2j+1)(W^3V)^{1/4}.\end{aligned} \tag{263}$$

The color-singlet state for the density of states is projected as

$$\begin{aligned}\rho_{(\mathrm{II})}(W,V) &= \mathcal{C}_{q\bar{q}g}(W,V)\int_{-\theta_c}^{\theta_c} d\mu(g)\exp\left[-\frac{1}{2}\lambda_{q\bar{q}}^{(2)}\sum_{i=1}^{N_c}\theta_i^2\right. \\ &\quad \left. -\frac{1}{2}\frac{2N_c\lambda_g^{(2)}}{2N_c}\sum_{i=1}^{N_c}\sum_{j=1}^{N_c}(\theta_i-\theta_j)^2\right] \\ &\doteq \mathcal{C}_{q\bar{q}g}(W,V)\int_{-\theta_c}^{\theta_c} d\mu(g) \\ &\quad \times \exp\left[-\frac{1}{2}\left(\lambda_{q\bar{q}}^{(2)} + 2N_c\lambda_g^{(2)}\right)\sum_{i=1}^{N_c}\theta_i^2\right].\end{aligned} \tag{264}$$

The result of Eq. (264) resembles Eq. (167), and its evaluation leads to

$$\begin{aligned}\rho_{(\mathrm{II})}(W,V) &= c_{q\bar{q}g}\frac{1}{W}(3d_{q\bar{q}g}W^3V)^{1/8}\left(\frac{1}{\lambda_{q\bar{q}}^{(2)} + 2N_c\lambda_g^{(2)}}\right)^{\frac{N_c^2-1}{2}} \\ &\quad \times \exp\left[\frac{4}{3}(3d_{q\bar{q}g}W^3V)^{1/4}\right],\end{aligned} \tag{265}$$

where the constant $c_{q\bar{q}g}$ reads

$$c_{q\bar{q}g} = \frac{1}{4N_c!(2\pi)^{N_c-1/2}}\frac{(2\pi)^{N_c/2}\prod_{k=1}^{N_c}k!}{\sqrt{2\pi N_c}}. \tag{266}$$

In terms of $\tilde{\Phi}_{q\bar{q}}^{(2)}$ and $\tilde{\Phi}_g^{(2)}$, Eq. (265) becomes

$$\begin{aligned}\rho_{(\mathrm{II})}(W,V) &= c_{q\bar{q}g}\left(\frac{3d_{q\bar{q}g}}{\tilde{\Phi}_{q\bar{q}}^{(2)} + 2N_c\tilde{\Phi}_g^{(2)}}\right)^{\frac{N_c^2-1}{2}} \\ &\quad \times \frac{1}{W}\left(\frac{1}{3d_{q\bar{q}g}W^3V}\right)^{\frac{N^2-2}{8}} \\ &\quad \times \exp\left[\frac{4}{3}(3d_{q\bar{q}g}W^3V)^{1/4}\right],\end{aligned} \tag{267}$$

where

$$\begin{aligned}\lambda_{q\bar{q}}^{(2)} &= (W^3V)^{1/4}\tilde{\Phi}_{q\bar{q}}^{(2)}/(3d_{q\bar{q}g})^{3/4}, \\ \lambda_g^{(2)} &= (W^3V)^{1/4}\tilde{\Phi}_g^{(2)}/(3d_{q\bar{q}g})^{3/4}.\end{aligned} \tag{268}$$

The Hagedorn density of states is given by $\rho_{(\mathrm{II})}(W,V) = \rho_{\mathrm{high}}(W,V)\delta(m-4BV)$ for the bags with the sharp surface boundary. It is found that Eq. (267) is identical to the result given in Eq. (177). The constraint of the thermal running parameter for Eq. (264) validity is given by

$$\tilde{\lambda} \equiv \frac{1}{2N_c}\left(\lambda_{q\bar{q}}^{(2)} + 2N_c\lambda_g^{(2)}\right) \geqslant \frac{1}{2}, \tag{269}$$

where $\tilde{\lambda}_{(\text{pre-})\mathrm{crit}} = \frac{1}{2}$. Using the standard MIT bag model, we get

$$\frac{1}{2N_c}\frac{1}{24d_{q\bar{q}g}^{3/4}B^{1/4}}(2j+1)(n_{\mathrm{fl}}+2N_c)m \geqslant \frac{1}{2}, \tag{270}$$

where $(W^3V)^{1/3} = 3^{3/4}m/(4B^{1/4})$ and $B^{1/4} = 180$ MeV. Equation (225) gives the minimum mass limit $m_{(\mathrm{II})\mathrm{min}}$, while the (pre-)critical mass threshold m_{crit} is determined by Eq. (270) with the condition $m_{\mathrm{crit}} \geqslant m_{(\mathrm{II})\mathrm{min}}$. The Hagedorn mass constraint is bounded from below by the (pre-)critical mass $m \geqslant m_{\mathrm{crit}}$. Nonetheless, Eq. (270) gives the following estimations

$$\begin{aligned}m \geqslant m_{\mathrm{crit}} &= 2060\ \mathrm{MeV}\ (\text{massless flavors} : n_{\mathrm{fl}} = 1), \\ m \geqslant m_{\mathrm{crit}} &= 2315\ \mathrm{MeV}\ (\text{massless flavors} : n_{\mathrm{fl}} = 2), \\ m \geqslant m_{\mathrm{crit}} &= 2482\ \mathrm{MeV}\ (\text{massless flavors} : n_{\mathrm{fl}} = 3).\end{aligned} \tag{271}$$

It is worth noting that Eq. (225) gives the constraint for the minimum mass limit for the Hagedorn threshold production where the (pre-)critical mass determined by Eq. (270) must lie above this minimum mass limit $m_{\mathrm{crit}} \geqslant m_{(\mathrm{II})\mathrm{min}}$. According to Eqs. (226) and (271), the minimum mass threshold and the

(pre-)critical mass for the two-flavor hadronic mass spectrum are found to be $m_{\rm crit} = 2315\,{\rm MeV} \geqslant m_{\rm (II)min} = 2029\,{\rm MeV}$. The experimental data book indicates that the maximum limit for the discrete mass spectrum is estimated to be around 2250–2300 MeV. The critical mass for the production of fireballs has to be just above the the known discrete mass spectrum. The present work predicts that the maximum limit for the two-flavor discrete hadronic mass spectrum is 2315 MeV, and above this limit the continuous Hagedorn spectrum is produced.

X. GAS OF BAGS WITH VAN DER WAALS REPULSION

A. Isobaric partition function

The partition function for a gas of bags in the Maxwell-Boltzmann statistics reads

$$Z(T,V) = \sum_{N\geqslant 0} \frac{1}{N!} \prod_{i=1}^{N} Q_i(\Lambda), \tag{272}$$

where

$$Q_i(\Lambda) = \int dm_i dv_i \int \left(V - \sum_{k=1}^{N} v_k\right) \frac{d^3p_i}{(2\pi)^3} \rho(\Lambda; m_i, v_i) \times e^{-E_i/T} \Theta\left(V - \sum_{k=1}^{N} v_k\right), \tag{273}$$

and v_i, m_i, and E_i are the hadron volume, mass, and total energy, respectively. The fugacity Λ is the constraint of all possible charge conservations such as baryonic, strangeness, etc., and is given by

$$\Lambda = \{e^{i\theta_B} \ldots\} \equiv \{e^{\frac{\mu_B}{T}} \ldots\}. \tag{274}$$

The density of states given by Eq. (272) consists all the discrete known mass spectrum particles and the continuous Hagedorn density of states as follows:

$$\rho(\Lambda; m_i, v_i, \ldots) = \rho_{\rm (I)}(m, v, T, \Lambda) + \rho_{\rm (II)}(m, v, T, \Lambda), \tag{275}$$

where $\rho_{\rm (I)}(m, v, T, \Lambda)$ corresponds to the discrete low-lying hadronic mass spectrum, while $\rho_{\rm (II)}(m, v, T, \Lambda)$ corresponds to the continuous Hagedorn mass spectrum. The discrete low-lying density of states of the known mass spectrum particles reads

$$\rho_{\rm (I)}(m, v, T, \Lambda) = \sum_{i}^{\rm baryons} D_{\rm FD}(m, v, T, \Lambda_i)\delta(m - m_i)\delta(v - v_H) + \sum_{i}^{\rm mesons} D_{\rm BE}(m, v, T, \Lambda_i)\delta(m - m_i)\delta(v - v_H). \tag{276}$$

The sum runs over the baryon and meson mass spectra that are satisfying the Fermi-Dirac and Bose-Einstein statistics, respectively. The terms $D_{\rm FD}(m, v, T, \Lambda_i)$ and $D_{\rm BE}(m, v, T, \Lambda_i)$ are the degeneracies as well as the single-particle statistic ensemble functions for Fermi and Bose particles, respectively. The continuous part $\rho_{\rm (II)}(m, v, T, \Lambda)$ is the Hagedorn density of states, and these states correspond to the hadronic bubbles with relatively large hadronic masses that could emerge as fireballs just above the highest mass of the known hadronic particle without strangeness $m \geqslant 2.0$ GeV represented by the discrete low-lying mass spectrum. In the simplest approximation, there is no reason to prefer the Fermi-Dirac or Bose-Einstein statistics for the exotic hadronic states such as Hagedorn states. The Hagedorn states are assumed to obey simply the classical Maxwell-Boltzmann statistics due to their relatively large masses. The grand canonical ensemble for a gas of noninteracting multiparticle species obeys the tensor product of their Fock spaces [38],

$$Z(T,V;\Lambda) = \prod_{\rm baryons} Z(T,V) \prod_{\rm mesons} Z(T,V) \times \prod_{\rm Hagedorns} Z(T,V)\cdot\theta\left(V - \sum_i v_i\right). \tag{277}$$

To overcome the volume step function problem in Eqs. (272) and (273), the isobaric ensemble trick is introduced. The isobaric partition function is calculated by taking the Laplace transformation of the grand partition function [35–39]

$$\begin{aligned}\hat{Z}(T,s;\Lambda) &\equiv \int_0^\infty dV \exp(-sV) Z(T,V;\Lambda) \\ &= 1\Big/\left[s - \int_i \exp(-v_i s)\varphi_{\mathcal{S}}(T; m_i, \Lambda_i)\right] \\ &= 1/[s - f_{\rm hadrons}(T,s)],\end{aligned} \tag{278}$$

where v_i is the hadron's Van der Waals excluded volume. It is reduced to a continuous Van der Waals variable v for the continuous mass spectrum. The isobaric function found in the denominator in the right-hand side of Eq. (278) is decomposed as follows

$$\begin{aligned}f_{\rm hadrons}(T,s) &= \int_i \exp(-v_i s)\rho(m, v, T, \Lambda)\varphi_{\mathcal{S}}(T; m_i, \Lambda_i), \\ &= \sum_i \int \exp(-v_i s)\rho_{\rm (I)}(m_i, v_i, T, \Lambda) \\ &\quad \times \varphi_{\mathcal{S}}(T; m_i, \Lambda_i)\,({\rm discrete\ low\text{-}lying}) \\ &\quad + \int dv\, dm \exp(-vs)\rho_{\rm (II)}(m, v, T, \Lambda) \\ &\quad \times \varphi_{\mathcal{S}}(T; m, \Lambda)\,({\rm continuous\ Hagedorn}) \\ &= f_{\rm low}(T,s) + f_{\rm fireballs}(T,s).\end{aligned} \tag{279}$$

The first term $f_{\rm low}(T,s)$ denotes the isobaric function consisting of all the known hadronic mass spectrum particles and resonances as well as their antiparticles embedded in the hot and dense medium. The masses of these particles are taken from the particle data book [45]. The nonstrange hadronic spectrum consists of 76 mesons and 64 baryons. This isobaric function is given as

$$f_{\rm low}(T,s) = \sum_i^{\rm mesons} [\varphi_{\rm BE}(T; m_i, \Lambda_i^\star) + \varphi_{\rm BE}(T; m_i, \overline{\Lambda_i^\star})] + \sum_i^{\rm baryons} [\varphi_{\rm FD}(T; m_i, \Lambda_i^\star) + \varphi_{\rm FD}(T; m_i, \overline{\Lambda_i^\star})]. \tag{280}$$

The ensemble functions for single-particle species obeying the Maxwell-Boltzmann, Fermi-Dirac, and Bose-Einstein statistics, respectively, read

$$\varphi_{\rm MB}(T;m_i,\Lambda_i)=(2J_i+1)\Lambda_i\int\frac{d^3k}{(2\pi)^3}e^{-\frac{1}{T}\sqrt{k^2+m_i^2}}, \quad (281)$$

$$\varphi_{\rm FD}(T;m_i,\Lambda_i)=(2J_i+1)\int\frac{d^3k}{(2\pi)^3}\times\ln\left[1+\Lambda_i e^{-\frac{1}{T}\sqrt{k^2+m_i^2}}\right], \quad (282)$$

and

$$\varphi_{\rm BE}(T;m_i,\Lambda_i)=-(2J_i+1)\int\frac{d^3k}{(2\pi)^3}\ln\left[1-\Lambda_i e^{-\frac{1}{T}\sqrt{k^2+m_i^2}}\right], \quad (283)$$

where J_i is the quantum number stemming from the internal degrees of freedom (e.g., spin multiplicity). The effective chemical potentials read

$$\Lambda_i^\star=e^{-vs}\Lambda_i,\quad \overline{\Lambda_i^\star}=e^{-vs}\overline{\Lambda}_i, \quad (284)$$

where the isobaric pressure times the Van der Waals volume ($s\times v$) enters as an exponential prefactor of the particle fugacity. The second term in Eq. (279) corresponds to the isobaric pressure of Hagedorn bubbles. The isobaric function for a gas of Hagedorn states reads

$$f_{\rm fireballs}(T,s)=\int_{v_0}^{\infty}dv\int_{m_0}^{\infty}dm\,e^{-vs}\rho_{\rm (II)}(m,v,T,\Lambda)\times\varphi_{\rm MB}(T;m,\Lambda), \quad (285)$$

where the first integration is over the hadron mass, while the second one is over the hadron excluded volume. The asymptotic behavior of the function $\varphi_{\rm MB}(T;m,\Lambda)$ in the limit of the large bag mass $m\gg T$ reads

$$\varphi_{\rm MB}(T;m,\Lambda)=\int\frac{d^3k}{(2\pi)^3}\exp(-\sqrt{k^2+m^2}/T)=\left[\frac{m^2T}{2\pi^2}\right]K_2(m/T)\approx\left(\frac{mT}{2\pi}\right)^{3/2}e^{-m/T}. \quad (286)$$

By introducing Eq. (286) in Eq. (285), Eq. (285) is reduced to

$$f_{\rm fireballs}(T,s)=\int_{v_0}^{\infty}dv\int_{m_0}^{\infty}dm\,e^{-vs}\rho_{\rm (II)}(m,v,T,\Lambda)\times\left(\frac{mT}{2\pi}\right)^{3/2}e^{-m/T}, \quad (287)$$

where $\rho_{\rm (II)}(m,v,T,\Lambda)$ measures the mass spectral density *and* the volume fluctuation of the continuous Hagedorn states.

It is known from the property of the Laplace transformation that the asymptotic behavior of $Z(T,V)$ as $V\to\infty$ is determined by the extreme right-hand singularity of $\hat{Z}(T,s;\Lambda)$ with respect to the isobaric variable s on the real axis. We denote this singularity point by s^*. The Laplace parameter s^* plays the role of the isobaric pressure. In the thermodynamic limit $V\to\infty$, the pressure reads

$$p=T\lim_{V\to\infty}\frac{1}{V}\ln Z(T,V)=Ts^*. \quad (288)$$

The isobaric partition function with the isobaric ensembles (T,s) is convenient for a system characterized by the external pressure $p=Ts$ rather than the fixed volume V. The isobaric partition function has another singularity besides the first singular point $s_0=s^*$. This singularity is determined by the nonlinear equation $s^*=f_{\rm hadrons}(T,s^*)$ given by Eq. (278). The second pole s_c is the singularity when the isobaric function $f_{\rm fireballs}(T,s_c)$ diverges because the fireball's internal pressure exceeds the external pressure of the gas of hadrons, i.e.,

$$f_{\rm fireballs}(T,s_c)\to\infty. \quad (289)$$

The density of states for the Hagedorn states described by the standard MIT bag model with a sharp surface boundary reads

$$\rho_{\rm (II)}(m,v)=\delta(m-4Bv)Z_{{\rm (II)}q\bar{q}g}(W,v), \quad (290)$$

where $W=m-Bv$, and the microcanonical ensemble

$$Z_{{\rm (II)}q\bar{q}g}(W,v)=Cv^{-N_c^2/2}x^{-(\frac{3N_c^2+2}{8})}\exp\left[\frac{4}{3}ax^{3/4}v\right], \quad (291)$$

with $(W,v)\to(x=W/v,v)$, is the microcanonical ensemble for a quark and gluon gas projected on the color-singlet state and confined in a spherical cavity with a specific volume v. This microcanonical ensemble has been derived in Secs. VIII and IX. Hence the isobaric pressure for the continuous spectrum of the hadronic bubbles becomes

$$f_{\rm fireballs}(T,s)=\int_{v_0}^{\infty}dv\int_{m_0}^{\infty}dme^{-vs}\delta(m-4Bv)\times Z_{{\rm (II)}q\bar{q}g}(W,v)\left(\frac{mT}{2\pi}\right)^{3/2}e^{-m/T}=C'(T)\int_{v_0}^{\infty}dv\,v^{-N_c^2/2+3/2}\exp[-v(s-s_0)], \quad (292)$$

where the bag's isobaric internal pressure is given by

$$s_0=\left[\frac{4}{3}\left(\tilde{\Phi}^{(0)}_{q\bar{q}g}\right)^{\frac{1}{4}}(3B)^{3/4}-\frac{4B}{T}\right]. \quad (293)$$

The integral prefactor, which is independent of the volume fluctuation, reads

$$C'(T)=C[3B]^{-(\frac{3N_c^2+2}{8})}\left(\frac{4BT}{2\pi}\right)^{3/2}. \quad (294)$$

In the case of QCD, we have $N_c=3$, $C^\star(T)=C'(T)|_{N_c=3}$ and the isobaric pressure for the Hagedorn gas reads

$$f_{\rm fireballs}(T,s)=C^\star(T)\int_{v_0}^{\infty}dv\,v^{-3}\exp[-v(s-s_0)]. \quad (295)$$

The pressure $p=Ts^*$ is typically calculated from the isobaric function extreme right singularity. The external isobaric pressure of the hadronic gas and the pressure of the Hagedorn

gas, respectively, read

$$s^* = f_{\text{hadrons}}(T, s^*), \qquad p_{\text{fireballs}} = T \times f_{\text{fireballs}}(T, s), \tag{296}$$

where

$$f_{\text{fireballs}}(T, s) = C^\star(T) \left(\frac{z_0}{v_0}\right)^2 \int_{z_0}^{\infty} dz\, z^{-3} e^{-z}, \tag{297}$$

and

$$z_0 = v_0\,(s - s_0). \tag{298}$$

B. Order of the phase transition

To analyze the phase transition, it is useful to introduce the exponential integral function

$$z_0^n \int_{z_0}^{\infty} dz\, z^{-n-1} e^{-z} = z_0^n \Gamma(-n, z_0). \tag{299}$$

This function diverges for $n \leqslant 0$ as follows:

$$\lim_{z_0 \to 0} z_0^n \int_{z_0}^{\infty} dz\, z^{-n-1} e^{-z} = \lim_{z_0 \to 0} z_0^n \Gamma(-n, z_0) \to \text{diverge}. \tag{300}$$

For $n = 0$, it diverges logarithmically. In contrast, it converges to $1/n$ for $n > 0$. Hence, the analysis to find the order of the phase transition in the limit $s \to s_0$ becomes a straightforward one. It is useful to adopt the approximation

$$s = s_{\text{hadrons}} + C^\star(T) \int_{v_0}^{\infty} dv\, v^{-\alpha} e^{-v(s-s_0)} \Big|_{s \to s_0}, \qquad s \approx C^\star(T) \int_{v_0}^{\infty} dv\, v^{-\alpha} e^{-v(s-s_0)} \Big|_{s \to s_0}. \tag{301}$$

Indeed, Eq. (301) leads to the following conclusions [28],

$$\begin{aligned} &\text{for } \alpha > 1 : s \to \text{finite (a possible phase transition)}, \\ &\text{for } \alpha \leqslant 1 : s \to \text{diverge (no phase transition)}. \end{aligned} \tag{302}$$

In the case $\alpha \leqslant 1$, the fireball pressure diverges in the limit $s = s_0$ and subsequently the phase transition does not exist. On the other hand, for $\alpha > 1$, the fireball isobaric pressure converges in the limit $s = s_0$, though it diverges as the bag's internal isobaric pressure exceeds the hadronic external isobaric pressure $s_0 > s$, and the phase transition to an explosive QGP takes place in the system.

The order of the phase transition is determined by examining the continuation of the isobaric pressure outside and inside the Hagedorn bag and its nth derivative as well. Its derivative with respect to temperature (or any thermodynamical ensemble) reads

$$s' = (C^\star(T))' \int_{v_0}^{\infty} dv\, v^{-\alpha} e^{-v(s-s_0)} - C^\star(T)(s' - s_0') \int_{v_0}^{\infty} dv\, v^{-\alpha+1} e^{-v(s-s_0)}. \tag{303}$$

The exponential integral in Eq. (303) at the point of the phase transition leads to the following conditions:

$$\begin{aligned} (s' - s_0') &\approx \frac{\text{finite value}}{\lim_{s \to s_0} \int_{v_0}^{\infty} dv\, v^{-\alpha+1} e^{-v(s-s_0)}} \\ &= 0, \quad \text{for } 2 \geqslant \alpha > 1 \text{(a higher order phase transition)}, \\ &\neq 0, \quad \text{for } \alpha > 2 \text{ (a first-order phase transition)}. \end{aligned} \tag{304}$$

In the summary, first- and second-order phase transitions take place under the following constraints:

$$\infty \geqslant \alpha > 2, \text{ (first-order phase transition)}, \tag{305}$$

and

$$2 \geqslant \alpha > 1 + \tfrac{1}{2}, \quad \text{(second-order phase transition)}, \tag{306}$$

respectively. The nth-order phase transition takes place whenever α takes the value

$$1 + \frac{1}{n-1} \geqslant \alpha > 1 + \frac{1}{n}, \quad (n\text{th-order phase transition}). \tag{307}$$

Finally, there is no phase transition for the bag of an internal structure of

$$\alpha \leqslant 1, \text{ (no phase transition)}. \tag{308}$$

The Hagedorn bubbles considered in the present work are color-singlet states with an internal structure of $\alpha = 3$. They may appear in RHIC and LHC as fireballs (i.e., the Hagedorn states). This means that the gas of fireballs (i.e., the Hagedorn phase) undergoes a first-order phase transition to an explosive QGP. However, when the explosive QGP appears, it expands rapidly. Nevertheless, in the context of an alternative scenario, it is reasonable to assume that the colored bags could appear in the system before the appearance of an explosive QGP. The isobaric function can be written as

$$f_{\text{fireballs}}(T, s)/f_{\text{colored}}(T, s) \sim \int_{v_0}^{\infty} dv\, v^{-3} e^{-v(s-s_0)} \Big/ \int_{v_0}^{\infty} dv\, v^{-\frac{1}{2}} e^{-v(s-s_0)}. \tag{309}$$

In this case, the phase transition from the Hagedorn phase to the gas of colored bags is a first-order phase transition. The surprise in this scenario is that the phase transition from the gas of colored bags to the explosive QGP is not possible, keeping in mind that in this scenario we only consider a simple color group symmetry with no other associated symmetry. This leads to the conclusion that the explosive QGP must take place for the quark and gluon bags with some specific internal structure.

On the other hand, it is also possible to think about a gas of colored bags with a specific internal color-flavor correlation associated with additional configuration-space internal symmetry such as $O(N)$ or $SO(N)$ or even any other associated nontrivial effect. Then the generalization of the isobaric function for a gas of exotic colored bags becomes

$$f_{\text{exotic}}(T, s) \sim \int_{v_0}^{\infty} dv v^{-\alpha_e} e^{-v(s-s_0)}, \tag{310}$$

with an internal structure $\frac{1}{2} < \alpha_e \leqslant \frac{3}{2}$. Then is this scenario, it is possible that the Hagedorn gas $f(T,s)_{\text{fireballs}}/f(T,s)_{\text{exotic}}$ undergoes a higher order phase transition to a gas of non-color-singlet bags. The resultant gas of non-color-singlet bags then undergoes a higher order phase transition to an explosive QGP.

XI. ROLE OF CHIRAL PHASE TRANSITION

In this section, the role of the chiral phase transition is considered in detail. A comprehensive review of the chiral fields can be found in Ref. [46]. In the context of the Gell-Mann–Lévy model, namely, the σ model, the quark is assumed to be coupled to the chiral field of the linear σ model. The model can also be studied in the context of the Nambu–Jona-Lasinio (NJL) model in a similar way. The analysis of the chiral restoration in the context of the NJL model and color deconfinement will be considered elsewhere [47]. We can extend the Lagrangian density of the σ model of Refs. [48,49] to include the flavor chemical potentials as follows:

$$\begin{aligned}\mathcal{L} = \overline{q}\Big[& i\gamma^{\mu}\partial_{\mu} - m_0 - g_{\text{YM}}\gamma^{\mu}A_{b\mu}\tau_b - g_{\sigma}(\sigma_a\lambda_a + i\gamma_5\lambda_a\pi_a) \\ & + i\frac{1}{\beta}(\theta_B + \theta_S + \cdots)\gamma^0\Big]q + \frac{1}{2}[\partial_{\mu}\sigma_a\partial^{\mu}\sigma_a \\ & + \partial_{\mu}\pi_a\partial^{\mu}\pi_a] - \frac{1}{4}F_{b\mu\nu}F_b^{\mu\nu} - U(\sigma,\vec{\pi}),\end{aligned} \tag{311}$$

where the axial scalar and axial pseudoscalar field potential is given by

$$\begin{aligned}U(\sigma,\vec{\pi}) = & \frac{\lambda_{\sigma}^2}{8}\left[\sigma_a^2 + \pi_a^2 - f^2\right]^2 \\ & + \frac{\eta_{\sigma}}{12}\Big[\text{tr}_F[(\sigma_a\lambda_a + i\pi_a\lambda_a)(\sigma_a\lambda_a - i\pi_a\lambda_a)]^2 \\ & - \frac{1}{3}[\text{tr}_F(\sigma_a\lambda_a + i\pi_a\lambda_a)(\sigma_a\lambda_a - i\pi_a\lambda_a)]^2\Big] \\ & - \frac{\kappa^2}{2}[\det(\sigma_a\lambda_a + i\pi_a\lambda_a) + \det(\sigma_a\lambda_a - i\pi_a\lambda_a)].\end{aligned} \tag{312}$$

The non-Abelian color-gluon field reads

$$F_{b\mu\nu} = \partial_{\mu}A_{b\nu} - \partial_{\nu}A_{b\mu} - g_{\text{YM}}f_{bb'b''}A_{b'\mu}A_{b''\nu}. \tag{313}$$

The quark satisfies the color fundamental representation defined by the following group transformation $U_{\text{fun}} = \exp(\imath\theta_a\tau_a)$, where τ_a is a set of the fundamental symmetric group $\text{SU}(N_c)$ generators. On the other hand, the gluon satisfies the adjoint group representation defined by the transformation $U_{\text{adj}} = \exp(\imath\phi_a T_a)$, where T_a is the set of adjoint generators of the same group that generates the fundamental generators. Furthermore, the adjoint color parameters ϕ_a are related to the fundamental ones by the relation $\phi_a \propto (\theta_i - \theta_j)$, where the index a runs over $1, \ldots, (N_c^2 - 1)$, and the i, j indices run over $1, \ldots, N_c$. The adjoint and fundamental indices are related by $a \equiv (ij)$. The set of generators that commute with the Hamiltonian is retained with the corresponding conservative parameters set θ_i. The details will be given elsewhere [47].

The last term in the Lagrangian

$$V_{U1} = -\frac{\kappa^2}{2}[\det(\sigma_a\lambda_a + i\pi_a\lambda_a) + \det(\sigma_a\lambda_a - i\pi_a\lambda_a)] \tag{314}$$

is the $U_{\text{axial}}(1)$ symmetry breaking term. For two flavors $N_f = 2$, we have $\eta_{\sigma} = 0$. The model can be simplified further by retaining only one scalar σ field and three pseudoscalar π_i fields and the constant $\kappa^2 = 0$ of the axial symmetry breaking term. The easiest way to analyze the chiral phase is to adopt the mean-field approximation by replacing the σ and π_i fields by the their expectation values or condensations $\sigma \approx \langle\sigma\rangle$ and $\pi_i \approx \langle\pi_i\rangle$, respectively. The trivial example is the set for the symmetric nuclear matter $\langle\pi_i\rangle = 0$. Finally, we neglect the interaction between the gluons and quarks by setting the non-Abelian coupling constant to $g_{\text{YM}} = 0$. The small coupling g_{YM} can be treated perturbatively [47].

The effective chiral Lagrangian reads

$$\mathcal{L} = \mathcal{L}_{q\overline{q}} + \mathcal{L}_g + \mathcal{L}_{\sigma}. \tag{315}$$

The quark term becomes

$$\begin{aligned}\mathcal{L}_{q\overline{q}} &\approx \overline{q}\left[i\gamma^{\mu}\partial_{\mu} - m_q^*(\sigma) + i\frac{1}{\beta}\theta_B\gamma^0\right]q \\ &\doteq \overline{q}\left[i\gamma^{\mu}\partial_{\mu} - m_q^*(\langle\sigma\rangle) + i\frac{1}{\beta}\frac{\mu_B}{T}\gamma^0\right]q,\end{aligned} \tag{316}$$

where the chiral constituent quark mass is given by $m_q^*(\langle\sigma\rangle) = m_0 + g_{\sigma}\langle\sigma\rangle$, while the conservative charge parameter such as the baryonic charge is defined by $\imath\theta_B = \frac{\mu_B}{T}$. Hereinafter, we shall neglect the chemical potential μ_B, because we are interested in the phase transition along the temperature axis for the diluted and hot nuclear matter. The hot hadronic matter at zero baryonic density simplifies the calculations drastically. The gluon-Lagrangian part in the limit of zero coupling constant, $g_{\text{YM}} = 0$, is reduced to

$$\mathcal{L}_g \approx -\tfrac{1}{4}F^a_{\mu\nu}F^{a\mu\nu}, \tag{317}$$

where the color-gluon field becomes

$$F^a_{\mu\nu} = \partial_{\mu}A^a_{\nu} - \partial_{\nu}A^a_{\mu}. \tag{318}$$

There is an additional term in the Lagrangian due the chiral interaction. This chiral-Lagrangian term is responsible for the chiral restoration phase transition at high temperature. The chiral-Lagrangian reads

$$\mathcal{L}_{\sigma} \approx \tfrac{1}{2}\partial_{\mu}\sigma\partial^{\mu}\sigma - U(\sigma) \doteq -U(\langle\sigma\rangle). \tag{319}$$

Hereinafter, the mean-field brackets are discarded and redefined as $\langle\sigma\rangle = \sigma$.

The partition function for a gas of quarks and gluons and chiral source is given by a tensor product of the quark, the gluon, and the chiral field Fock spaces:

$$Z_{q\overline{q}g\sigma}(\beta, V; \sigma) = Z_{q\overline{q}}(\beta, V; \sigma) \cdot Z_g(\beta, V) \cdot Z_{\sigma}(\beta, V; \sigma). \tag{320}$$

However, the chiral potential is to be subtracted from the quark and gluon bag energy when the microcanonical ensemble is computed. The whole idea is that the hadronic bags are

embedded in the chiral field background, and the constituent quarks are coupled to the external chiral field.

The color-singlet state is projected as

$$\begin{aligned} Z_{\text{singlet}\sigma}(\beta, V;\sigma) &= \int d\mu(g) Z_{q\bar{q}g\sigma}(\beta, V;\sigma), \\ &= \int d\mu(g) Z_{q\bar{q}}(\beta, V;\sigma)\cdot Z_g(\beta, V) \\ &\quad \times Z_\sigma(\beta, V;\sigma), \\ &= \left[\int d\mu(g) Z_{q\bar{q}}(\beta, V;\sigma)\cdot Z_g(\beta, V)\right] \\ &\quad \times Z_\sigma(\beta, V;\sigma). \end{aligned} \tag{321}$$

The quark-antiquark partition function with an internal color degree of freedom is given by

$$\begin{aligned} Z_{q\bar{q}}(\beta, V;\sigma) = \exp\Bigg[(2j+1)\frac{1}{N_c}\text{tr}_c \int \frac{V d^3\vec{p}}{(2\pi)^3} \\ \times \ln\left[1 + (\mathbf{R}_{\text{fun}}(g) + \mathbf{R}^*_{\text{fun}}(g)) e^{-\beta\sqrt{\vec{p}^2+m_q^{*2}(\sigma)}}\right. \\ \left. + e^{-2\beta\sqrt{\vec{p}^2+m_q^{*2}(\sigma)}}\right]\Bigg]. \end{aligned} \tag{322}$$

The gluon partition function is not modified by the chiral field, and it reads

$$\begin{aligned} Z_g(\beta, V) = \exp\Bigg[-\frac{(2j+1)}{N_c^2-1}\text{tr}_c \int \frac{V d^3\vec{p}}{(2\pi)^3} \\ \times \ln\left[1 - \mathbf{R}_{\text{adj}}(g) e^{-\beta\sqrt{\vec{p}^2+m_g^{*2}}}\right]\Bigg], \end{aligned} \tag{323}$$

where the gluon mass remains $m_g = 0$ in the hadronic phase. Finally, the σ energy partition function is calculated from the σ potential as

$$Z_\sigma(\beta, V;\sigma) = e^{-\beta V U(\sigma)}. \tag{324}$$

The microcanonical ensemble is calculated by finding the inverse Laplace transform of the mixed-canonical ensemble

$$Z(W, V;\sigma) = \frac{1}{2\pi i}\int_{\beta_c - i\infty}^{\beta_c + i\infty} d\beta\, e^{\beta W} Z_{\text{singlet}\sigma}(\beta, V;\sigma). \tag{325}$$

The σ-potential background is to be subtracted from the bag energy in order to correctly scale the quark and gluon bag energy. The σ field is the scalar chiral field interaction among the bags, and it is coupled to the constituent quarks. The quark and gluon bag energy $\widetilde{W}$ is scaled and redefined as

$$\widetilde{W} = W - V U_\sigma(\sigma). \tag{326}$$

Hence, the microcanonical ensemble of the chiral quark and gluon bag is calculated as

$$\begin{aligned} Z(\widetilde{W}, V;\sigma) &= \frac{1}{2\pi i}\int_{\beta_c - i\infty}^{\beta_c + i\infty} d\beta\, e^{\beta\widetilde{W} + \beta V U_{\sigma(\sigma)}} Z_{\text{singlet}\sigma}(\beta, V;\sigma) \\ &= \frac{1}{2\pi i}\int_{\beta_c - i\infty}^{\beta_c + i\infty} d\beta\, e^{\beta\widetilde{W}} e^{\beta V U_{\sigma(\sigma)}} Z_{\text{singlet}\sigma}(\beta, V;\sigma). \end{aligned} \tag{327}$$

The resultant microcanonical ensemble given by Eq. (327) is equivalent to starting from the beginning with a mixed-canonical ensemble as a tensor product of the Fock spaces of chiral quark and gluon projected in the color-singlet state as

$$Z(\widetilde{W}, V;\sigma) = \frac{1}{2\pi i}\int_{\beta_c - i\infty}^{\beta_c + i\infty} d\beta\, e^{\beta\widetilde{W}} Z_{\text{singlet}}(\beta, V;\sigma), \tag{328}$$

where $\widetilde{W}$ is the quark and gluon bag energy, while the chiral color-singlet mixed-canonical partition function is given by

$$\begin{aligned} Z_{\text{singlet}}(\beta, V;\sigma) &= \int d\mu(g) Z_{q\bar{q}}(\beta, V;\sigma)\cdot Z_g(\beta), \\ &= \int d\mu(g) Z_{q\bar{q}g}(\beta, V;\sigma). \end{aligned} \tag{329}$$

It is demonstrated in Secs. VII and VIII that the nonchiral hadronic phase undergoes a third-order phase transition from a hadronic gas dominated by the low-lying mass spectrum to another hadronic gas dominated by the continuous Hagedorn mass spectrum. It is interpreted that low-lying mass spectrum corresponds to the discrete hadronic mass spectrum found experimentally and consisting of meson, baryons, and any exotic hadronic mass spectrum that could be found in the data book [45]. On the other hand, the Hagedorn states are the highly excited metastable hadronic states produced just above the discrete low-lying mass spectrum. The density of states for the continuous Hagedorn mass spectrum is calculated from the microcanonical ensemble. In the calculation of the color-singlet canonical ensemble, the multi-integrations over the colors are performed. The standard procedure is to adopt the saddle points approximation. In the limit of chiral Hagedorn states, the quark and gluon canonical ensemble is approximated by expanding the exponential around the color saddle points up to the quadratic term similar to the same procedure performed on the nonchiral Hagedorn states. The quadratic expansion of the chiral quark ensemble given by Eq. (322) with respect to the color saddle points reads

$$\ln Z_{q\bar{q}}(\beta, V, \sigma) = \Phi^{(0)}_{q\bar{q}\sigma} - \frac{1}{2}\Phi^{(2)}_{q\bar{q}\sigma}\sum_{i=1}^{N_c}\theta_i^2. \tag{330}$$

The coefficients of the zeroth and quadratic terms read, respectively,

$$\begin{aligned} \Phi^{(0)}_{q\bar{q}\sigma} &= 2N_c \int \frac{V d^3\vec{p}}{(2\pi)^3} 2\ln\left[1 + e^{-\beta\sqrt{\vec{p}^2+m_q^{*2}(\sigma)}}\right] \\ &= \frac{V}{\beta^3}\frac{2N_c}{\pi^2}\int_0^\infty dx\, x^2 \ln\left(1 + e^{-\sqrt{x^2+\beta^2 m_q^{*2}(\sigma)}}\right) \\ &= \frac{V}{\beta^3}\widetilde{\Phi}^{(0)}_{q\bar{q}\sigma}(\beta m_q^*(\sigma)) \\ &= \frac{V}{\beta^3}\widetilde{\Phi}^{(0)}_{q\bar{q}\sigma}(\overline{\beta} m_q^*(\sigma)), \end{aligned} \tag{331}$$

and

$$\begin{aligned} \Phi^{(2)}_{q\bar{q}\sigma} &= 2N_c \frac{1}{N_c}\int \frac{V d^3\vec{p}}{(2\pi)^3} \frac{2e^{-\beta\sqrt{\vec{p}^2+m_q^{*2}(\sigma)}}}{\left(1 + e^{-\beta\sqrt{\vec{p}^2+m_q^{*2}(\sigma)}}\right)^2} \\ &= \frac{V}{\beta^3}\frac{2}{\pi^2}\int_0^\infty dx x^2 \frac{e^{-\sqrt{x^2+\beta^2 m_\sigma^{*2}(\sigma)}}}{\left(1 + e^{-\sqrt{x^2+\beta^2 m_\sigma^{*2}(\sigma)}}\right)^2} \end{aligned}$$

$$= \frac{V}{\beta^3}\widetilde{\Phi}^{(2)}_{q\bar{q}\sigma}(\beta m^*_q(\sigma)) = \frac{V}{\beta^3}\widetilde{\Phi}^{(2)}_{q\bar{q}\sigma}(\overline{\beta} m^*_q(\sigma)), \tag{332}$$

where $m^*_\sigma(\sigma) = (m_0 + g_\sigma\sigma)$. The first-order term is not needed in the expansion thanks to the saddle point constraint of extremization.

The same thing can be performed for the gluon part given by Eq. (323). The only difference is that in the gluon ensemble, the expansion is carried over the adjoint color variables rather the fundamental ones as in the chiral quark-antiquark ensemble. The gluonic quadratic color expansion is identical to that found in the nonchiral Hagedorn, that is,

$$\ln Z_g(\beta) = \Phi^{(0)}_g - \frac{1}{2}\Phi^{(2)}_g \sum_{n=1}^{N_c}\sum_{m=1}^{N_c}(\theta_n - \theta_m)^2, \tag{333}$$

where

$$\Phi^{(0)}_g = \frac{V}{\beta^3}\widetilde{\Phi}^{(0)}_g, \quad \text{where} \quad \widetilde{\Phi}^{(0)}_g = 2\left(N_c^2 - 1\right)\frac{\pi^2}{90}, \qquad \Phi^{(2)}_g = \frac{V}{\beta^3}\widetilde{\Phi}^{(2)}_g, \quad \text{where} \quad \widetilde{\Phi}^{(2)}_g = \frac{1}{3}. \tag{334}$$

The resultant mixed-canonical ensemble that generates the density of states for the color-singlet chiral Hagedorn in Eq. (329) is approximated to

$$Z_{\text{singlet}}(\beta, V; \sigma) \approx \int d\mu(g)_{\text{sp}} Z_{q\bar{q}}(\beta, V; \sigma) Z_g(\beta, V), \tag{335}$$

where $\int d\mu(g)_{\text{sp}}$ is the invariance measure given by the GSP method and Eq. (22). After evaluating the multi-integrations over the color variables using the saddle points approximation, the chiral color-singlet mixed-canonical ensemble is reduced to

$$Z_{(\text{II})q\bar{q}g}(\beta, V; \sigma) = \mathcal{N}_{q\bar{q}g}\left(\frac{\beta^3/V}{2N_c\tilde{\Phi}^{(2)}_g + \widetilde{\Phi}^{(2)}_{q\bar{q}\sigma}(\overline{\beta} m^*_\sigma)}\right)^{\frac{N_c^2-1}{2}} \times \exp\left[\frac{V}{\beta^3}\left(\widetilde{\Phi}^{(0)}_{q\bar{q}\sigma}(\overline{\beta} m^*_\sigma) + \widetilde{\Phi}^{(0)}_g\right)\right], \tag{336}$$

where the prefactor normalization coefficient $\mathcal{N}_{q\bar{q}g}$ is identical to the nonchiral mixed-canonical ensemble given by Eq. (169).

The chiral color-singlet microcanonical ensemble is found by calculating the inverse Laplace transform of the mixed-canonical ensemble as

$$Z_{(\text{II})q\bar{q}g}(W, V; \sigma) = \mathcal{N}_{q\bar{q}g}\frac{1}{2\pi i}\int_{\beta_c - i\infty}^{\beta_c + i\infty} d\beta e^{\beta W}\beta^{\frac{3}{2}(N_c^2-1)} \times \left(\frac{1/V}{2N_c\widetilde{\Phi}^{(2)}_g + \widetilde{\Phi}^{(2)}_{q\bar{q}\sigma}(\overline{\beta} m^*_\sigma)}\right)^{\frac{N_c^2-1}{2}} \times \exp\left[\frac{V}{\beta^3}\left(\widetilde{\Phi}^{(0)}_{q\bar{q}\sigma}(\overline{\beta} m^*_\sigma) + \widetilde{\Phi}^{(0)}_g\right)\right]. \tag{337}$$

The inverse Laplace transform is evaluated using the steepest-descent method. The Laplace stationary saddle point is determined by extremizing the exponential under the integral in Eq. (337) with respect to the Laplace transform variable β. Unfortunately, the solution of the Laplace saddle point is found to be a transcendental one and cannot be written in a closed form. However, we are concerned with the solution near the chiral restoration phase transition where the constituent quark masses approach their current ones. In the limit of small constituent quark masses such as light flavors, the Laplace saddle point is found by iteration. In this kind of transcendental problem, the solution converges rapidly. The saddle point solution is found as follows:

$$\begin{aligned}
\beta_0^{(1)} &= \left[\frac{3V}{W}\left(\widetilde{\Phi}^{(0)}_{q\bar{q}\sigma}(\overline{\beta} m^*_\sigma \approx 0) + \tilde{\Phi}^{(0)}_g\right)\right]^{\frac{1}{4}}, \\
\beta_0^{(2)} &= \left[\frac{3V}{W}\left(\widetilde{\Phi}^{(0)}_{q\bar{q}\sigma}\left(\beta_0^{(1)} m^*_\sigma\right) + \tilde{\Phi}^{(0)}_g\right)\right]^{\frac{1}{4}}, \\
&\vdots \\
\beta_0 &\approx \beta_0^{(I_n)}, \quad \text{and} \quad \overline{\beta} \approx \beta^{(I_n - 1)},
\end{aligned} \tag{338}$$

where I_n is the number of iteration. In the present kind of transcendental equation, we assume that the value $\beta_0 = \beta_0^{(2)}$ (i.e., $I_n = 2$ and $\overline{\beta} = \beta_0^{(1)}$) is a sufficient approximation in the limit below but close to the chiral restoration phase transition with small constituent quark masses such as up and down flavors. This approximation is also justified for the strangeness. The microcanonical ensemble takes the form

$$Z_{(\text{II})q\bar{q}g}(W, V; \sigma) = \frac{1}{2\sqrt{2\pi}}\mathcal{N}_{q\bar{q}g}N_{\tilde{\Phi}}V^{-\frac{(N_c^2-2)}{8}}W^{-\frac{(3N_c^2+2)}{8}} \times \exp\left[\frac{4}{3}\left(\tilde{\Phi}^{(0)}_{q\bar{q}g\sigma}(\overline{\beta} m^*_\sigma)\right)^{\frac{1}{4}}W^{3/4}V^{1/4}\right], \tag{339}$$

for the chiral color-singlet bag of quarks and gluons. The preexponential coefficient $N_{\tilde{\Phi}}$ is dimensionless and reads

$$N_{\tilde{\Phi}} = \frac{\left(\widetilde{\Phi}^{(0)}_{q\bar{q}g\sigma}(\overline{\beta} m^*_\sigma)\right)^{\frac{3N_c^2-2}{8}}}{\left(2N_c\widetilde{\Phi}^{(2)}_g + \widetilde{\Phi}^{(2)}_{q\bar{q}\sigma}(\overline{\beta} m^*_\sigma)\right)^{\frac{N_c^2-1}{2}}}. \tag{340}$$

The neutrality of the prefactor coefficient $N_{\tilde{\Phi}}$ does not generate a power function with respect to the bag's energy or volume. In this sense, its variation with respect to the chiral constituent quark mass does not play a significant role in the chiral restoration phase transition and subsequently this variation is neglected. Therefore, it is reasonable to ignore the chiral effect in $N_{\tilde{\Phi}}$ and to approximate it to

$$N_{\tilde{\Phi}} \approx \frac{\left(\widetilde{\Phi}^{(0)}_{q\bar{q}g\sigma}(0)\right)^{\frac{3N_c^2-2}{8}}}{\left(2N_c\widetilde{\Phi}^{(2)}_g + \widetilde{\Phi}^{(2)}_{q\bar{q}\sigma}(0)\right)^{\frac{N_c^2-1}{2}}} \approx \frac{\left[2 \times 2N_c 7\pi^2/720 + 2\left(N_c^2 - 1\right)\pi^2/90\right]^{(3N_c^2-2)/8}}{(2N_c/6 + 1/3)^{(N_c^2-1)/2}}. \tag{341}$$

In contrast, the exponential plays a significant role in the chiral phase transition. It is decisive in determining the scalar chiral σ

mean field and the order of the chiral phase transition. It must be written explicitly as a function of the chiral constituent quark mass as follows:

$$\widetilde{\Phi}^{(0)}_{q\bar{q}g\sigma}(\overline{\beta}m^*_\sigma) = \widetilde{\Phi}^{(0)}_{q\bar{q}\sigma}(\overline{\beta}m^*_\sigma) + \widetilde{\Phi}^{(0)}_{g}. \tag{342}$$

The explicit expression with respect to the chiral constituent quark mass reads

$$\begin{aligned}\widetilde{\Phi}^{(0)}_{q\bar{q}\sigma}(\overline{\beta}m^*_\sigma) &= \frac{2N_c}{\pi^2}\int_0^\infty dx\, x^2 \ln\left[1 + e^{-\sqrt{x^2+(\overline{\beta}m^*_\sigma)^2}}\right], \\ &= \frac{2N_c}{3\pi^2}\int_0^\infty dx \frac{x^4}{\sqrt{x^2+(\overline{\beta}m^*_\sigma)^2}} \\ &\quad\times \frac{1}{\left[1 + e^{-\sqrt{x^2+(\overline{\beta}m^*_\sigma)^2}}\right]}.\end{aligned} \tag{343}$$

The variation of the exponential with respect to the scalar chiral σ mean field is essential for calculating the scalar chiral σ field. This can be done by extremizing the isobaric pressure. The explicit variation of $\widetilde{\Phi}^{(0)}_{q\bar{q}\sigma}(\overline{\beta}m^*_\sigma)$ with respect to the scalar chiral σ field takes the form

$$\begin{aligned}&\frac{\delta}{\delta\sigma}\left(\widetilde{\Phi}^{(0)}_{q\bar{q}\sigma}(\overline{\beta}m^*_\sigma)\right) \\ &= -\left(\frac{2N_c}{\pi^2}\int_0^\infty dx\, x^2 \frac{1}{\left[e^{\sqrt{x^2+(\overline{\beta}m^*_\sigma)^2}}+1\right]}\right. \\ &\quad\left.\times \frac{\overline{\beta}^2 m^*_\sigma}{\sqrt{x^2+(\overline{\beta}m^*_\sigma)^2}}\right)\frac{\delta m^*_\sigma}{\delta\sigma}.\end{aligned} \tag{344}$$

The variable transformations $x = W/V$ and $v = V$ transform the independent variable set as follows $\{W, V\} \to \{x, v\}$. However, this transformation set simplifies the analysis of phase transition in terms of the bag's energy density and volume rather than the bag's energy and volume. Nonetheless, according to the standard MIT bag model, the bag's mass is given by subtracting the bag's energy constant, i.e., $W = m - Bv$, where BV is interpreted as the bag's vacuum energy. The microcanonical ensemble as a function of two independent variables $\{x, v\}$ is displayed as

$$\begin{aligned}Z_{(\mathrm{II})q\bar{q}g}(x, v; \sigma) \equiv{}& \frac{1}{2\sqrt{2\pi}}\mathcal{N}_{q\bar{q}g} N_{\widetilde{\Phi}} v^{-\frac{N_c^2}{2}} x^{-\frac{3N_c^2+2}{8}} \\ &\times \exp\left[\frac{4}{3}\left(\widetilde{\Phi}^{(0)}_{q\bar{q}g\sigma}(\overline{\beta}m^*_\sigma)\right)^{\frac{1}{4}} x^{3/4} v\right].\end{aligned} \tag{345}$$

The Hagedorn density of states in the context of the MIT bag model with a sharp surface boundary becomes

$$\begin{aligned}\rho_{\mathrm{bags}} &= \delta(m - 4Bv) Z_{(\mathrm{II})q\bar{q}g}(x, v; \sigma), \\ &= \frac{1}{v}\delta(x - 3B) Z_{(\mathrm{II})q\bar{q}g}(x, v; \sigma).\end{aligned} \tag{346}$$

The advantage of adopting the standard bag model with a sharp surface boundary condition is that it simplifies the model dramatically. However, in the realistic physical situations, it is expected that the bag surface boundary has an extended surface in the extreme hot bath rather than a sharp one. Furthermore, it would be reasonable to think that the bag's surface boundary is distorted and becomes a fuzzy one. It is argued that the bag's surface boundary is important in the determining the order of the phase transition and the existence of the tricritical point in the phase transition diagram [28,50]. Nonetheless, the surface distortion may cause a mechanical instability. Such a mechanical instability is ignored here. The Hagedorn isobaric pressure is calculated by integrating the degenerate single-particle ensemble function over the mass and volume distribution function. It is reasonable to assume that the gas of Hagedorn states is satisfying the Maxwell-Boltzmann statistics in order to simplify the model analysis. The Hagedorn isobaric function is integrated over the continuous mass and volume variables as follows:

$$f_{\mathrm{fireballs}}(T, s) = \int_{v_0}^\infty \int_{m_0}^\infty dv\, dm\, e^{-vs} \rho_{\mathrm{bags}}(m, v) \varphi_{\mathrm{MB}}(T; m). \tag{347}$$

Because the initial Hagedorn mass is relatively heavy, it is adequate to adopt the following approximation:

$$\begin{aligned}f_{\mathrm{fireballs}}(T, s) &= \int_{v_0}^\infty \int_{m_0}^\infty dv\, dm\, e^{-vs} \rho_{\mathrm{bags}}(m, v) \\ &\quad\times \left(\frac{mT}{2\pi}\right)^{3/2} e^{-m/T} \\ &= \int_{v_0}^\infty \int_{x_0}^\infty dv\, dx e^{-vs} \delta(x - 3B) Z_{(\mathrm{II})q\bar{q}g} \\ &\quad\times (x, v; \sigma)\left(\frac{(x + B)vT}{2\pi}\right)^{3/2} e^{-(x+B)v/T}.\end{aligned} \tag{348}$$

The integration over the δ function eliminates the energy density integration and reduces the isobaric function to an integration only over the Hagedorn excluded volume as follows:

$$\begin{aligned}f_{\mathrm{fireballs}}(T, s) &= \int_{v_0}^\infty dv\, e^{-vs} Z_{(\mathrm{II})q\bar{q}g}(x, v; \sigma)\Big|_{x=3B} \\ &\quad\times \left(\frac{4BT}{2\pi}\right)^{3/2} v^{3/2} e^{-(4B/T)v}.\end{aligned} \tag{349}$$

To simplify the analysis, the chiral isobaric function for the Hagedorn gas is shortened to

$$f_{\mathrm{fireballs}}(T, s) = C'(T)\int_{v_0}^\infty dv\, v^{-\frac{(N_c^2-3)}{2}} e^{-v(s-s_0)}, \tag{350}$$

where the integral prefactor function reads

$$C'(T) = \frac{1}{2\sqrt{2\pi}}\mathcal{N}_{q\bar{q}g} N_{\widetilde{\Phi}} (3B)^{-\frac{3N_c^2+2}{8}} \left(\frac{4BT}{2\pi}\right)^{3/2}. \tag{351}$$

It is worth noting that Eq. (350) differs from Eq. (295) where the former equation includes the scalar chiral σ field unlike the later one. Furthermore, the Hagedorn bag's internal isobaric pressure is given by

$$p_{\mathrm{int}}/T = s_0 = \frac{4}{3}\left(\widetilde{\Phi}^{(0)}_{q\bar{q}g\sigma}(\overline{\beta}m^*_\sigma)\right)^{\frac{1}{4}} (3B)^{3/4} - 4B/T. \tag{352}$$

On the other hand, the chiral low-lying mass spectrum is realized as the discrete hadronic mass spectrum found

experimentally and displayed in the data book [45]. The scalar chiral σ mean-field potential interacts and couples to the hadrons and generates the hadron masses. At highly extreme conditions, the chiral symmetry will be restored, and the hadrons with light flavors will dissolve to massless states, while the scalar chiral σ potential vanishes. Under the above assumption, the density of states for the low-lying mass spectrum is generalized to take into consideration the chiral discrete mass spectrum as follows:

$$\begin{aligned}\rho_{\text{low}}(m, v, T, \Lambda) &= \sum_{B}^{\text{baryons}} (2J_B + 1) D_{\text{FD}}(\Lambda_B)\delta(m - m_B^*(\sigma))\delta(v - v_H) \\ &+ \sum_{M}^{\text{mesons}} (2J_M + 1) D_{\text{BE}}(\Lambda_M)\delta(m - m_M^*(\sigma))\delta(v - v_H).\end{aligned} \tag{353}$$

The sums run over the baryon and the meson mass spectra those are satisfying Fermi-Dirac and Bose-Einstein statistics, respectively. The coupling of the scalar chiral σ field to the constituent quark generates the hadron mass as follows

$$M^*_{\text{hadron}} = g_{H\sigma}\sigma + n_q m_{q0} \approx n_q g^{\text{input}}_{q\sigma}\sigma, \tag{354}$$

where $n_q = 2, 3$ for meson and baryon, respectively, and m_{q0} is the quark current mass, which is usually massless for light flavors $m_{q0} \approx 0$. In general, the coupling constants $g_{H\sigma}$ or $g^{\text{input}}_{q\sigma}$ are determined by the phenomenology in order to fit the experimental hadronic mass spectrum. However, the above procedure is boring and produces a tremendous number of fitting parameters. To reduce the number of phenomenological parameters $g_{H\sigma}$ and to include the effect of the discrete hadronic mass spectrum, we assume that the effective discrete hadronic mass spectra for baryons and mesons are, respectively, generated by

$$\begin{aligned} m_B^*(\sigma) &= (M_B - M_{\text{nucleon}}) + 3g_{q\sigma}\sigma, \\ m_M^*(\sigma) &= \left(M_M - \tfrac{2}{3}M_{\text{nucleon}}\right) + 2g_{q\sigma}\sigma. \end{aligned} \tag{355}$$

In the computational calculations, a special consideration is given for light mesons such as pions, because they are replaced by the scalar σ mean field. Furthermore, the ω meson is replaced by the vector mean field, while the other nonstrange hadrons are left as hadron particles. The generalization of the isobaric function of the discrete low-lying hadronic mass spectrum, namely, the chiral low-lying isobaric function, is given by

$$\begin{aligned} f_{\text{low}}(T, s) = &\sum_{B}^{\text{baryons}} [\varphi_{\text{FD}}(T, s; m_B^*(\sigma), \Lambda_B^\star) \\ &+ \varphi_{\text{FD}}(T, s; m_B^*(\sigma), \overline{\Lambda}_B^\star)] \\ &+ \sum_{M}^{\text{mesons}} [\varphi_{\text{BE}}(T, s; m_M^*(\sigma), \Lambda_M^\star) \\ &+ \varphi_{\text{BE}}(T, s; m_M^*(\sigma), \overline{\Lambda}_M^\star)]. \end{aligned} \tag{356}$$

The ensemble functions for single-particle species obeying the Fermi-Dirac and Bose-Einstein statistics read, respectively,

$$\begin{aligned}&\varphi_{\text{FD}}(T, s; m_B^*(\sigma), \Lambda_B^\star) \\ &\quad = (2J_B + 1)\int \frac{d^3k}{(2\pi)^3} \ln\left[1 + \Lambda_B e^{-vs} e^{-\frac{1}{T}\sqrt{k^2 + m_B^{*2}(\sigma)}}\right],\end{aligned} \tag{357}$$

and

$$\begin{aligned}&\varphi_{\text{BE}}(T, s; m_M^*(\sigma), \Lambda_M^\star)) \\ &\quad = -(2J_M + 1)\int \frac{d^3k}{(2\pi)^3} \ln\left[1 - \Lambda_M e^{-vs} e^{-\frac{1}{T}\sqrt{k^2 + m_M^{*2}(\sigma)}}\right].\end{aligned} \tag{358}$$

The pressure $p = Ts^*$ is determined by finding the isobaric extreme right-hand singularity as follows:

$$\begin{aligned} s^* &= f_{\text{fireballs}}(T, s^*) + f_{\text{low}}(T, s^*) + f_\sigma(T, s^*) \\ &= f_{\text{fireballs}}(T, s^*) + f_{\text{low}}(T, s^*) - U(\sigma), \end{aligned} \tag{359}$$

where the isobaric term of the scalar chiral σ field is given by $f_\sigma(T, s^*) = -U(\sigma)$.

The value of the scalar chiral σ mean field is determined by extremizing the chiral isobaric pressure as follows

$$\frac{\partial}{\partial\sigma} s^* = 0. \tag{360}$$

The chiral variation of the Hagedorn isobaric function reads

$$\begin{aligned}\frac{\partial}{\partial\sigma} f_{\text{fireballs}}(T, s^*) = C'(T)\int_{v_0}^{\infty} dv\, v^{-\alpha+1} e^{-v(s-s_0)} \frac{\partial s_0}{\partial\sigma} \\ + (\cdots)\frac{\partial s^*}{\partial\sigma}.\end{aligned} \tag{361}$$

The chiral variation of the bag's internal pressure reads

$$\frac{\partial p_{\text{int}}}{\partial\sigma} = T\frac{\partial s_0}{\partial\sigma}, \tag{362}$$

where

$$\frac{\partial s_0}{\partial\sigma} = \frac{1}{3}\left(\frac{3B}{\widetilde{\Phi}^{(0)}_{q\bar{q}g\sigma}(\overline{\beta}m_\sigma^*)}\right)^{3/4} \times \frac{\delta\widetilde{\Phi}^{(0)}_{q\bar{q}g\sigma}(\overline{\beta}m_\sigma^*)}{\delta\sigma}. \tag{363}$$

The asymptotic approximation of the chiral variation of the Hagedorn isobaric function reads

$$\begin{aligned}\frac{\partial}{\partial\sigma} f_{\text{fireballs}}(T, s^*) \propto -m_q^*\int_{v_0}^{\infty} dv\, v^{-\alpha+1} e^{-v(s-s_0)} \\ + (\cdots)\frac{\partial s^*}{\partial\sigma}.\end{aligned} \tag{364}$$

The variation of the chiral isobaric function of the discrete low-lying mass spectrum with respect to the scalar chiral σ field reads

$$\begin{aligned}\frac{\partial}{\partial\sigma} f_{\text{low}}(T, s^*) = &\sum_{B}^{\text{baryons}} \left[\varphi^{(\sigma)}_{\text{FD}}(T, s^*; m_B^*(\sigma), \Lambda_B^\star)\right. \\ &\left. + \varphi^{(\sigma)}_{\text{FD}}(T, s^*; m_B^*(\sigma), \overline{\Lambda}_B^\star)\right] \\ &+ \sum_{M}^{\text{mesons}} \left[\varphi^{(\sigma)}_{\text{BE}}(T, s^*; m_M^*(\sigma), \Lambda_M^\star)\right.\end{aligned}$$

$$+\varphi^{(\sigma)}_{\rm BE}(T,s;m^*_M(\sigma),\overline{\Lambda^\star_M})\big] + (\cdots)\frac{\partial s^*}{\partial\sigma}. \quad (365)$$

The explicit expressions used in the above equations are displayed as

$$\frac{\partial}{\partial\sigma}\varphi_{\rm FD}(T,s^*;m^*_B(\sigma),\Lambda^\star_B) = \varphi^{(\sigma)}_{\rm FD}(T,s^*;m^*_B(\sigma),\Lambda^\star_B) + (\cdots)\frac{\partial s^*}{\partial\sigma},$$

$$\varphi^{(\sigma)}_{\rm FD}(T,s^*;m^*_B(\sigma),\Lambda^\star_B) = -(2J_B+1)g_{q\sigma}\int\frac{dkk^2}{2\pi^2}\frac{\frac{m^*_q(\sigma)}{T}\Big/\sqrt{k^2+m^{*2}_B(\sigma)}}{\left[\Lambda_B^{-1}e^{vs^*}e^{\frac{1}{T}\sqrt{k^2+m^{*2}_B(\sigma)}}+1\right]}, \quad (366)$$

and

$$\frac{\partial}{\partial\sigma}\varphi_{\rm BE}(T,s^*;m^*_M(\sigma),\Lambda^\star_M) = \varphi^{(\sigma)}_{\rm BE}(T,s^*;m^*_M(\sigma),\Lambda^\star_M) + (\cdots)\frac{\partial s^*}{\partial\sigma},$$

$$\varphi^{(\sigma)}_{\rm BE}(T,s^*;m^*_M(\sigma),\Lambda^\star_M) = -(2J_M+1)g_{q\sigma}\int\frac{dkk^2}{2\pi^2}\frac{\frac{m^*_q(\sigma)}{T}\Big/\sqrt{k^2+m^{*2}_M(\sigma)}}{\left[\Lambda_M^{-1}e^{vs^*}e^{\frac{1}{T}\sqrt{k^2+m^{*2}_M(\sigma)}}-1\right]}, \quad (367)$$

where the result $\partial m^*_q(\sigma)/\partial\sigma = g_{q\sigma}$ is adopted. Finally, the variation of the scalar chiral σ potential is written for simplicity as

$$-\frac{\partial U(\sigma)}{\partial\sigma} \equiv M^2_\sigma(\sigma)\sigma + (\cdots), \quad (368)$$

where $M_\sigma(\sigma)$ is interpreted as the effective mass of the scalar chiral σ field particle. The dots term represents the remaining terms that do not affect our final interpretation and conclusion in the chiral restoration phase transition.

The scalar chiral σ mean-field condensate is determined by extremizing the total isobaric pressure (i.e., grand potential) in the following way:

$$T\frac{\partial s^*}{\partial\sigma} = 0,$$
$$-\frac{\partial U(\sigma)}{\partial\sigma} = -\frac{\partial}{\partial\sigma}[f_{\rm fireballs}(T,s^*) + f_{\rm low}(T,s^*)]. \quad (369)$$

Equation (369) is approximated and simplified to

$$M^2_\sigma(\sigma)\sigma = -\frac{\partial}{\partial\sigma}[f_{\rm fireballs}(T,s^*) + f_{\rm low}(T,s^*)]. \quad (370)$$

It has been pointed out that the hadronic phase exhibits the Gross-Witten point in a way that the gas of the discrete low-lying mass spectrum undergoes a third-order phase transition from the discrete low-lying hadronic mass spectrum phase to a hadronic phase dominated by the continuous Hagedorn mass spectrum. This leaves three possibilities in order to study the chiral phase transition.

In case (I), we have mixed low-lying and Hagedorn phases near the Gross-Witten point. In this case, the Gross-Witten and chiral restoration phase transitions overlap around the Gross-Witten point, although the chiral restoration phase transition is a cross-over one unlike the third-order Gross-Witten phase transition. Moreover, both transitions take place below and far away from the deconfinement phase transition to an explosive QGP.

In case (II), the chiral restoration phase transition takes place in the hadronic phase dominated by the discrete low-lying hadronic mass spectrum particles. In this scenario [i.e., case (II)], the chiral restoration phase transition is a smooth cross-over and is located below the Gross-Witten point and far away from the phase transition to an explosive QGP. In case (II), the scalar chiral σ mean field is determined by solving the equation of extremization,

$$M^2_\sigma(\sigma)\sigma \approx -\frac{\partial U(\sigma)}{\partial\sigma} = -\frac{\partial}{\partial\sigma}[f_{\rm low}(T,s^*)]. \quad (371)$$

This equation produces a smooth cross-over chiral restoration phase transition where the scalar chiral σ mean field decreases smoothly. This class of equation has been studied extensively in the context of the Walecka model, where the Van der Waals effect is neglected. When the bag's excluded volume is ignored, we get the standard σ model

$$M^2_\sigma(\sigma)\sigma \approx -\frac{\partial}{\partial\sigma}[f_{\rm low}(T,s^*)] = 2(J_B+1)g_{q\sigma}\sum_B\int\frac{dkk^2}{2\pi^2}\frac{\frac{m^*_q(\sigma)}{T}\Big/\sqrt{k^2+m^{*2}_B(\sigma)}}{\left[e^{\frac{1}{T}\sqrt{k^2+m^{*2}_B(\sigma)}}+1\right]} + 2(J_M+1)g_{q\sigma} \times\sum_M\int\frac{dkk^2}{2\pi^2}\frac{\frac{m^*_q(\sigma)}{T}\Big/\sqrt{k^2+m^{*2}_M(\sigma)}}{\left[e^{\frac{1}{T}\sqrt{k^2+m^{*2}_M(\sigma)}}-1\right]}, \quad (372)$$

where the fugacities are set to $\Lambda_B = 1$ and $\Lambda_M = 1$, because the present analysis focuses on the region near zero baryonic chemical potential along the temperature axis. In this case, the chiral restoration phase transition takes place before the Gross-Witten point, in contrast to case (I) where the chiral restoration phase transition overlaps the Gross-Witten point and is located far from the deconfinement phase transition to an explosive QGP. Hence, case (II) seems to fail to produce the continuous Hagedorn threshold, since it generates massless hadron masses before the continuous Hagedorn mass spectrum is reached. Since in this scenario the Hagedorn mass threshold is much higher than the maximum discrete mass spectrum, the continuous Hagedorn states production is denied. The self-consistent phase transition from the hadronic phase to a QGP is not possible in the context of case (II), because the gas of bags will never be produced, unlike in cases (I) and (III). Hence, the Gibbs construction becomes essential in case (II) if we want to study the phase transition to QGP. It is hard to picture an explosive QGP phase transition in this case. However, case (I) appears to be more physical than case (II), since in the former case the chiral restoration phase transition overlaps the third-order Gross-Witten point. This overlapping mechanism virtually makes the Hagedorn

phase difficult to be detected directly experimentally [51]. Furthermore, in this case, the chiral restoration phase transition is supposed to take place prior to the color-deconfinement phase transition to an explosive QGP. Technically speaking, it will be hard to distinguish the color-deconfinement from the chiral restoration phase transition. Nonetheless, the indirect detection and analysis can distinguish the explosive QGP from the static hadronic phase [52,53].

Finally, case (III) is the most important case. Indeed, in this case, the chiral phase transition takes place in a hadronic phase dominated by the Hagedorn gas. The chiral restoration phase transition takes place at least just above the Gross-Witten point and at most simultaneously with the point of the deconfinement phase transition to an explosive QGP. The scalar chiral σ mean field is determined by extremizing the isobaric pressure as follows:

$$-\frac{\partial U(\sigma)}{\sigma} \approx M_\sigma^2(\sigma)\sigma \doteq -\frac{\partial}{\partial\sigma}[f_{\text{fireballs}}(T, s^*)]. \quad (373)$$

Hence, the hadronic matter dominated by the fireballs (i.e., the Hagedorn states) leads to the following equation

$$M_\sigma^2(\sigma)\sigma \doteq (\cdots)m_q^* \int_{v_0}^{\infty} dv v^{-\alpha+1} e^{-v(s-s_0)}. \quad (374)$$

Equation (374) has very important characteristics that have been discussed in detail in Sec. X and Ref. [28]. At the point just below the phase transition from the Hagedorn phase to an explosive QGP, it is shown that Eq. (374) has the following characteristic properties:

$$\begin{aligned} M_\sigma^2(\sigma)\sigma &\propto m_q^* \lim_{s\to s_0}(s-s_0)^{\alpha-2}\Gamma(-\alpha+2, v_0(s-s_0)), \\ &\sim \text{finite for } \alpha > 2, \\ &\sim \infty \text{ for } \alpha \leqslant 2 \to \sigma = 0, \end{aligned} \quad (375)$$

where $\Gamma(-n, x)$ is the exponential integral function of order n where $n > 0$. The integral on the right-hand side of Eq. (374) diverges whenever the bag's internal isobaric pressure s_0 exceeds the external one s. The phase transition from the hadronic phase to an explosive QGP takes place in the limit $(s - s_0) \to 0$ when the bag's internal isobaric pressure s_0 reaches the external isobaric hadronic pressure s from below. The solution $\sigma = 0$ is the only nontrivial solution for the scalar chiral σ mean-field condensate when the explosive QGP takes place subsequent the point $(s - s_0) = 0^-$. The abrupt vanishing of the scalar chiral σ mean field indicates evidently that the chiral symmetry restoration phase transition takes place below or at most at the same point of the phase transition to an explosive QGP. Actually, the point $s = s_0$ decides the order of the chiral phase transition when it takes place simultaneously with the deconfinement phase transition to an explosive QGP. However, if the cross-over chiral restoration phase transition takes place prior to the deconfinement phase transition, then it takes place far from the explosive QGP phase transition.

The same analysis done in Sec. X to determine the order of the phase transition can be carried out for the chiral symmetry restoration phase transition. As the isobaric ensemble reaches the limit $(s - s_0) = 0^+$ just below the point of the phase transition, the scalar chiral σ mean-field solution is finite for the gas of bags with an internal structure of $\alpha > 2$, while it must vanish for $\alpha \leqslant 2$ in order to get the physical solution. This means that for the gas of bags with internal structures of $\alpha \leqslant 2$, the chiral restoration phase transition takes place below the point of the deconfinement phase transition to an explosive QGP. In this case, the order of the phase transition will be a rapid cross-over transition. Furthermore, the chiral restoration phase transition must be completed far from the point at which the phase transition to an explosive QGP is reached. If the smooth cross-over phase transition is not completed prior to the deconfinement point, then the chiral restoration is prohibited for $\alpha \leqslant 2$.

On the other hand, the case is completely different for the gas of bags with the internal structure of $\alpha > 2$. In this case, the gas of bags undergoes the chiral restoration phase transition simultaneously at the same point of the explosive QGP phase transition. The order of the chiral restoration phase transition is found to be second order for $\alpha = 3$, whereas it is a higher order for $3 \geqslant \alpha > 2$. Finally, the chiral phase transition is first order for the gas of bags with an internal structure of $\alpha > 3$.

In the context of a model consisting of hadronic matter dominated by fireballs with an internal structure of $\alpha = 3$ (i.e., the color-singlet bag), the scenario of the phase transition is summarized as follows. The gas of the discrete low-lying hadronic mass spectrum particles undergoes a third-order phase transition to the Hagedorn phase at the Gross-Witten point. The chiral restoration phase transition likely takes place in the hadronic matter that is dominated by the continuous Hagedorn states. The chiral restoration phase transition is located above the critical Gross-Witten point, and it takes place simultaneously with the point of the phase transition to an explosive QGP. The chiral restoration phase transition is of the second order, and it takes place just below or almost simultaneously with the point of the phase transition to an explosive QGP. Finally, the Hagedorn phase undergoes a first-order phase transition to an explosive QGP. Nonetheless, this scenario does not exclude the possibility for the sharp cross-over chiral restoration phase transition to take place subsequent to Gross-Witten point but far away from the point of the phase transition to an explosive QGP. However, in the case that the smooth cross-over chiral restoration phase transition is not completed yet in the Hagedorn phase, then the second-order chiral restoration phase transition must take place simultaneously with the point of the phase transition to an explosive QGP.

Indeed, in this scenario, it seems likely that the chiral restoration phase transition takes place in the continuous Hagedorn spectrum phase rather than in the discrete low-lying mass spectrum phase. The continuity of the Hagedorn mass spectrum makes the Hagedorn phase domain narrow in the hot bath. The narrowness of the Hagedorn phase range, besides the restoration phase transition being above the Gross-Witten point and taking place at most simultaneously with the deconfinement phase transition, makes the continuous Hagedorn states difficult to distinguish from the QGP. It also makes it harder to distinguish the chiral restoration phase transition from the deconfinement phase transition. For example, it has been argued that the heavy Hagedorn states have large widths [51]. Nevertheless, this scenario is inconclusive, although it explains

the existence of the Gross-Witten point, the chiral restoration and deconfinement, and even the existence of the tricritical point for some class of bag internal structures. The existence of the tricritical point is essential in the multiprocess scenario.

Other alternative scenarios for a hadronic gas dominated by fireballs can also be imagined. The fireball internal structure α varies under extreme conditions because of the color-flavor correlations and the modification of the bag's volume fluctuations. When the bag's internal structure is of order $\alpha > 3$, then both the chiral restoration and the color deconfinement are of first-order phase transitions if they take place simultaneously. In contrast, the chiral restoration phase transition is of a higher order for the gas of bags with the internal structure of $3 \geqslant \alpha > 2$. The phase transition to an explosive QGP is first order for $\alpha > 2$ and a higher order for $2 \geqslant \alpha > 1$.

In the class of scenarios in which the chiral restoration and deconfinement phase transitions overlap, the nth-order chiral restoration phase transition takes place simultaneously with the first-order phase transition to an explosive QGP. Nonetheless, the Gross-Witten point remains a third-order phase transition point. However, the simultaneous phase transition to the chiral restoration and to an explosive QGP is not conclusive. If the fireball has the internal structure of $2 \geqslant \alpha > 1$, then the deconfinement phase transition is of nth order, while the chiral phase transition must take place far from the point of phase transition to an explosive QGP. Moreover, the gas of hadronic bags with the internal structure of $\alpha \leqslant 1$ never undergo the phase transition to an explosive QGP. It is interesting to note that most of the above scenarios are precursors to the scenario that the smooth cross-over chiral restoration phase transition takes place below and far from the point of the phase transition to an explosive QGP, and moreover as the chiral restoration phase transition approaches the point of the phase transition to QGP, the cross-over restoration phase transition becomes more sharp and rapid.

XII. CONCLUSIONS

To study the chiral restoration and deconfinement phase transitions in QCD, the hadronic density of states must be known for the entire energy domain below the point of the phase transition to the true deconfined QGP. The theoretical procedure for finding the hadronic density of states is carried out by computing the microcanonical ensemble. The canonical ensemble for the color-singlet bag of constituent particles with the underlying symmetric group SU(N_c) [and U(N_c)] has been considered in detail. The color structure has attracted much attention in order to understand confinement/deconfinement in QCD [10,13–15,28–31,34] or even the extended gauge field theories such as AdS/CFT [21–23]. However, sometime ago, Gross and Witten argued for the existence of the tricritical Gross-Witten point, which is thought to play a significant role in the phase transition mechanism. It has been derived using the spectral density of color eigenvalues method originally introduced by Brezin *et al*. [8]. Recently, the Gross-Witten critical point and the deconfinement mechanism have been reviewed in the context of the Brezin *et al*. [8] method to study the QGP in QCD [10,11,13–15] and black hole formation in AdS/CFT [22–26].

In the present work, we have introduced a simpler alternative method to derive the color-singlet canonical ensemble for the asymptotic large thermal running parameter λ/N_c^2. Furthermore, we have demonstrated in detail how to locate the Gross-Witten critical point for the phase transition. This novel method suits the realistic and complicated physical situations. For the small thermal running parameter λ/N_c^2, the saddle points are distributed uniformly over the entire color circle range $|\theta_i| \leqslant \pi$. Since the saddle points are distributed uniformly over the entire range, the Vandermonde determinant contributes to the action as an additional effective potential term. The integral of the resultant ensemble has been evaluated trivially. However, this procedure fails when the saddle points congregate around the origin rather than distribute uniformly over the entire color circle range $|\theta_i| \leqslant \pi$ and the Vandermonde effective potential develops a virtual singularity. In this case, a further consideration must be taken into account to regulate the action involving the Vandermonde effective potential and finally to evaluate the canonical ensemble correctly. Therefore, this behavior indicates that the solution changes its analytical function characteristic and a subsequent phase transition takes place. The solution of the asymptotic large λ/N_c^2 is evaluated using the Gaussian-like saddle points (GSP) method. The action is expanded around the stationary Fourier color variables where only the quadratic terms are retained, while the Vandermonde determinant is regulated in a nontrivial way. Fortunately, in this procedure, the stationary Fourier color points are found dominant around the origin, and this simplifies the problem dramatically. In spite of the action complexity due to the realistic physical situation involved, it will always be an easy way to find the quadratic expansion around the saddle color points, and the resultant integration over the color variables is evaluated using the standard Gaussian quadrature.

The critical point for the Hagedorn phase transition is determined midway of the interpolation between the two different analytical solutions for the small and the large λ/N_c^2, respectively. The GSP method is compared with the spectral density of color eigenvalues method (i.e., spectral density method, see, for example, Refs. [7,8,23]) and the exact numerical solution as well. It is found that the exact numerical solution fits precisely the results of the GSP method for the large thermal running parameter $\lambda/N_c^2 > \lambda_0/N_c^2$. Furthermore, it is found to be in good agreement with the spectral density method. When the large λ/N_c^2 is extrapolated to the small $\lambda/N_c^2 < \lambda_0/N_c^2$, the solution becomes slippery; and when λ/N_c^2 reaches some critical value, it is deflected to increase. This solution is concave up and has a minimum at the critical point $\lambda_{(\mathrm{II})\mathrm{min}}$. This point is the threshold point for the acceptable physical solution (II). The minimum point for the extrapolation of the asymptotic large-λ/N_c^2 solution is actually the minimal threshold point. The extreme left-hand side interval for the asymptotic large-λ/N_c^2 solution is presumed to start from the threshold point $\lambda_{(\mathrm{II})\mathrm{min}}$. The extrapolation down below this threshold point is unphysical and is declined as a solution. This means that beyond the threshold point, the asymptotic large-λ/N_c^2 solution (II) is

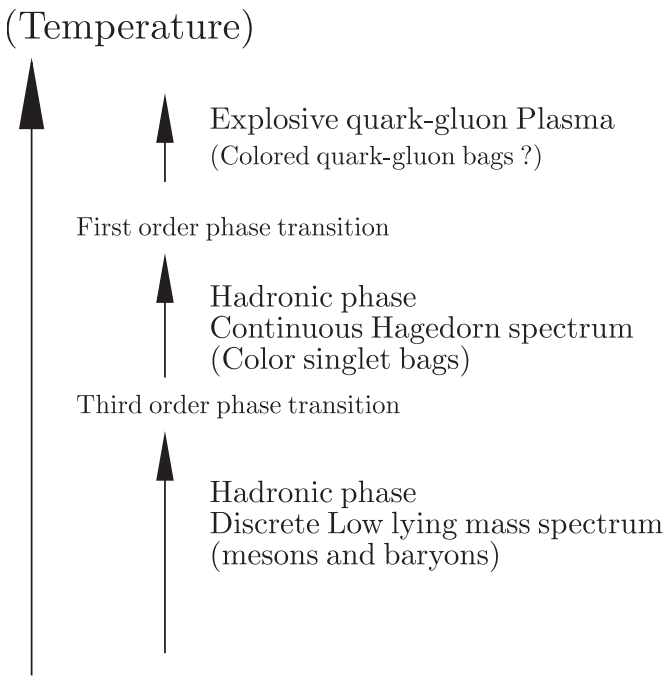

FIG. 11. Phase transition scenario in the context of the present model. At low temperature, the diluted nuclear matter is dominated by the low-lying hadronic mass spectrum such pions, nucleons, etc. At the Hagedorn critical temperature, the system undergoes a third-order phase transition to a system dominated by the highly excited hadronic states known as Hagedorn states or fireballs. When the system is thermally excited to higher temperature, the hadronic phase undergoes a first-order phase transition to an explosive QGP.

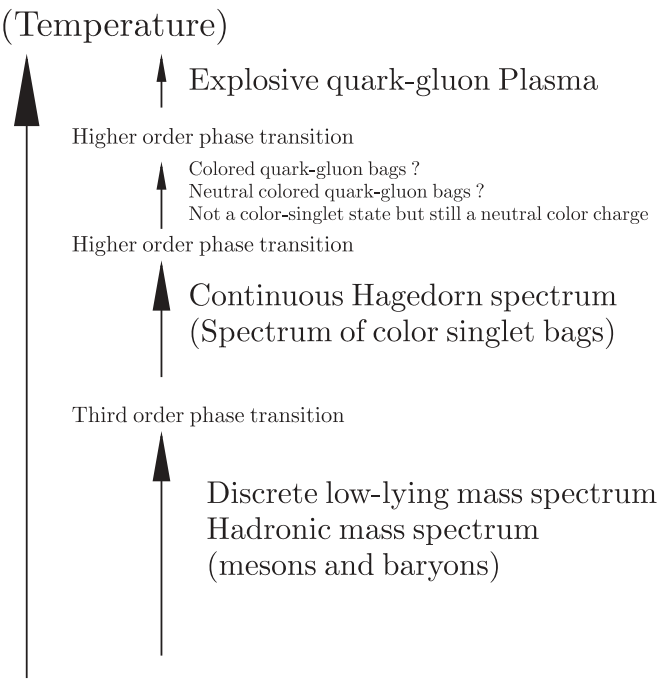

FIG. 12. Same as Fig. 11, but with an alternative scenario for the phase transition. The hadronic phase dominated by Hagedorn states undergoes a higher order phase transition to another phase dominated by highly excited neutral color bound quark-gluon bags (i.e., bound state but with a color nonsinglet state). At higher temperature, the gas of colored quark and gluon bags undergoes a higher order phase transition to an explosive real deconfined QGP. In this scenario, the phase transition to an explosive QGP takes place only through more complicated processes.

deflected and changes its analyticity in order to match and satisfy the asymptotic small-λ/N_c^2 solution (I). Solution (I) is found in agreement with the exact numerical results for the small λ/N_c^2, and it is found to adopt standard approximations. The action is expanded to λ-power expansion and then is evaluated using the group orthogonality over the full color range. The ultimate limit of the approximation validity is given by the point $\lambda_{(\mathrm{I})\max}$; beyond this point, the solution will be broken. The action structure is simplified dramatically in the range $\lambda \leqslant \lambda_{(\mathrm{I})\max}$. For example, the quantum statistics can be approximated always to Maxwell-Boltzmann statistics and so on. However, the asymptotic small- and large-λ/N_c^2 solutions (i.e., solutions (I) and (II), respectively) may split by a small additional constant. This constant is simply the approximation redundant in particular when both solutions are extrapolated far from their asymptotic limits. The critical point λ_0/N_c^2 for the phase transition from the asymptotic small-λ/N_c^2 to large-λ/N_c^2 solutions is located near or above $\lambda \geqslant \lambda_{(\mathrm{II})\min}$ but below $\lambda \leqslant \lambda_{(\mathrm{I})\max}$. It is roughly the midway interpolation between the small and large solutions. The advantage of the Gaussian-like saddle points method is its simplicity in that it can deal with a complicated physical problem such as the deconfinement phase transition in QCD.

The QCD phase transition is studied in the context of the color-singlet state of quark and gluon bags. It is found that the density of states for low-lying masses is a discrete spectrum. The low-lying density of states is determined by the known hadronic mass spectrum particles that are found experimentally and are available in the data book [45]. The Hagedorn states appear just above the low-lying known mass spectrum. The mass spectrum for the Hagedorn states is continuous. The gas dominated by the low-lying mass spectrum particles undergoes a third-order phase transition to a hadronic phase dominated by the Hagedorn states. When the system is thermally excited beyond the Hagedorn phase, the hadronic phase undergoes another phase transition to an explosive QGP.

The scenario for the phase transition is depicted in Fig. 11. In the diluted nuclear matter when the temperature increases and reaches the critical one, the gas of the discrete low-lying hadronic mass spectrum particles undergoes a third-order phase transition to a gas of continuous Hagedorn states (i.e., the high-lying hadronic states). Furthermore, when the system is thermally excited above this temperature, the gas of Hagedorn states undergoes another first-order or higher order phase transition to an explosive QGP. Moreover, the scenario for the phase transition can be extended to consider the multiple intermediate processes. An alternate scenario is depicted in Fig. 12. The gas of Hagedorn states undergoes a higher order phase transition to a gas of neutral colored bags or even nonsinglet bags. These bags are not color-singlet states but carry a neutral color charge, and this charge is fixed by the effective color chemical potentials. Subsequently, the

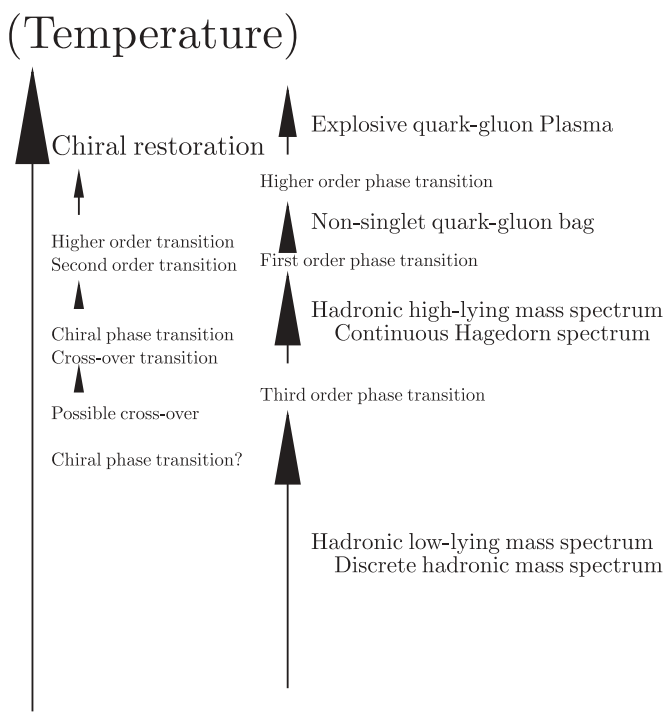

FIG. 13. Consistent chiral and deconfinement phase transition scenario.

gas of neutral colored bags undergoes a higher order phase transition to a gas of colored bags. The nonsinglet bags are not colored bags and not true deconfined colors but rather bags with specific internal color structures. In the colored bags, the quarks and gluons are still bounded in finite size blobs, and they carry total color charge. The phase transition to the colored bags with conserved color charges might be associated with breaking the group symmetry $SU(N_c)$ to $U(1)^{N_c-1}$. These colored bags become unstable, and when the system is perturbed slightly and thermally excited, the system eventually undergoes another higher order phase transition to a real deconfined QGP.

The possible consistent color-deconfinement and chiral restoration phase transition scenarios are depicted in Fig. 13. It is illustrated that the discrete low-lying hadronic mass spectrum undergoes a third-order phase transition to the Hagedorn phase. The gas of continuous Hagedorn states with internal structures $\alpha > 2$ undergoes a first-order phase transition to an explosive QGP. However, it is possible in some alternative scenarios that the Hagedorn phase undergoes a higher order phase transition to the gas of nonsinglet bags (i.e., with $\alpha \leqslant 2$), and the subsequent gas of exotic states undergoes a higher order phase transition to an explosive QGP. The chiral phase transition for the gas of Hagedorn states with the internal structure $\alpha = 3$ is found to be second order, and it takes place below or at most simultaneously with the deconfinement first-order phase transition to an explosive QGP. However, in the case that the chiral phase transition persists to take place in the gas of discrete low-lying hadronic mass spectrum states prior to the Hagedorn phase, then the chiral phase transition will be a smooth cross-over one. In this case, it will be hard to reach the Hagedorn threshold production, and subsequently the Hagedorn states will not be produced and no explosive QGP will be generated. The QGP in this scenario can be found by the Gibbs construction. It is possible in other scenarios that the the chiral phase transition coincides with the Gross-Witten point and it will be a cross-over transition. It seems that the chiral restoration phase transition likely takes place in the Hagedorn phase at most just below the deconfinement phase transition or at least coincides with the Gross-Witten point. In some scenarios, it is likely that the chiral phase transition coincides with the Gross-Witten point, whereas in other scenarios, the chiral restoration phase transition likely takes place simultaneously with the deconfinement phase transition to an explosive QGP. Indeed, the Hagedorn bag's internal structure α is found essential in the phase transition diagram. Furthermore, it is also possible that the Hagedorn phase undergoes a higher order phase transition through a multiprocess internal-structure phase transition, while the chiral restoration phase transition is a smooth cross-over transition and takes place in the continuous Hagedorn phase. The order of the chiral phase transition becomes sharper and of a lower order as its point approaches the deconfinement point to an explosive QGP. The QCD phase transition diagram is proved to be very rich and nontrivial.

ACKNOWLEDGMENTS

I.Z. gratefully acknowledges support from the Frankfurt Institute for Advanced Studies. He is indebted to Walter Greiner and Horst Stöcker for their encouragement and discussions, Melissa Franklin and John Huth for their support during his visit to Harvard University, and George Brandenburg for the hospitality of the Laboratory for Particle Physics and Cosmology at Harvard University. The authors thank J. Schaffner-Bielich for collaboration in the earlier stages of the present work and H. T. Elze. The authors also thank the Frankfurt Center for Scientific Computing. This work was supported by the Alexander von Humboldt Foundation and Harvard University.

[1] R. Hagedorn, Nuovo Cimento Suppl. **3**, 147 (1965).
[2] S. C. Frautschi, Phys. Rev. D **3**, 2821 (1971).
[3] J. I. Kapusta, Phys. Rev. D **23**, 2444 (1981).
[4] J. I. Kapusta, Nucl. Phys. **B196**, 1 (1982).
[5] K. Redlich and L. Turko, Z. Phys. C **5**, 201 (1980).
[6] L. Turko, Phys. Lett. **B104**, 153 (1981).
[7] D. J. Gross and E. Witten, Phys. Rev. D **21**, 446 (1980).
[8] E. Brezin, C. Itzykson, G. Parisi, and J. B. Zuber, Commun. Math. Phys. **59**, 35 (1978).
[9] C. B. Lang, P. Salomonson, and B. S. Skagerstam, Nucl. Phys. **B190**, 337 (1981).
[10] B. S. Skagerstam, Z. Phys. C **24**, 97 (1984).
[11] S. I. Azakov, P. Salomonson, and B. S. Skagerstam, Phys. Rev. D **36**, 2137 (1987).
[12] J. Hallin and D. Persson, Phys. Lett. **B429**, 232 (1998).

[13] A. Dumitru, Y. Hatta, J. Lenaghan, K. Orginos, and R. D. Pisarski, Phys. Rev. D **70**, 034511 (2004).
[14] A. Dumitru, J. Lenaghan, and R. D. Pisarski, Phys. Rev. D **71**, 074004 (2005).
[15] A. Dumitru, R. D. Pisarski, and D. Zschiesche, Phys. Rev. D **72**, 065008 (2005).
[16] Y. Nambu, B. Bambah, and M. Gross, Phys. Rev. D **26**, 2875 (1982).
[17] B. Bambah, Phys. Rev. D **29**, 1323 (1984).
[18] M. Gross, Phys. Rev. D **27**, 432 (1983).
[19] S. Jaimungal and L. D. Paniak, Nucl. Phys. **B517**, 622 (1998).
[20] C. R. Gattringer, L. D. Paniak, and G. W. Semenoff, Ann. Phys. (NY) **256**, 74 (1997).
[21] H. J. Schnitzer, Nucl. Phys. **B695**, 267 (2004).
[22] B. Sundborg, Nucl. Phys. **B573**, 349 (2000).
[23] O. Aharony, J. Marsano, S. Minwalla, K. Papadodimas, and M. Van Raamsdonk, Adv. Theor. Math. Phys. **8**, 603 (2004).
[24] O. Aharony, J. Marsano, S. Minwalla, K. Papadodimas, and M. Van Raamsdonk, Phys. Rev. D **71**, 125018 (2005).
[25] O. Aharony, S. Minwalla, and T. Wiseman, Class. Quant. Grav. **23**, 2171 (2006).
[26] L. Alvarez-Gaume, C. Gomez, H. Liu, and S. R. Wadia, Phys. Rev. D **71**, 124023 (2005).
[27] B. Muller and J. Rafelski, Phys. Lett. **B116**, 274 (1982).
[28] I. Zakout, C. Greiner, and J. Schaffner-Bielich, Nucl. Phys. **A781**, 150 (2007).
[29] H. T. Elze, W. Greiner, and J. Rafelski, Phys. Lett. **B124**, 515 (1983).
[30] H. T. Elze, W. Greiner, and J. Rafelski, Z. Phys. C **24**, 361 (1984).
[31] H. T. Elze and W. Greiner, Phys. Rev. A **33**, 1879 (1986).
[32] H. T. Elze and W. Greiner, Phys. Lett. **B179**, 385 (1986).
[33] H. T. Elze, D. E. Miller, and K. Redlich, Phys. Rev. D **35**, 748 (1987).
[34] M. I. Gorenstein, S. I. Lipskikh, V. K. Petrov, and G. M. Zinovev, Phys. Lett. **B123**, 437 (1983).
[35] M. I. Gorenstein, V. K. Petrov, and G. M. Zinovev, Phys. Lett. **B106**, 327 (1981).
[36] M. I. Gorenstein, V. K. Petrov, V. P. Shelest, and G. M. Zinovev, Theor. Math. Phys. **52**, 843 (1982).
[37] M. I. Gorenstein, S. I. Lipskikh, and G. M. Zinovev, Z. Phys. C **22**, 189 (1984).
[38] M. I. Gorenstein, W. Greiner, and S. N. Yang, J. Phys. G **24**, 725 (1998).
[39] G. Auberson, L. Epele, and G. Mahoux, Nuovo Cimento A **94**, 339 (1986).
[40] M. I. Gorenstein, M. Gazdzicki, and W. Greiner, Phys. Rev. C **72**, 024909 (2005).
[41] G. Auberson, L. Epele, G. Mahoux, and F. R. A. Simao, J. Math. Phys. **27**, 1658 (1986).
[42] R. Balian and C. Bloch, Ann. Phys. (NY) **60**, 401 (1970).
[43] R. Balian and C. Bloch, Ann. Phys. (NY) E **84**, 559 (1974).
[44] R. Balian and C. Bloch, Ann. Phys. (NY) **64**, 271 (1971).
[45] S. Eidelman *et al.* (Particle Data Group), Phys. Lett. **B592**, 1 (2004).
[46] G. Ripka, *Quarks Bound by Chiral Fields: The Quark Structure of the Vacuum and of Light Mesons and Baryons* (Clarendon, Oxford, U.K., 1997), pp. 1–205.
[47] I. Zakout, work in progress.
[48] J. A. Mcgovern and M. C. Birse, Nucl. Phys. **A506**, 367 (1990).
[49] J. A. Mcgovern and M. C. Birse, Nucl. Phys. **A506**, 392 (1990).
[50] K. A. Bugaev, Phys. Rev. C **76**, 014903 (2007).
[51] K. A. Bugaev, V. K. Petrov, and G. M. Zinovjev, arXiv:0801.4869 [hep-ph].
[52] H. Stoecker, B. Betz, and P. Rau, in *CPOD2006 Proceedings*, PoS(CPOD2006)029 (SISSA, Trieste, Italy, 2006).
[53] B. Betz, P. Rau, and H. Stocker, Int. J. Mod. Phys. E **16**, 3082 (2008) [hep-th].